Copyright

by

Nicholas Phillip Fey

2011

The Dissertation Committee for Nicholas Phillip Fey Certifies that this is the approved version of the following dissertation:

The influence of prosthetic foot design and walking speed on below-knee amputee gait mechanics

Committee:

Richard R. Neptune, Supervisor

Lawrence D. Abraham

Ronald E. Barr

Richard H. Crawford

Raul G. Longoria

The influence of prosthetic foot design and walking speed on below-knee amputee gait mechanics

by

Nicholas Phillip Fey, B.S.M.E.; M.S.E.

Dissertation

Presented to the Faculty of the Graduate School of

The University of Texas at Austin

in Partial Fulfillment

of the Requirements

for the Degree of

Doctor of Philosophy

The University of Texas at Austin

December 2011

Dedication

This dissertation is dedicated to my parents, Timothy and Sharlene; siblings, Natalie and C.W.; and fiancée, Carrie, for inspiring me to aim high in life and in education.

Acknowledgements

I would like to thank my advisor Dr. Richard Neptune for welcoming me into his research group and setting an excellent example of how to conduct research and be a professional in Academia. Throughout graduate school, he has continually put me in a position to be successful. I have had the opportunity to contribute to several uniquely remarkable research projects in addition to gaining collegiate teaching experience, for which I am truly grateful.

Thank you to the current and past members of the Neuromuscular Biomechanics Laboratory who provided a delightful work environment and many stimulating conversations along the way. I am thankful to have been surrounded by great people and friends on a daily basis.

Thank you to our research collaborators at the VA Center of Excellence for Limb Loss Prevention and Prosthetic Engineering and the Andrew J. Gitter Research Center GAIT Lab, especially Dr. Glenn Klute, Jan Pecoraro, Hannah Sutton, Gordon Bosker, Gail Walden, Bill Rogers and Albert Portillo who provided outstanding research facilities and assistance.

Thank you to the members of my dissertation committee, Dr. Lawrence Abraham, Dr. Ronald Barr, Dr. Richard Crawford and Dr. Raul Longoria, for dedicating their time and effort in helping me achieve my research goals.

My graduate research was made possible through funding by the National Science Foundation, Department of Veterans Affairs, and The University of Texas at Austin Cockrell School of Engineering.

The influence of prosthetic foot design and walking speed on below-knee amputee gait mechanics

Nicholas Phillip Fey, Ph.D.

The University of Texas at Austin, 2011

Supervisor: Richard R. Neptune

Unilateral below-knee amputees commonly experience asymmetrical gait patterns and develop comorbidities in their intact (non-amputated) and residual (amputated) legs, with the mechanisms leading to these asymmetries and comorbidities being poorly understood. Prosthetic feet have been designed in an attempt to minimize walking asymmetries by utilizing elastic energy storage and return (ESAR) to help provide body support, forward propulsion and leg swing initiation. However, identifying the influence of walking speed and prosthetic foot stiffness on amputee gait mechanics is needed to develop evidence-based rationale for prosthetic foot selection and treatment of comorbidities. In this research, experimental and modeling studies were performed to identify the influence of walking speed and prosthetic foot stiffness on amputee walking mechanics.

The results showed that when asymptomatic and relatively new amputees walk using clinically prescribed prosthetic feet across a wide range of speeds, loading asymmetries exist between the intact and residual knees. However, knee intersegmental joint force and moment quantities in both legs were not higher compared to non-amputees, suggesting that increased knee loads leading to joint disorders may develop in response to prolonged prosthesis usage or the onset of joint pathology over time. In addition, the results showed that decreasing ESAR foot stiffness can increase prosthesis range of motion, mid-stance energy storage, and late-stance energy return. However, the prosthetic foot contributions to forward propulsion and swing initiation were limited due to muscle compensations

needed to provide body support and forward propulsion in the absence of residual leg ankle muscles.

A study was also performed that integrated design optimization with forward dynamics simulations of amputee walking to identify the optimal prosthetic foot stiffness that minimized metabolic cost and intact knee joint forces. The optimal stiffness profile stiffened the toe and mid-foot while making the ankle less stiff, which decreased the intact knee joint force during mid-stance while reducing the overall metabolic cost of walking.

These studies have provided new insight into the relationships between prosthetic foot stiffness and amputee walking mechanics, which provides biomechanics-based rationale for prosthetic foot prescription that can lead to improved amputee mobility and overall quality of life.

Table of Contents

List of Tables xii

List of Figures xiii

Introduction 1

Review of Related Literature 5

- Amputation Prevalence 5
- Amputee Walking Abnormalities 5
- Prosthetic Foot Function and Type 7
- Selective Laser Sintering Applications 7
- Optimization Techniques and Forward Dynamics Simulations 8
- Muscle Function in Non-Amputee Walking using Forward Dynamics Simulations 9
- Experimental Differences of Amputee Walking 11
- Intact Knee Osteoarthritis Development 12

Aim 1: 3D Intersegmental Knee Loading in Below-Knee Amputees across Steady-State Walking Speeds 15

- Introduction 15
- Methods 18
  - Subjects 18
  - Procedures 19
  - Data Analyses 19
  - Statistical Analyses 21
- Results 21
  - Joint Moments – Intact to Control Comparison 21
  - Joint Moments – Intact to Residual Comparison 24
  - Intersegmental Forces – Intact to Control Comparison 25
  - Intersegmental Forces – Intact to Residual Comparison 27
- Discussion 28

Aim 2: The Influence of Energy Storage and Return Foot Stiffness on Walking Mechanics and Muscle Activity in Below-Knee Amputees 33
Introduction 33
Methods 35
Subjects 36
Protocol 36
Kinematics and Kinetics 38
Electromyography 38
Prosthetic Energy Storage and Return and Mechanical Efficiency 39
Statistical Analyses 39
Results 40
Ground Reaction Forces 40
Joint Kinematics and Kinetics 43
Electromyography 46
Prosthetic Energy Storage and Return and Mechanical Efficiency 48
Discussion 50
Aim 3: The Effect of Altering Stiffness on Prosthetic Foot and Muscle Function during Below-Knee Amputee Walking 56
Introduction 56
Methods 57
Musculoskeletal Model 58
Musculotendon Actuators 60
Energy Storage and Return Prosthetic Foot Model 61
Prosthetic Foot Stiffness 62
Dynamic Optimization 64
Muscle and Prosthetic Foot Function 65
Experimental Tracking Data 66
Results 67
Experimental Tracking Data 67
Prosthetic Foot Deflections, Torques and Energy Storage and Return 70
Contributions to Walking Ground Reaction Forces 73

Contributions to Trunk Power 79
Contributions to Residual Leg Power 80
Discussion 81
Prosthetic Foot Function is Influenced by Stiffness 82
Individual Compensations in Response to Altered Prosthetic Foot Function 83
Comparison of Energy Storage and Return 87
Conclusions and Limitations 88
Aim 4: Optimization of Prosthetic Foot Stiffness to Reduce Metabolic Cost and Intact Knee Loading of Below-Knee Amputee Walking 90
Introduction 90
Methods 92
Musculoskeletal Model 92
Musculotendon Actuators 94
Energy Storage and Return Prosthetic Foot Model 95
Prosthetic Foot Stiffness 96
Metabolic Cost and Joint Contact Forces 97
Dynamic Optimization 97
Muscle and Prosthetic Foot Function 100
Experimental Tracking Data 101
Results 102
Minimization of Metabolic Cost and Intact Knee Contact Force 102
Experimental Tracking Data 104
Individual Joint Contact Forces and Muscle Metabolic Cost 108
Contributions to Residual Leg Walking Ground Reaction Forces 111
Individual Muscle Contributions to Walking Ground Reaction Forces 112
Prosthetic and Muscular Contributions to Trunk Propulsion and Support 115
Prosthetic and Muscular Contributions to Residual Leg Power 118
Discussion 119
Reducing Metabolic Cost 120

Reducing the Intact Knee Contact Force 121
Reducing Both Metabolic Cost and Intact Knee Contact Force 122
Limitations and Future Work 123
Conclusions 125

Conclusions and Future Research 126

Appendix A: Additional Aims 3 and 4 Methods 130
Experimental Tracking Data 130
Musculotendon Actuators 131
Energy Storage and Return Prosthetic Foot Model 132
Muscle and Prosthetic Foot Function 135
Distribution of Ground Contact Elements 137
Prosthetic Foot Damping 138

Appendix B: Additional Aim 3 Results 142
Tracking Comparisons of the Amputee Walking Simulations 142
Prosthetic Foot Deflections, Torques and Energy Storage and Return 145

Appendix C: Additional Aim 4 Results 149
Tracking Comparisons of the Amputee Walking Simulations 149
Prosthetic Foot Deflections, Torques, and Energy Storage and Return 152
Total Prosthetic Foot Energy Storage and Return 154
Total Metabolic Power of Amputee Walking 156

References 157

Vita..... 165

List of Tables

Table 1.1: Group average, mean (standard deviation), net internal joint moment impulses (N*m*s/kg) of the residual, intact and control knees during stance across steady-state walking speeds.. 24

Table 1.2: Group average, mean (standard deviation), net internal joint force impulses (N*s/kg) of the residual, intact and control knees during stance across steady-state walking speeds.. 27

Table 2.1: Below-knee amputee subject characteristics. 36

Table 2.2: Mean (standard deviation) GRFs, joint angles, and joint moments of the residual and intact leg for each prosthetic foot condition. 42

Table 4.1: Metabolic cost and intact knee (right knee) contact force objectives. Also included in this table are the optimized scale factors which varied the prosthetic foot stiffness distribution.. 103

Table A1: Prosthetic foot segment geometry (length, thickness and depth), which were used to calculate individual segment volumes and masses. ...134

List of Figures

Figure 1.1: The local femoral reference frame used to express intersegmental moments and forces.. 20
Figure 1.2: Group average net internal joint moments (N*m/kg) of the residual, intact and control knees across steady-state walking speeds. 22
Figure 1.3: Group average net internal joint moment impulses (N*m*s/kg) of the residual, intact and control knees across steady-state walking speeds.23
Figure 1.4: Group average net internal joint forces (N/kg) of the residual, intact and control knees across steady-state walking speeds. 26
Figure 2.1: ESAR prosthetic feet fabricated using SLS additive manufacturing technology.. 35
Figure 2.2: Group average ground reaction force (GRF) data. 41
Figure 2.3: Group average joint moment data of the residual and intact legs.. 45
Figure 2.4: Group average smoothed EMG data of the intact and residual legs. ..47
Figure 2.5: Group average residual leg ankle power curves and group average (+/- standard deviation) prosthetic energy stored, energy returned and efficiency quantities. 49
Figure 3.1: Amputee musculoskeletal model. 59
Figure 3.2: Schematic of prosthetic foot model consisting of 22 rigid segments connected in series. 62
Figure 3.3: Nominal, compliant and stiff prosthetic foot stiffness distributions calculated from the three SLS ESAR feet.. 64
Figure 3.4: Optimization framework used to generate simulations of amputee walking. 65

Figure 3.5: ESAR prosthetic feet fabricated using SLS additive manufacturing technology that encompassed a wide range of stiffness levels.. 67
Figure 3.6: Representative simulation tracking comparison from the nominal amputee walking simulation.. 68
Figure 3.7: Comparison of excitation timing with group average experimental EMG data of amputee subjects (for only those muscles in which EMG data were collected).. 69
Figure 3.8: Representative keel (left column, KR1-KR13) and heel (right column, HR1-HR5) rotational element angular deflections (top row), torques (middle row) and powers (bottom row) in the nominal amputee walking simulation.. 71
Figure 3.9: Prosthetic foot shape deformations during the nominal, compliant and stiff amputee walking simulations.. 72
Figure 3.10: Keel (KR1-KR13), heel (HR1-HR5) and total (keel + heel) power curves in the nominal, compliant and stiff simulations. 73
Figure 3.11: Mean contributions of the prosthetic foot, residual (left leg) and intact (right leg) muscles, and gravity to A/P and vertical GRF of the residual leg.. 75
Figure 3.12: Mean individual residual (left leg) muscle contributions to A/P and vertical GRF of the residual leg. 77
Figure 3.13: Mean individual intact (right leg) muscle contributions to A/P and vertical GRF of the intact leg. 78
Figure 3.14: Mean prosthetic foot and residual (left leg) and intact (right leg) muscle contributions to horizontal (top row) and vertical (bottom row) trunk power.. 80

Figure 3.15: Mean prosthetic foot and individual muscle contributions to total residual leg power.. 81
Figure 3.16: Amputee group average residual leg ankle power curves which were calculated experimentally to estimate the prosthetic foot energy storage and return characteristics of the prosthetic feet. 88
Figure 4.1: Amputee musculoskeletal model. 93
Figure 4.2: Schematic of prosthetic foot model consisting of 22 rigid segments connected in series. 96
Figure 4.3: Optimization framework used to generate simulations of amputee walking. 98
Figure 4.4: Nominal prosthetic foot stiffness distribution calculated from the SLS ESAR foot. 100
Figure 4.5: ESAR prosthetic foot fabricated using SLS additive manufacturing technology that was worn during the amputee walking trials. 102
Figure 4.6: Prosthetic foot shape deformations throughout each of the three amputee walking simulations. 104
Figure 4.7: Representative simulation tracking comparison from the amputee walking simulation for minimizing metabolic cost. 106
Figure 4.8: Comparison of simulation excitation timing (plotted below each x-axis) with group average experimental EMG data (+1 SD) of amputee subjects walking with the SLS ESAR foot (only those muscles in which EMG data were collected are plotted). 107
Figure 4.9: Intact (right leg) and residual (left leg) knee and hip contact forces for each walking simulation. 109

Figure 4.10: Individual muscle group metabolic cost profiles of intact (right leg) and residual (left leg) muscle groups.. 110
Figure 4.11: Contributions of the prosthetic keel and heel, muscles (left and right legs), and gravity to residual leg A/P and vertical ground reaction forces during the first (left column) and second (right column) halves of residual leg stance. 112
Figure 4.12: Mean individual residual (left leg) muscle contributions to A/P and vertical GRF of the residual leg.. 113
Figure 4.13: Mean individual intact (right leg) muscle contributions to A/P and vertical GRF of the intact leg. 115
Figure 4.14: Mean prosthetic foot and residual (left leg) muscle contributions to horizontal (top row) and vertical (bottom row) power delivered to the trunk. 117
Figure 4.15: Mean intact (right leg) muscle contributions to horizontal (top row) and vertical (bottom row) power delivered to the trunk. 118
Figure 4.16: Mean prosthetic foot and individual muscle contributions to total power delivered to the leg. 119
Figure A1: Schematic of Hill-type musculotendon actuator. 131
Figure A2: Musculotendon contraction dynamics included muscle force-length, muscle force-velocity, and tendon force-strain relationships. 132
Figure A3: Prosthetic foot segment definitions.. 133
Figure A4: The distribution of 31 ground contact elements (indicated by square symbols) attached to the distal segments of the feet.. 137
Figure A5: In order to estimate the damping of the three prosthetic feet, a linear regression equation was computed.. 139

Figure A6: In order to estimate the damping of the three prosthetic feet, a linear regression equation was computed. 140
Figure A7: In order to estimate the damping of the three prosthetic feet, a linear regression equation was computed. 141
Figure B1: Representative simulation tracking comparison from the nominal amputee walking simulation.. 142
Figure B2: Representative simulation tracking comparison from the compliant amputee walking simulation. 143
Figure B3: Representative simulation tracking comparison from the stiff amputee walking simulation. 144
Figure B4: Keel (left column, KR1-KR13) and heel (right column, HR1-HR5) rotational element angular deflections (top row), torques (middle row) and powers (bottom row) in the nominal amputee walking simulation. 146
Figure B5: Keel (left column, KR1-KR13) and heel (right column, HR1-HR5) rotational element angular deflections (top row), torques (middle row) and powers (bottom row) in the compliant amputee walking simulation. 147
Figure B6: Keel (left column, KR1-KR13) and heel (right column, HR1-HR5) rotational element angular deflections (top row), torques (middle row) and powers (bottom row) in the stiff amputee walking simulation. 148
Figure C1: Representative simulation tracking comparison from the amputee walking simulation for minimizing metabolic cost. 149

Figure C2: Representative simulation tracking comparison from the amputee walking simulation for minimizing both metabolic cost and intact knee contact force.. 150
Figure C3: Representative simulation tracking comparison from the amputee walking simulation for minimizing intact knee contact force. 151
Figure C4: Keel (left column, KR1-KR13) and heel (right column, HR1-HR5) rotational element angular deflections (top row), torques (middle row) and powers (bottom row) in the amputee walking simulation for minimizing metabolic cost. 152
Figure C5: Keel (left column, KR1-KR13) and heel (right column, HR1-HR5) rotational element angular deflections (top row), torques (middle row) and powers (bottom row) in the amputee walking simulation for minimizing both metabolic cost and intact knee contact force.. 153
Figure C6: Keel (left column, KR1-KR13) and heel (right column, HR1-HR5) rotational element angular deflections (top row), torques (middle row) and powers (bottom row) in the amputee walking simulation for minimizing intact knee contact force. 154
Figure C7: Keel, heel and total (keel + heel) power curves in the amputee walking simulations.. 155
Figure C8: Metabolic cost profiles of the intact (right leg) and residual (left leg) legs as well as the total (right + left) metabolic cost profile for the three simulations. 156

Introduction

In the U.S., the number of people living with the loss of a limb is projected to dramatically increase by the year 2050 due to a rise in secondary illness and traumatic injuries, with approximately 40% of these losses being major lower-leg amputations (Dillingham et al., 2002; Ziegler-Graham et al., 2008). Comorbidities of unilateral below-knee amputees during walking include chronic leg and back pain (Burke et al., 1978; Ephraim et al., 2005; Kulkarni et al., 2005; Smith et al., 1999) relative to non-amputees. Joint pain is most frequently reported in the intact (non-amputated) leg knee, and long term prosthetic use is associated with increased prevalence of joint disorders such as osteoarthritis in the intact knee that are detrimental to their mobility (for review, see Gailey et al., 2008). Examining the mechanical knee loading characteristics of amputees remains an active area of research and can provide insight into the development of such joint disorders.

Studies analyzing sagittal plane knee loading quantities have identified increased intact leg loading relative to the residual (amputated) leg, leading some to suggest that the reduced residual leg loads are a mechanism to protect the residual leg (e.g., Beyaert et al., 2008). However, protecting the residual leg may lead to long-term detrimental consequences in the intact leg due to increased dependence on the intact leg. In general, previous studies examining amputee knee loading have focused on either sagittal or frontal plane comparisons at self-selected walking speeds (SSWS), and often do not compare their results to non-amputee control subjects. In addition, the influence of altering the task demands of walking (e.g., speed) on amputee knee loading has not been investigated. Such an investigation is needed since knee loading has been shown to be influenced by altered walking speed in non-amputees (e.g., Mundermann et al., 2004).

Thus, altering walking speed in amputees may offer new insight into the knee loading characteristics that are detrimental to knee joint health. The purpose of Aim 1 was to examine three-dimensional mechanical knee loading across a wide range of steady-state walking speeds in below-knee amputees and non-amputees to identify potential mechanisms that may lead to amputee knee joint disorders.

Below-knee amputations also lead to distinct walking characteristics that include altered residual leg muscle activation patterns (e.g., Winter and Sienko, 1988), increased metabolic cost (e.g., Waters et al., 1976) and reduced walking speed (e.g., Robinson et al., 1977). These differences between amputees and non-amputees are attributed to the functional loss of the ankle plantar flexor muscles, which provide essential body support, forward propulsion and leg swing initiation subtasks during non-amputee walking (Neptune et al., 2001). Thus, proper prosthetic foot selection and design is critical to reduce the effects of limb loss.

Advancements in prosthetic foot design have lead to the development of carbon fiber energy storage and return (ESAR) feet, which are designed to restore some functions of the ankle plantar flexors and improve amputee walking by storing and releasing elastic energy during stance. However, the appropriate stiffness level that governs ESAR for a given amputee is not well-defined. Studies are needed that quantify the influence of specific prosthetic foot stiffness during amputee gait to develop evidence-based rationale for prosthetic selection. However, a difficulty in executing such studies is the complexity of creating custom ESAR feet. One solution to overcome this difficulty is to use selective laser sintering (SLS) technology, which was recently used in a manufacturing framework to produce ESAR prosthetic feet of a desired stiffness and shape (South et al. 2010). The purpose of Aim 2 was to use this framework to identify the influence of ESAR foot stiffness on gait characteristics by manufacturing SLS ESAR feet

with a range of stiffness levels and quantify their effect on below-knee amputee walking. Using experimental biomechanical techniques, we investigated the influence of ESAR foot stiffness on kinematics, kinetics, muscle activity, prosthetic energy storage and return, and mechanical efficiency during amputee walking.

Although much insight into the influence of foot stiffness on walking performance was gained from these experimental analyses, these studies are limited by the level of detail to which the dynamic interactions between prosthetic feet and the musculoskeletal system can be examined. Identifying causal relationships between foot stiffness, muscle and prosthetic foot contributions to walking subtasks, and important biomechanical quantities of interest would further develop quantitative rationale for prosthetic foot prescription and improve amputee mobility. In previous studies of non-amputee walking, musculoskeletal models and forward dynamics simulations have provided much insight into muscle function and coordination (e.g., Anderson and Pandy, 2003; Liu et al., 2006; Neptune et al., 2001). Therefore, the purpose of Aim 3 was to develop forward dynamics simulations of below-knee amputee walking using a range of prosthetic foot stiffness levels to identify how foot stiffness influences muscle and prosthetic foot function in terms of their contributions to body support, forward propulsion and leg swing initiation.

Forward dynamics simulations have also provided insight into the estimation of *in vivo* quantities such as joint contact forces and metabolic cost (Sasaki and Neptune, 2010; Shelburne et al., 2005; Umberger, 2010). Joint contact forces and metabolic cost are important biomechanical quantities to consider since amputees are more likely to develop joint disorders than non-amputees and experience an increased metabolic cost of walking. The design of prosthetic devices that reduce metabolic cost and joint loading (e.g., joint contact forces) of amputees will likely provide substantial improvements in amputee

mobility. Thus, the purpose of Aim 4 was to couple design optimization of ESAR prosthetic feet with forward dynamics simulations of amputee walking to identify optimal prosthetic foot designs that minimize metabolic cost and joint loading of below-knee amputees.

Review of Related Literature

The following literature review covers a range of topics relevant to this research and provided a foundation to effectively investigate amputee walking and prosthetic foot design.

AMPUTATION PREVALENCE

Amputation prevalence has been identified as an important health risk in the U.S.. Below-knee amputation was the second most common form of amputation in the U.S. from 1988 to 1996 (second only to toe amputation) with primary causes linked to traumatic injuries and vascular disease (Dillingham et al., 2002). In 2005, approximately 1.6 million persons were living with limb loss in the U.S. (~40% major lower limb amputations) (Ziegler-Graham et al., 2008). By 2050, the number of people with limb loss is expected to more than double to 3.6 million (Ziegler-Graham et al., 2008).

AMPUTEE WALKING ABNORMALITIES

Unilateral below-knee amputations result in a number of walking abnormalities relative to non-amputees. Temporal and ground reaction force (GRF) asymmetry between legs is increased, with increased time spent and GRF magnitude developed during the intact leg stance phase (Nolan et al., 2003; Sanderson and Martin, 1997; Silverman et al., 2008; Vrieling et al., 2008). In addition, amputees experience increased metabolic cost (e.g., Czerniecki, 1996; Genin et al., 2008; Waters et al., 1976), asymmetric joint loading between legs (Bateni and Olney, 2002; Beyaert et al., 2008; Gitter et al., 1991; Nolan and Lees, 2000; Powers et al., 1998; Silverman et al., 2008), and altered residual leg muscle activation patterns (e.g., Fey et al., 2010; Klute et al., 2001; Winter and Sienko, 1988).

Amputees also suffer from chronic leg and back pain (Burke et al., 1978; Ephraim et al., 2005; Kulkarni et al., 2005; Smith et al., 1999) and experience a reduced self-selected walking speed (Hermodsson et al., 1994; Perry et al., 1997; Powers et al., 1998; Robinson et al., 1977).

These abnormalities may be attributed to the functional loss of the muscles that once spanned the ankle joint pre-amputation. Specifically, the ankle plantar flexors (soleus and gastrocnemius) are critical to non-amputee walking. Ankle plantar flexors provide body support, forward propulsion, and swing initiation in non-amputees (Anderson and Pandy, 2003; Liu et al., 2006; Neptune et al., 2001). Thus, the primary goal of prosthetic foot designs has been to provide these important biomechanical functions. However, current passive prosthetic feet are unable to completely replace these functions. As a result, a number of compensatory strategies have been identified in amputee walking using both experimental and modeling studies (e.g., Fey et al., 2010; Silverman et al., 2008; Zmitrewicz et al., 2007). Our group has shown that across a wide range of walking speeds (0.6-1.5 m/s) amputees have been shown to reduce the braking GRF impulse during the first half of residual leg stance to compensate for a reduced propulsive impulse that occurs during the second half of residual leg stance (Silverman et al., 2008). We have also shown that amputees compensate for a reduced positive residual ankle power (push-off) prior to toe-off by increasing the output of their residual leg hip extensors during the first half of residual leg stance to reduce the braking impulse (increasing net propulsion) (Fey et al., 2010; Silverman et al., 2008). Proper prosthetic foot selection and design may be critical to help reduce these effects of limb loss and required compensations that occur post-amputation.

PROSTHETIC FOOT FUNCTION AND TYPE

In contrast to previous research aimed at identifying walking abnormalities relative to non-amputees, a considerable knowledge gap exists in terms of prosthetic foot design. The influence of specific design characteristics (e.g., stiffness) during amputee walking remains unclear. Traditional solid ankle cushion heel feet attempt to reduce contact forces during initial loading response but store and release minimal elastic energy (e.g., Ehara et al., 1993) due to a high stiffness and limited deflection. Carbon fiber energy storage and return (ESAR) feet attempt to replace lost ankle function by storing and releasing elastic energy. Carbon fiber is a strong and lightweight composite material that exhibits beneficial mechanical properties for prosthetic foot function. However, the technology to manufacture carbon fiber feet is labor intensive. Also, the appropriate stiffness level for a given amputee to maximize function is not well-understood (Hafner et al., 2002b). Currently, clinician experience and patient feedback are the primary methods for prosthetic selection rather than quantitative assessment of biomechanical data. Therefore, studies that quantify the effect of prosthetic design variables (e.g., stiffness characteristics) independently are needed to improve both subject-specific prosthetic design and prescription.

SELECTIVE LASER SINTERING APPLICATIONS

Previously, to manufacture custom ESAR feet of varying stiffness levels was infeasible due to the labor intensive manufacturing technology used. In this research we have applied a powerful manufacturing technique called selective laser sintering (SLS) to produce ESAR prosthetic feet of varying stiffness levels (Fey et al., 2011; South et al., 2010). Selective laser sintering is a powerful freeform manufacturing process with few manufacturing constraints. It is a form of rapid manufacturing in which layers of powder

are successively and selectively melted (sintered) together until a solid part is produced (Beaman, 1997). As a result, nearly any complex part can be realized. In addition, the process is highly automated and hands-off. With these beneficial features, it has been used to manufacture a variety of biomechanics-related devices such as ankle-foot orthoses (Faustini et al., 2008), below-knee prosthetic sockets (Faustini et al., 2005; Faustini et al., 2006a; Faustini et al., 2006b; Rogers et al., 2007), ESAR prosthetic ankles (Ventura et al., 2011; Ventura et al., 2011) and ESAR prosthetic feet of a desired stiffness and shape (Fey et al., 2011; South et al., 2010).

OPTIMIZATION TECHNIQUES AND FORWARD DYNAMICS SIMULATIONS

Due to the small number of manufacturing constraints using SLS and its corresponding large design space, a design optimization framework would be useful to produce and investigate custom prosthetic designs. Previous studies have used topology or parametric optimization techniques on a variety of tasks to optimize the layout of a product or component (Eschenauer and Olhoff, 2001; Ohsaki and Swan, 2002; Soto, 2001). In biomechanics-related applications, topology optimization techniques have been used to generate implant scaffold designs (Lin et al., 2004), simulate bone morphology and growth (Xinghua et al., 2005), and design compliant features in amputee prosthetic sockets (Faustini et al., 2005). However, the application of optimization techniques to produce custom prosthetic foot designs remains unexplored. In addition, forward dynamics simulations of human movement have been effective in assessing individual muscle function (Neptune et al., 2001) and estimation of important in vivo quantities such as muscle work, metabolic cost and joint contact forces (Sasaki et al., 2009; Sasaki and Neptune; Shelburne et al., 2005; Umberger, 2010). These applications most commonly develop detailed musculoskeletal models that represent the human body in

terms of bones, ligaments, tendons and muscles. Often, the goal of these studies is to solve for the muscle control strategy that allows these musculoskeletal models to emulate experimentally-derived clinical data (optimal tracking). After these models successfully track experimental data, they can be used in a variety of analyses to study human locomotion. In this research, we used these types of analyses to evaluate and optimize the prosthetic foot stiffness characteristics to improve important biomechanical quantities in amputee walking (i.e., metabolic cost and joint contact forces), which are difficult or nearly impossible to measure experimentally.

Some studies have coupled forward dynamics simulations of human movement with finite element models of the natural foot to calculate soft tissue deformation and loading (Halloran et al., 2009; Halloran et al., 2010). However, solving the finite element model at various time steps of the simulations accounted for greater than 99% of the total computation time. Thus, coupling forward dynamics simulations of human movement with a finite element prosthetic foot model to optimize a prosthetic foot design would present even greater computational expense. Other modeling and simulation studies of human movement have successfully incorporated design optimization and evaluated its influence on biomechanical objectives. These studies include optimizing bicycle seat configuration (Rankin and Neptune, 2010) and chainring shape (Rankin and Neptune, 2008) to maximize power delivered to the crank. Similar methods were developed in this research to optimize the stiffness characteristics of ESAR prosthetic feet.

MUSCLE FUNCTION IN NON-AMPUTEE WALKING USING FORWARD DYNAMICS SIMULATIONS

A thorough understanding of muscle function in non-amputee walking is necessary to interpret differences in experimental quantities such as muscle activity, joint

kinetics and ground reaction forces in pathological populations such as amputees. Specifically, the primary contributors to the walking subtasks of body support, forward propulsion and swing initiation in able-bodied non-amputees were considered since contributions of these muscles to each subtask may change as prosthetic foot stiffness characteristics are altered. Previous studies have shown the primary contributors to body support during the first half of stance are the dorsiflexors, gluteus maximus, gluteus medius and vasti muscles (Anderson and Pandy, 2003; Liu et al., 2006; Neptune et al., 2004; Neptune et al., 2008). Also when active during the first half of stance, the rectus femoris provides body support (Neptune et al., 2004). During mid stance, the primary contributors to body support are the gluteus medius (Anderson and Pandy, 2003) and ankle plantar flexors (Anderson and Pandy, 2003; Neptune et al., 2001). In late stance and pre-swing, the primary contributors to body support are the ankle plantar flexors (Anderson and Pandy, 2003; Neptune et al., 2001). In terms of forward propulsion, the gluteus maximus and vasti muscles are the primary contributors to braking (negative forward propulsion) during the first half of stance (Liu et al., 2006; Neptune et al., 2004), whereas the biarticular hamstrings produce forward propulsion throughout stance when active (Liu et al., 2006; Neptune et al., 2004). During mid to late stance, the ankle plantar flexors are the primary producers of propulsion (Liu et al., 2006; Neptune et al., 2001; Neptune et al., 2004), while the rectus femoris acts to transfer energy from the leg to the trunk for forward propulsion (Neptune et al., 2004). Leg swing initiation is primarily provided by the gastrocnemius, iliacus and psoas muscles (Neptune et al., 2004). This understanding of muscle function during non-amputee walking was essential for our goal of designing ESAR prosthetic feet to replace the function of the ankle plantar flexors, which above shows they are critical in providing body support, forward propulsion and leg swing initiation.

EXPERIMENTAL DIFFERENCES OF AMPUTEE WALKING

Previous studies have identified differences in various GRF, joint kinetic and muscle activity quantities during unilateral below-knee amputee walking using a variety of prosthetic feet. A number of studies have used inverse-dynamics-based analyses to compare GRFs and joint kinetics between amputee and non-amputee walking. Studies have shown amputees have greater intact leg GRFs and stance time compared to their residual leg and non-amputees (e.g., Engsberg et al., 1991; Nolan et al., 2003; Sanderson and Martin, 1997; Vrieling et al., 2008). Increased intact leg hip (Bateni and Olney, 2002; Nolan and Lees, 2000; Silverman et al., 2008) and knee (Beyaert et al., 2008; Nolan and Lees, 2000; Sanderson and Martin, 1997) joint moments and powers compared to non-amputees have also been shown. Within the residual leg, kinetic differences include reduced knee extensor moment and power (Beyaert et al., 2008; Powers et al., 1998; Sanderson and Martin, 1997; Winter and Sienko, 1988) and increased hip extensor moment and power (Bateni and Olney, 2002; Gitter et al., 1991; Winter and Sienko, 1988) compared to non-amputees.

Studies investigating changes in muscle activity during amputee walking have identified significant differences in the muscle activity of several residual leg muscles compared to the intact leg and non-amputees. In particular, increased magnitude and duration of the residual leg uniarticular knee extensors (Culham et al., 1986; Fey et al., 2010; Isakov et al., 2000; Perry and Shanfield, 1993; Pinzur et al., 1991; Powers et al., 1998; Rietman et al., 2002; Torburn et al., 1990; Winter and Sienko, 1988), biarticular hamstrings (Culham et al., 1986; Fey et al., 2010; Isakov et al., 2000; Isakov et al., 2001; Perry and Shanfield, 1993; Pinzur et al., 1991; Powers et al., 1998; Rietman et al., 2002; Schmalz et al., 2001; Torburn et al., 1990; Winter and Sienko, 1988) and gluteus

maximus (Perry and Shanfield, 1993; Torburn et al., 1990; Winter and Sienko, 1988) muscles have been reported. Intact leg muscle activity has consistently been found to be similar to non-amputees (Culham et al., 1986; Czerniecki, 1996; Fey et al., 2010; Rietman et al., 2002).

However, in many of these studies, amputee subjects wore differing prosthetic feet with a wide range of design characteristics, and may have contributed to inconsistencies across studies. Thus, one aspect of this research was to isolate the influence of specific prosthetic design characteristics (e.g., foot stiffness) during amputee walking.

INTACT KNEE OSTEOARTHRITIS DEVELOPMENT

During amputee walking, pain is most frequently reported in the intact leg knee joint and long term prosthetic use is associated with increased prevalence of joint disorders and an early onset of knee osteoarthritis (for review, see Gailey et al., 2008). Prevalence of osteoarthritis in unilateral amputees is higher in the intact knee compared to the residual knee (Burke et al., 1978). In addition, the development of intact-knee osteoarthritis in older unilateral below-knee amputees (83%) is higher than non-amputees (50%) (Lemaire and Fisher, 1994). However, the mechanism leading to the greater prevalence of intact knee osteoarthritis in amputees remains unclear. Studies analyzing amputee walking have primarily focused on sagittal plane quantities and identified bilateral loading asymmetry between residual and intact legs. Some studies have suggested that reduced residual leg loads compared to the intact leg are indicative of a mechanism to protect the residual leg (e.g., Beyaert et al., 2008), which may have long-term detrimental consequences in the intact leg. Studies examining intersegmental joint forces between legs have produced conflicting results. One study found a significantly

smaller peak horizontal force and no difference in vertical force of the intact knee compared to non-amputees (Hurley et al., 1990), while others found no significant difference in peak vertical and horizontal forces of the intact knee compared to non-amputees, but reported a significantly greater vertical force impulse (Lemaire and Fisher, 1994). Thus, while studies have shown the intact leg experiences greater sagittal plane GRFs and joint moments and powers compared to the residual leg and non-amputees, their relationships with the intersegmental forces are not well-understood.

Previous studies investigating the mechanisms leading to osteoarthritis in non-amputees have found that an increased knee abduction (internal) moment is associated with higher medial compartment forces and joint degradation in the knee of patients with osteoarthritis (Miyazaki et al., 2002; Sharma et al., 1998) and is proportional to osteoarthritis disease severity (for review, see Foroughi et al., 2009; Mundermann et al., 2004). However, a recent review of the association between knee abduction moment and osteoarthritis in non-amputees was inconclusive. In patients with low disease severity, there was no consistent increase in the knee abduction moment compared to controls (Foroughi et al., 2009), suggesting an increased abduction moment may not be the cause of osteoarthritis. Similar studies of amputee walking have found intact knee abduction moment to be significantly greater (~56%) than in the residual leg and have suggested the increased moment is the mechanism for joint degradation (Royer and Koenig, 2005; Royer and Wasilewski, 2006). However, there was no significant difference in knee loads compared to non-amputees (Royer and Koenig, 2005). Others have shown up to a 44% difference in the abduction moment between intact and residual knees, although they were not statistically compared (Underwood et al., 2004). Recent studies analyzing below-knee amputee walking have shown differences in GRFs, joint work and muscle adaptation between residual, intact and control legs are not always consistent across

walking speeds (Fey et al., 2010; Silverman et al., 2008), which will affect joint forces and moments. Thus, another aspect of this research was to examine intact knee intersegmental moments and forces across speeds that may provide further insight into potential mechanisms leading to joint disorders such as osteoarthritis in amputees.

Aim 1: 3D Intersegmental Knee Loading in Below-Knee Amputees across Steady-State Walking Speeds

INTRODUCTION

Limb loss prevalence in the U.S. is projected to dramatically increase over the next 40 years, with the primary causes related to dysvascular disease and traumatic injuries (Ziegler-Graham et al., 2008). Unilateral below-knee amputees often develop comorbidities that include joint disorders in both the intact and residual legs (e.g., Gailey et al., 2008) and chronic pain in their legs (e.g., Ephraim et al., 2005) and lower backs (e.g., Burke et al., 1978; Ephraim et al., 2005). Pain is most frequent in the intact leg knee joint, and long-term prosthetic use is associated with increased prevalence of joint disorders (for review, see Gailey et al., 2008). For example, the prevalence of osteoarthritis in unilateral amputees is higher in the intact knee compared to the residual knee (Burke et al., 1978). In addition, the development of intact-knee osteoarthritis in older unilateral below-knee amputees (83%) is higher than non-amputees (50%) (Lemaire and Fisher, 1994). However, the mechanisms leading to the development of such disorders are unclear.

Previous studies seeking to identify these mechanisms in amputees have examined a variety of factors including bone mineral density (Royer and Koenig, 2005), strength (Lloyd et al., 2010) and mechanical loading (Lloyd et al., 2010; Royer and Koenig, 2005; Royer and Wasilewski, 2006) of the knee joint, which were generally greater in the intact leg compared to residual leg and non-amputees. For example, sagittal plane knee strength of amputees were found to be asymmetric compared to non-amputees (Lloyd et al., 2010). However, frontal plane knee moments at self-selected walking speeds (SSWS) and hip abduction strength were not significantly asymmetric compared to non-amputees (Lloyd et al., 2010). Previous studies investigating joint disorders in

non-amputees have also examined mechanical loading of the knee in addition to other factors such as joint laxity, varus alignment and serum hyaluronan level (Miyazaki et al., 2002; Sharma et al., 1998). These studies have shown increased knee loading is associated with knee joint disorders (Miyazaki et al., 2002; Sharma et al., 1998) and is proportional to disease severity (for review, see Foroughi et al., 2009; Mundermann et al., 2004). In addition, other factors such as specific walking patterns (Fregly et al., 2009), gait retraining (Barrios et al., 2010) and altered walking speed (Mundermann et al., 2004) have been shown to influence knee loading in non-amputees and may offer effective non-invasive treatment interventions for amputees. However, the relationships between these quantities, specifically knee loading and walking speed in amputees, remain unclear. Since unilateral amputees commonly walk using passive prosthetic feet on their residual leg, which cannot perform net positive work, compensation from other muscles to provide body support and propulsion and differences in walking mechanics as walking speed increases may influence the joint loads that develop in amputees.

Studies analyzing sagittal plane mechanical loading during amputee walking have identified bilateral loading asymmetry between the residual and intact legs. Greater intact leg ground reaction forces (GRFs) and stance time (e.g., Sanderson and Martin, 1997; Silverman et al., 2008) as well as intersegmental joint moments and powers (e.g., Beyaert et al., 2008; Gitter et al., 1991) have been reported. Some studies have suggested that reduced residual leg loads compared to the intact leg are indicative of a mechanism to protect the residual leg (e.g., Beyaert et al., 2008; Nolan et al., 2003), which may have long-term detrimental consequences in the intact leg. Other studies examining intersegmental joint forces between legs have produced conflicting results. One study found a significantly smaller peak horizontal force and no difference in vertical force of the intact knee compared to non-amputees (Hurley et al., 1990), while others found no

significant difference in peak vertical and horizontal forces of the intact knee compared to non-amputees, but reported a significantly greater vertical force impulse (Lemaire and Fisher, 1994). Thus, while studies have shown the intact leg experiences greater sagittal plane GRFs and joint moments and powers, consistently greater intact leg intersegmental forces have not been observed.

Previous analyses of frontal plane loading during amputee walking have shown the intact knee abduction moment peak magnitude to be significantly greater (~56%) than in the residual leg at their SSWS (Royer and Koenig, 2005; Royer and Wasilewski, 2006). However, there was no significant difference in knee loads compared to non-amputees (Royer and Koenig, 2005). Others have shown up to a 44% difference in the abduction moment magnitude between intact and residual knees, although they were not statistically compared (Underwood et al., 2004).

Previous observational studies examining amputee knee loading have emphasized loading magnitudes, and typically do not control walking speed. Recent studies analyzing below-knee amputee walking have shown differences in GRFs, joint work and muscle activity between residual, intact and control legs are not always consistent across walking speeds (Fey et al., 2010; Silverman et al., 2008), which will influence both the magnitude and duration of knee loading characteristics. In this study, we analyzed amputees and non-amputees walking at different speeds to identify the influence of speed on knee loading. Since the loading magnitude and duration change with speed, both factors would influence the mechanical loading dose and response characteristics. Therefore, in order to quantify this relationship, knee loading impulses (i.e., the time-integral of the corresponding load) were compared during stance of both amputees and non-amputees.

The overall objective of this study was to examine three-dimensional mechanical knee loading across a wide range of steady-state walking speeds in below-knee amputees

and non-amputees. Four hypotheses were evaluated at each walking speed: (1) net intersegmental joint moment impulses and (2) force impulses of the intact knee of amputees will be greater than non-amputee control subjects, and (3) net intersegmental joint moment impulses and (4) force impulses of the intact knee of amputees will be greater than in the residual knee. In addition, we expected the influence of walking speed on moment and force impulses to be different between the residual and intact knees of amputees, and between the intact knee of amputees and non-amputee control subjects.

METHODS

Subjects

Each subject provided informed consent to an Institutional Review Board approved protocol. Subjects were pain free and asymptomatic of joint disorders. Fourteen unilateral, below-knee amputees (11 traumatic, 3 vascular; 13 males, 1 female; 45 (9) years mean (standard deviation); 90.6 (18.6) kg; 1.76 (0.10) m) and 10 control non-amputees (7 males, 3 females; 33 (12) years; 70.9 (13.6) kg; 1.76 (0.11) m) were analyzed. Time from amputation was ≥1.5 years and averaged 6 (3) years. The vascular and traumatic amputee groups did not substantially differ in terms of body weight or activity level, and all amputee subjects were at least limited community ambulators. Each amputee used their own prosthesis (9 energy storage and return, ESAR, and 5 solid ankle cushioned heel, SACH, prosthetic feet). Prosthesis alignment and fit were verified by a licensed prosthetist.

Procedures

Each subject walked along a 10-m walkway at four randomly-ordered, steady-state speeds of 0.6, 0.9, 1.2 and 1.5 m/s. For each walking trial, speed was measured using infrared timing gates. To be included in the analysis, the speed was required to be within 0.06 m/s of the target speed. Bilateral kinematic marker data (Silverman et al., 2008) were measured at 120 Hz using an eight-camera motion capture system (Vicon, Oxford Metrics, Inc.). Reflective markers were placed on the C-7 vertebrae and bilaterally on the acromion, iliac crest, posterior superior iliac spine, anterior superior iliac spine, greater trochanter, lateral and medial femoral condyles, lateral and medial malleoli, heel, dorsal foot, and the first, second and fifth metatarsal heads. To minimize skin movement artifact, marker clusters were also placed bilaterally on the shank and thigh. Markers on the foot of the residual leg were placed symmetric to the intact leg. GRF data were measured at 1200 Hz using four embedded force plates (Advanced Mechanical Technology, Inc.). Repeated trials were collected until at least five complete gait cycles per foot were measured at each speed.

Data Analyses

Inverse dynamics analysis was performed to calculate net intersegmental joint moments and forces using Visual3D (C-Motion, Inc.), which were expressed in the local orthogonal femoral frame (Fig. 1.1). Kinematic data were low-pass filtered using a 4^{th}-order Butterworth filter with a cut-off frequency of 6 Hz, and GRF data were low-pass filtered with a cut-off frequency of 20 Hz. Inertial properties of the residual leg were adjusted for the amputees and were based on previous measurements of residual limb mass and center-of-mass location for below-knee amputees (Mattes et al., 2000). Residual shank mass was reduced to 50% of the intact leg shank mass (2.3% body

weight). Residual shank center-of-mass location was moved more proximally to 25% of the total shank length measured relative to the knee. Joint moments and forces were normalized by each subject's body mass.

Knee intersegmental joint moment and force impulses (i.e., time integral of the corresponding moment or force) were computed over the stance phase (ipsilateral heel strike to toe off). Knee extension, flexion, abduction, internal rotation, and external rotation moment impulses and lateral (positive x-direction), anterior (positive y-direction), posterior (negative y-direction), and distal (negative z-direction) force impulses of the residual, intact and control legs were compared at each walking speed. Control subject data from the left and right legs were averaged for the analyses.

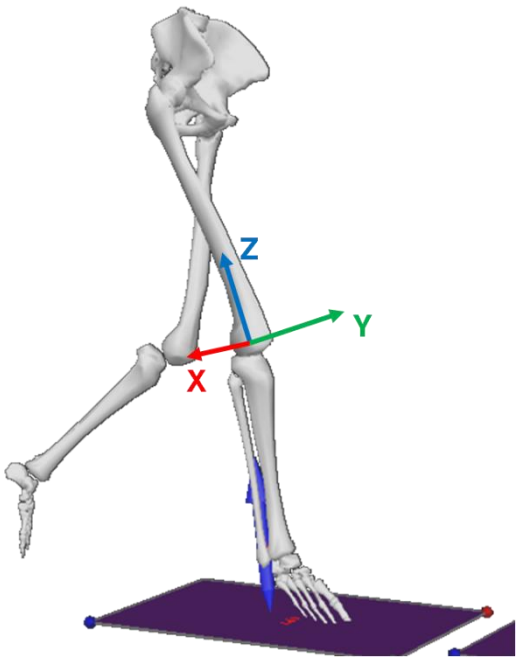

Figure 1.1: The local femoral reference frame used to express intersegmental moments and forces was defined as positive x-direction oriented laterally, positive z-direction oriented proximally and axially along the femur, and positive y-direction orthogonal to x- and z-direction axes and oriented anteriorly.

Statistical Analyses

For each impulse tested, two, two-factor repeated-measures ANOVAs were performed to compare quantities across legs, group and speed (SPSS 16.0 GP, SPSS, Inc.). The two ANOVAs included: (1) intact and residual legs (two-factor, leg and speed), and (2) intact and control legs (two-factor, group and speed). The leg factor consisted of two levels (residual leg, intact leg). The group factor consisted of two levels (amputee, non-amputee). The speed factor consisted of four levels (0.6, 0.9, 1.2 and 1.5 m/s). If a significant main or interaction effect was found (α=0.05), pairwise comparisons were made using a Bonferroni adjustment for multiple comparisons to determine which factors were significantly different. To further assess how these impulses varied with respect to walking speed, a polynomial decomposition was evaluated in each ANOVA to determine if there was a significantly different linear trend with walking speed in the intact, residual and control legs (α=0.05).

RESULTS

Joint Moments – Intact to Control Comparison

The hypothesis that the intact knee moment impulses would be greater than in the control subjects was not supported in any of the moment impulses tested. In contrast, the knee abduction moment impulse was significantly lower (group, $p=0.039$; speed*group, $p<0.001$) in the intact knee compared to control subjects at 0.6 and 0.9 m/s ($p\leq0.031$) and showed a significantly different linear relationship between intact and control legs as walking speed increased ($p<0.001$, Figs. 1.2 and 1.3, Table 1.1).

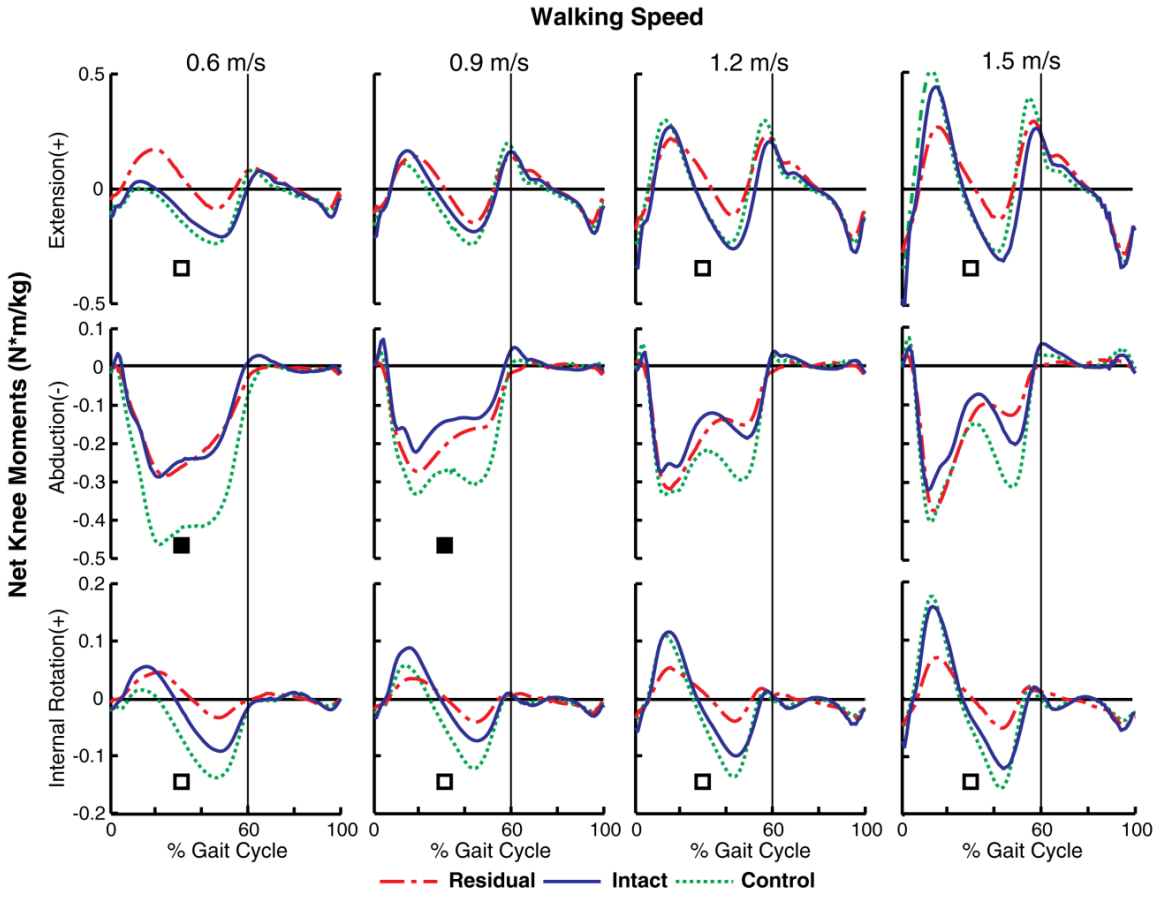

Figure 1.2: Group average net internal joint moments (N*m/kg) of the residual, intact and control knees across steady-state walking speeds. Significant pairwise differences between intact and control knees (■) and between intact and residual knees (□) are indicated.

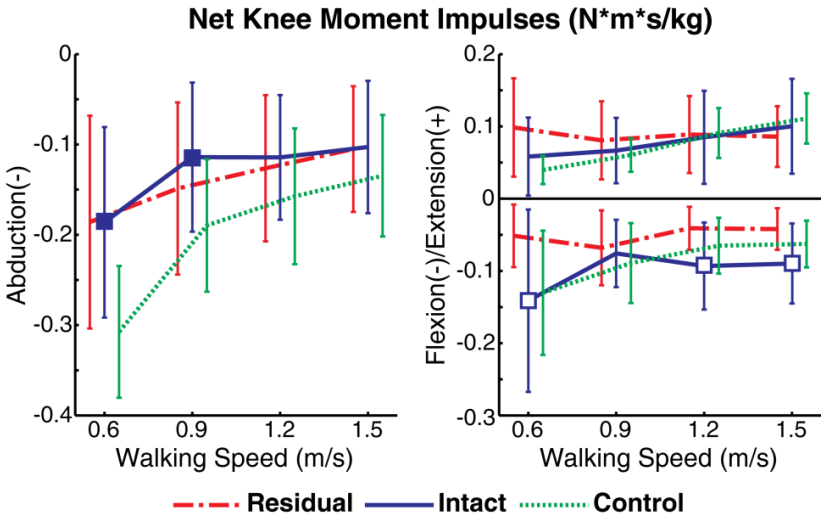

Figure 1.3: Group average net internal joint moment impulses (N*m*s/kg) of the residual, intact and control knees across steady-state walking speeds. Vertical bars represent one standard deviation of the experimental data. Significant pairwise differences between intact and control knees (■) and between intact and residual knees (□) are indicated.

Table 1.1: Group average, mean (standard deviation), net internal joint moment impulses (N*m*s/kg) of the residual, intact and control knees during stance across steady-state walking speeds. Significant pairwise differences (α=0.05) between intact and control knees and intact and residual knees are indicated by the shaded regions.

		0.6 m/s	0.9 m/s	1.2 m/s	1.5 m/s
Extension (N*m*s/kg)	Residual	0.099 (0.068)	0.081 (0.054)	0.089 (0.053)	0.086 (0.042)
	Intact	0.058 (0.054)	0.067 (0.045)	0.085 (0.064)	0.100 (0.066)
	Control	0.040 (0.020)	0.060 (0.023)	0.091 (0.035)	0.111 (0.035)
Flexion (N*m*s/kg)	Residual	**-0.051 (0.043)**	-0.068 (0.052)	**-0.041 (0.030)**	**-0.042 (0.029)**
	Intact	**-0.141 (0.126)**	-0.076 (0.047)	**-0.093 (0.060)**	**-0.090 (0.055)**
	Control	-0.130 (0.086)	-0.089 (0.055)	-0.065 (0.039)	-0.063 (0.032)
Abduction (N*m*s/kg)	Residual	-0.186 (0.118)	-0.149 (0.096)	-0.126 (0.081)	-0.110 (0.070)
	Intact	**-0.186 (0.105)**	**-0.114 (0.083)**	-0.114 (0.069)	-0.103 (0.073)
	Control	**-0.307 (0.073)**	**-0.190 (0.073)**	-0.157 (0.075)	-0.135 (0.067
Internal Rot. (N*m*s/kg)	Residual	0.025 (0.017)	0.019 (0.015)	0.017 (0.010)	0.019 (0.014)
	Intact	0.026 (0.017)	0.026 (0.016)	0.027 (0.019)	0.030 (0.020)
	Control	0.012 (0.008)	0.015 (0.008)	0.020 (0.010)	0.025 (0.009)
External Rot. (N*m*s/kg)	Residual	**-0.020 (0.013)**	**-0.019 (0.015)**	**-0.012 (0.008)**	**-0.014 (0.009)**
	Intact	**-0.044 (0.034)**	**-0.026 (0.015)**	**-0.029 (0.020)**	**-0.029 (0.016)**
	Control	-0.067 (0.042)	-0.039 (0.024)	-0.033 (0.017)	-0.030 (0.014)

Joint Moments – Intact to Residual Comparison

The hypothesis that the intact knee moment impulses would be greater than in the residual knee was supported by the knee flexion moment impulse (leg, p=0.001; leg*speed, p=0.033) at 0.6, 1.2 and 1.5 m/s ($p \leq 0.009$) (Figs. 1.2 and 1.3, Table 1.1). This hypothesis was also supported by the knee external rotation moment impulse (leg, p=0.001; leg*speed, p=0.025), which was larger in the intact knee compared to the residual knee at all speeds ($p \leq 0.041$). In addition, the knee extension moment impulse had a significant leg*speed interaction effect (p=0.015) with a significantly different linear relationship as speed increased between the intact and residual legs (p=0.003, Fig. 1.3). The residual knee extension moment impulse did not significantly change with

speed, while the intact knee extension moment impulse increased as speed increased (0.6 to 1.5 m/s, p=0.043; 0.9 to 1.5 m/s, p=0.019). However, there were no significant pairwise differences between intact and residual knee extension moment impulse. In addition, the internal rotation moment impulse had a significantly different linear relationship as speed increased between the intact and residual legs (p=0.025).

Intersegmental Forces – Intact to Control Comparison

The hypothesis that the intact knee force impulses would be greater than in the control subjects was not supported, as there were no significant differences found between intact and control knees at any speed (Fig. 1.4, Table 1.2).

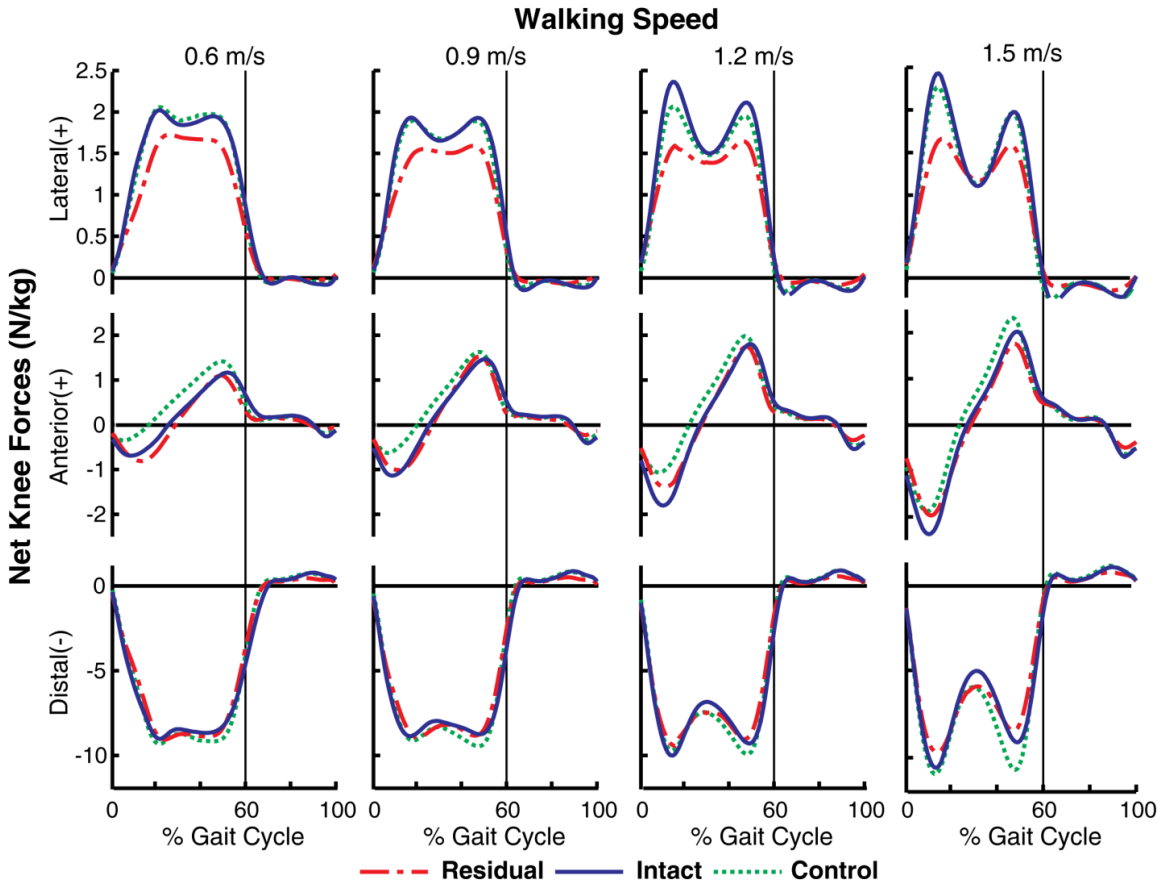

Figure 1.4: Group average net internal joint forces (N/kg) of the residual, intact and control knees across steady-state walking speeds.

Table 1.2: Group average, mean (standard deviation), net internal joint force impulses (N*s/kg) of the residual, intact and control knees during stance across steady-state walking speeds. There were no significant differences between legs at any speed.

		0.6 m/s	0.9 m/s	1.2 m/s	1.5 m/s
Lateral (N*s/kg)	Residual	1.26 (0.44)	1.01 (0.34)	0.88 (0.31)	0.77 (0.28)
	Intact	1.50 (0.35)	1.19 (0.27)	1.09 (0.25)	0.95 (0.20)
	Control	1.54 (0.49)	1.19 (0.37)	1.02 (0.34)	0.86 (0.28)
Anterior (N*s/kg)	Residual	0.40 (0.31)	0.41 (0.31)	0.36 (0.24)	0.38 (0.21)
	Intact	0.51 (0.42)	0.47 (0.30)	0.44 (0.24)	0.45 (0.16)
	Control	0.69 (0.46)	0.58 (0.36)	0.54 (0.28)	0.50 (0.21)
Posterior (N*s/kg)	Residual	-0.36 (0.27)	-0.33 (0.21)	-0.35 (0.18)	-0.40 (0.18)
	Intact	-0.27 (0.24)	-0.30 (0.23)	-0.39 (0.23)	-0.46 (0.22)
	Control	-0.14 (0.17)	-0.17 (0.16)	-0.23 (0.14)	-0.32 (0.15)
Distal (N*s/kg)	Residual	-6.81 (0.83)	-5.82 (0.63)	-4.98 (0.44)	-4.41 (0.30)
	Intact	-7.07 (0.85)	-5.92 (0.49)	-5.12 (0.43)	-4.56 (0.42)
	Control	-7.30 (0.82)	-6.17 (0.64)	-5.33 (0.56)	-4.71 (0.54)

Intersegmental Forces – Intact to Residual Comparison

The hypothesis that the intact knee joint force impulses would be greater than in the residual knee was not supported in any of the force impulses. Differences in lateral force impulses approached significance (leg, $p=0.062$) between intact and residual knees (Fig. 1.4, Table 1.2). Posterior force impulse had a significant leg*speed interaction effect ($p<0.001$) and significantly different linear relationships as speed increased between intact and residual legs ($p=0.002$, Fig. 1.4, Table 1.2), but there were no differences between intact and residual legs at any speed. A significant speed effect ($p=0.001$) was found in the posterior force impulse. However, as walking speed increased, the posterior force impulse did not significantly change in the residual knee and significantly increased with walking speed in the intact knee (0.6 to 1.2 m/s,

$p<0.001$; 0.6 to 1.5 m/s, $p<0.001$; 0.9 to 1.2 m/s, $p<0.001$; 0.9 to 1.5 m/s, $p<0.001$; 1.2 to 1.5 m/s, $p=0.021$).

DISCUSSION

We expected the amputee intact knee loading would be greater than in the non-amputee subjects. In contrast, intact knee abduction moment impulse was actually smaller compared to control subjects at 0.6 and 0.9 m/s (Figs. 1.2 and 1.3, Table 1.1) and no differences were found in the intersegmental forces of the amputee and non-amputee knees. Previously, an increased internal knee abduction (external knee adduction) moment magnitude was associated with osteoarthritis disease progression (Miyazaki et al., 2002) and severity (Mundermann et al., 2004) in non-amputees. However, the non-amputee subjects were either already experiencing osteoarthritis and/or were substantially older (Miyazaki et al., 2002; Mundermann et al., 2004; Sharma et al., 1998). Thus, it is not clear whether the increased knee abduction moment of osteoarthritic non-amputees contributes to disease onset or is an adaptation resulting from disease onset and progression. An increased intact knee abduction moment peak magnitude at SSWS was previously shown in amputee subjects (Royer and Koenig, 2005; Royer and Wasilewski, 2006) that were free of joint pain and of similar age, 41 (10) years mean (standard deviation), to our amputee subjects, 45 (9) years. However, the post-amputation times for their subjects were substantially larger compared to our amputee subjects (17 (11) years compared to 6 (3) years). These previous studies along with our current knee abduction moment results suggest prolonged prosthetic usage and/or aging may lead to frontal plane knee loading asymmetries over time.

In the sagittal plane, the larger intact knee flexor moment impulse compared to the residual knee at 0.6, 1.2 and 1.5 m/s supported our third hypothesis (Figs. 1.2 and 1.3,

Table 1.1). Previously, these same subjects showed increased residual leg quadriceps activity across walking speeds (Fey et al., 2010), which would act to reduce residual knee flexion moment and may provide additional body support in the absence of the ankle plantar flexors (e.g., Neptune et al., 2004). Increased residual leg hamstring activity was also shown in these subjects across all speeds (Fey et al., 2010), which would act to increase hip extension and knee flexion moments. Based on these results, increased residual leg hamstring activity may increase hip extensor moments (e.g., Gitter et al., 1991; Silverman et al., 2008) and have a smaller effect at the knee. Further work is needed to examine if the increased intact knee flexor moment impulse is unfavorable to intact knee health.

Significantly different linear relationships as walking speed increased were found in the residual knee extension, abduction and internal rotation moment impulses and posterior force impulse compared to the intact knee. In addition, residual knee extension moment impulse (Figs. 1.2 and 1.3, Table 1.1) and posterior force impulse (Fig. 1.4, Table 1.2) did not significantly change as walking speed increased, while they did increase in the intact and control knees. It is unclear whether these different relationships with walking speed result in less favorable loading conditions in the intact knee as amputees modulate speed. Future studies analyzing amputees during accelerated/decelerated walking or typical maneuvering tasks such as standing and hopping on their intact leg may provide insight since ~40% of day to day walking in adults located in urban environments are short duration bouts of less than twelve steps (Orendurff et al., 2008). This is especially important for below-knee amputees since they are commonly classified as limited community ambulators, which are characterized by a reduced walking range (Johnson et al., 1995). Thus, amputees may experience increased

intact leg loading demands during these types of non-steady-state activities or perform these activities with greater regularity that may be detrimental to knee joint health.

No differences in intersegmental joint force impulses were found between legs. A important limitation of analyzing intersegmental joint forces is that they underestimate net joint contact forces by not accounting for co-contraction of antagonistic muscles or compressive forces due to ligaments (e.g., Zajac et al., 2002). Therefore, differences in knee contact forces may exist. However, intersegmental forces do quantify the contributions of GRFs and body segment inertial forces to the net knee contact force, and therefore provide useful insight into knee loading. Since studies have identified increases in intact leg GRFs compared to the residual leg (e.g., Nolan et al., 2003; Silverman et al., 2008), it was reasonable to expect larger knee intersegmental forces would develop. Previous studies examining intersegmental joint forces of amputees between intact and control legs have produced conflicting results and found either a smaller intact knee intersegmental horizontal force and no difference in vertical forces when testing younger amputees (36 (7) years) (Hurley et al., 1990), or found no significant difference in peak vertical and horizontal forces of the intact knee and a significantly greater vertical force impulse when testing elderly amputees years; (72 (4) years) (Lemaire and Fisher, 1994). These previous studies and our intersegmental force results again suggest that longer prosthetic use and/or aging may play a role in developing higher intact knee loading over time.

An interesting finding was that as walking speed increased, we observed the highest degree of symmetry between residual and intact knee moments and forces at 0.9 m/s (Fig. 1.2, Table 1.1). This finding is consistent with previous work (Nolan et al., 2003) who tested amputees walking at 0.5, 0.9 and 1.2 m/s and found the highest degree of vertical ground reaction force symmetry occurred at 0.9 m/s. Other studies have shown

amputees exhibit a slower SSWS (e.g., Waters et al., 1976) and an increased metabolic cost at a given walking speed compared to non-amputees, which is minimized at their slower SSWS (e.g., Genin et al., 2008; Waters et al., 1976). Since the highest degree of loading symmetry occurs at a slower walking speed compared to the SSWS (~1.3 m/s) of non-amputees (e.g., Waters et al., 1976), unilateral amputees may prefer slower walking speeds to maintain a higher degree of bilateral knee loading symmetry in addition to reducing metabolic cost.

A potential limitation in this study is the amputees analyzed included multiple etiologies (traumatic, n=11; vascular, n=3). Also, amputees walked using their own clinically prescribed prostheses which included ESAR (n=9) and SACH (n=5) feet. To assess whether this influenced our results, the analyses were performed on two subsets of amputees (the traumatic amputees and the amputees that used ESAR feet). We found the statistical results were similar and our overall conclusions remained unchanged.

In summary, intact knee mechanical loading during steady-state walking was similar or even lower at some speeds compared to the control subjects. Thus, in terms of intersegmental joint moments and forces, it does not appear that the intact knee is at a higher risk of overloading compared to non-amputees. However, there were sagittal and transverse plane bilateral loading asymmetries in the flexion and external rotation moment impulses, which were larger in the intact knee at multiple speeds. In addition, the residual knee extension moment impulse and posterior force impulse were insensitive to walking speed increases, while these quantities increased in the intact and control knees. Future modeling studies are needed to quantify the contributions of muscles, ligaments and external loads to the knee contact forces (e.g., Winby et al., 2009) to determine if these bilateral asymmetries across speed lead to less favorable intact knee loading that contributes to joint disorders over time. In addition, factors other than mechanical loading

and walking speed such as non-steady-state task demands and frequency, bone mineral density (Royer and Koenig, 2005), joint laxity and varus alignment (Miyazaki et al., 2002; Sharma et al., 1998), joint contact geometry and localized stress distribution (Koo and Andriacchi, 2007), and specific walking patterns (Fregly et al., 2009) may also play important roles in the development of joint disorders in lower-limb amputees that warrants further research.

Aim 2: The Influence of Energy Storage and Return Foot Stiffness on Walking Mechanics and Muscle Activity in Below-Knee amputees

INTRODUCTION

The number of people living with limb loss in the U.S. is projected to dramatically increase over the next 40 years (Ziegler-Graham et al., 2008), with approximately 40% representing major lower limb amputations. Unilateral below-knee amputations often lead to temporal and ground reaction force bilateral asymmetries (Nolan et al., 2003; Sanderson and Martin, 1997; Silverman et al., 2008; Vrieling et al., 2008), altered residual leg muscle activity (e.g., Fey et al., 2010; Winter and Sienko, 1988), higher metabolic cost (Czerniecki, 1996; Genin et al., 2008; Waters et al., 1976) and reduced walking speed (Hermodsson et al., 1994; Perry et al., 1997; Powers et al., 1998; Robinson et al., 1977) relative to non-amputee walking. Many differences between amputee and non-amputee walking can be attributed to the absence of the ankle plantar flexor muscles, which provide needed body support, forward propulsion and swing initiation during non-amputee walking (Neptune et al., 2001). As a result, previous studies have identified a number of neuromotor adaptations used by amputees to provide these important biomechanical functions (e.g., Silverman et al., 2008; Winter and Sienko, 1988). To help minimize the necessary adaptations and improve amputee walking ability, proper prosthetic foot prescription and design is critical.

Some amputees use low or non-energy storage and return feet (e.g., solid ankle cushioned heel, SACH), which reduce ground contact forces during the initial loading response following heel-strike as well as provide body support. However, these prosthetic feet provide minimal energy storage and return over the stance phase (e.g., Ehara et al., 1993) due to their high stiffness and limited deflection, and therefore provide few biomechanical advantages (for review, see Hafner et al., 2002a). In an effort to improve

performance, carbon fiber energy storage and return (ESAR) feet have been developed that store and release elastic energy during stance (Hafner et al., 2002a; Hafner et al., 2002b) and provide body support, forward propulsion and leg swing initiation (Zmitrewicz et al., 2007). However, the appropriate ESAR stiffness level for a given amputee is not well-defined (Hafner et al., 2002b). Currently, clinicians base prosthetic prescription on a patient's body weight and activity level. The latter is evaluated subjectively using clinician experience as well as patient self-report and feedback, rather than objective biomechanical data. Thus, studies are needed to systematically vary foot stiffness to assess its influence on gait characteristics, which has the potential to improve amputee mobility by developing quantitative rationale for prosthetic foot prescription.

However, one challenge to such studies is the difficulty in generating ESAR feet of varying stiffness levels using traditional manufacturing techniques. One solution to overcome this difficulty is to use an additive manufacturing technology known as selective laser sintering (SLS), which has been used to fabricate ankle-foot orthoses (Faustini et al., 2008), below-knee prosthetic sockets (Faustini et al., 2005; Faustini et al., 2006a; Faustini et al., 2006b; Rogers et al., 2007) and prosthetic ankles (Ventura et al., 2011). We recently developed a SLS-based framework to fabricate ESAR feet that replicated the geometry and dynamic response of a commercially available carbon fiber ESAR foot (South et al., 2010). The purpose of this study was to use this framework to identify the influence of ESAR foot stiffness on gait characteristics by manufacturing SLS ESAR feet with a range of stiffness levels and quantify their effect on below-knee amputee walking. Specifically, we investigated the influence of ESAR foot stiffness on gait kinematics, kinetics, muscle activity and prosthetic energy stored, returned and mechanical efficiency during overground walking.

METHODS

Prosthetic foot stiffness was modified by altering keel and heel geometry (for details, see South et al., 2010) to yield three SLS feet: one that closely matched the nominal stiffness of a widely prescribed carbon fiber foot (Highlander™, FS 3000, Freedom Innovations, LLC), one that was 50% stiffer than this foot, and one that was 50% more compliant. The feet (Fig. 2.1) were mechanically tested using a uniaxial load cell (ATS, Inc.). Each foot was clamped to the base of the machine and loaded axially by a flat plate attached to the load cell in similar configurations as specified in the ISO 10328 standard for structural testing of lower-limb prostheses. The feet were tested in three different configurations: toe-only contact, heel-only contact and foot-flat (South et al., 2010). Foot mass increased as stiffness increased (compliant=355 g, nominal=426 g, stiff=449 g). To assure all feet had identical mass, small amounts of lead were placed near the center-of-mass of the compliant and nominal feet. These feet were then used in the overground walking trials.

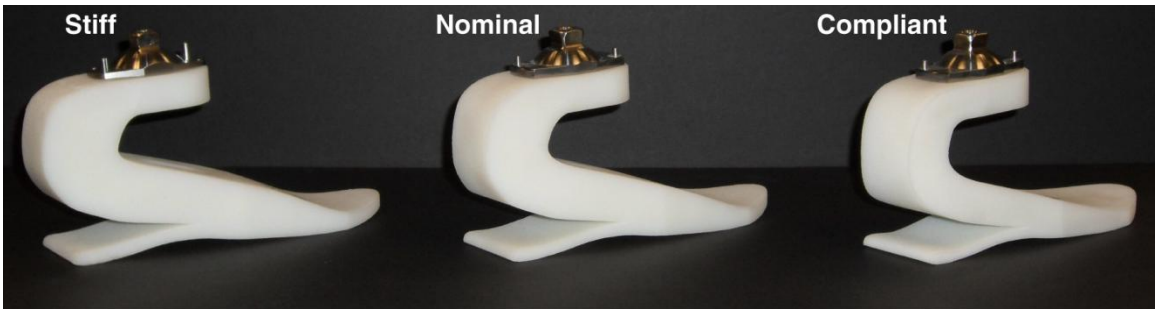

Figure 2.1: ESAR prosthetic feet fabricated using SLS additive manufacturing technology that approximately matched the nominal carbon fiber stiffness (Nominal), and were 50% more stiff (Stiff) and 50% more compliant (Compliant). All feet were manufactured from Rilsan™ D80 (Nylon 11 powder, Arkema) using a Vanguard HiQ Sinterstation (3D Systems, Inc.).

Subjects

Twelve unilateral below-knee amputees participated in the study (Table 2.1). All subjects were asymptomatic of musculoskeletal disorders and pain and were proficient walkers who did not use assistive devices.

Table 2.1: Below-knee amputee subject characteristics.

	Mean	Std. Dev.	Max	Min	#Subjects
Age (years)	51.9	17.1	72	25	-
Height (m)	1.78	0.06	1.91	1.66	-
Body mass (kg)	83.0	15.8	120.7	65.3	-
Post-amputation time (years)	13.9	14.4	42	0.8	-
Gender					
Male	-	-	-	-	12
Female	-	-	-	-	0
Cause of Amputation					
Traumatic injury	-	-	-	-	10
Secondary illness	-	-	-	-	2
Prescribed Prostheses					
Energy storage and return (ESAR)	-	-	-	-	12
Non-ESAR	-	-	-	-	0

Protocol

The experimental protocol was a crossover design in which amputees walked with the three different prosthetic feet in a randomized order. Prior to use, a certified and licensed prosthetist with 15 years clinical experience ensured proper fit and alignment. Subjects were allowed as much time as needed until they felt comfortable with each foot, which did not exceed five minutes for any subject. Subjects provided informed consent to an Institutional Review Board approved protocol prior to participation. Subjects walked overground along a 10-meter walkway consisting of four embedded force plates

(Advanced Mechanical Technology, Inc. and Bertec Corporation) at 1.2 +/- 0.06 m/s, which was verified using infrared timing gates. Repeated trials were collected at each condition until at least five force plate contacts per leg were measured.

Ground reaction force (GRF) and kinematic marker data were measured at 1200 Hz and 120 Hz, respectively, using a motion capture system (Vicon Nexus, Oxford Metrics, Inc.). Reflective markers were placed on the C-7 vertebrae and bilaterally on the acromion, iliac crest, posterior superior iliac spine, anterior superior iliac spine, greater trochanter, lateral and medial femoral condyles, lateral and medial malleoli, heel, dorsal foot, and the first, second and fifth metatarsal heads. Marker clusters (each consisting of four markers) were also placed bilaterally on the shank and thigh. Markers on the residual leg were placed symmetrically to the intact leg.

Electromyographic (EMG) data were collected at 2160 Hz using surface EMG electrodes (2, 10-mm disposable self-adhesive Ag/AgCl sensor contacts, 16-mm interelectrode distance; TeleMyo 900, Noraxon U.S.A., Inc.) from eight intact leg muscles including the tibialis anterior (TA), medial gastrocnemius (GAS), soleus (SOL), vastus medialis (VAS), rectus femoris (RF), biceps femoris long head (BF), gluteus medius (GMED) and gluteus maximus (GMAX), and from five residual leg muscles including VAS, RF, BF, GMED and GMAX. A ground electrode was placed on the sacrum. Common mode rejection and amplification characteristics included: effective 130 dB at DC (0 Hz), >100 dB at 50/60 Hz, and minimum 85 dB through 10-500 Hz operating range; <1.2 μV root-mean-square (RMS) noise level, 2000 fixed overall gain and >10 MΩ input impedance. Electrodes were placed on the muscle belly along the line of action between the origin and insertion points based on guidelines provided by Perotto and Delagi (1994). Each location was shaved and cleaned with alcohol prior to electrode placement.

Kinematics and Kinetics

An inverse dynamics analysis was performed to calculate net intersegmental joint moments using Visual3D (C-Motion, Inc.). Kinematic data were low-pass filtered using a 4^{th}-order Butterworth filter with a cut-off frequency of 6 Hz, while the GRF data were low-pass filtered with a cut-off frequency of 20 Hz. Inertial properties of the residual leg were adjusted in the inverse dynamics model based on previous work (Mattes et al., 2000). GRFs and joint moments were normalized by body weight and body mass, respectively. For the residual and intact legs, sagittal plane GRFs and joint angles and ankle, knee and hip moments were averaged across trials for each condition.

Electromyography

Raw EMG signals were filtered and processed in MATLAB (MathWorks, Inc.). Data were demeaned and then smoothed using a moving, symmetric 80-ms root-mean-square (RMS) window. Timing of the gait cycle events of each leg were exported using Visual3D. The smoothed EMG data were extracted in MATLAB based on the nearest time point for each event. The data from each gait cycle were then time-normalized to represent 100% of the gait cycle. The data for each gait cycle were then integrated within specific regions of the gait cycle (Perry, 1992) that corresponded to the loading response and mid-stance (0-30% gait cycle), terminal stance and pre-swing (30-60% gait cycle), swing (60-100% gait cycle) in addition to over the entire gait cycle (0-100% gait cycle). These integrated EMG (iEMG) quantities were averaged at each condition and then normalized for each subject by the 0-100% gait cycle iEMG magnitude from the nominal stiffness condition.

Prosthetic Energy Storage and Return and Mechanical Efficiency

Residual leg ankle power was computed as the product of the residual leg ankle moment and angular velocity. Prosthetic foot energy storage and return characteristics were estimated by evaluating the time integrals of the residual leg ankle power. For each condition, the integrals of the residual leg negative ankle power (energy stored) and positive ankle power (energy returned) (J/kg) were computed during stance for each gait cycle and averaged across trials for each subject. Mechanical efficiency was calculated as the ratio of energy returned divided by the energy stored during stance.

Statistical Analyses

All statistical analyses were performed using SPSS 16.0 GP (SPSS, Inc.). Differences in peak GRFs, sagittal-plane joint angles and moments, iEMG magnitudes, and prosthetic energy quantities were analyzed. Braking, propulsion and the first (V1) and second (V2) vertical peak GRFs were analyzed. Sagittal-plane joint angles including ankle plantarflexion, dorsiflexion, knee flexion and hip extension peaks were also compared. Joint moment comparisons included dorsiflexion, plantarflexion, knee extension in early (K1) and late (K3) stance, knee flexion (K2), hip extension (H1) and hip flexion (H2) peaks. The iEMG quantities over each phase of the gait cycle (0-30% gait cycle, 30-60% gait cycle, and swing) were also compared for each muscle. Finally, the prosthetic energy stored, returned and mechanical efficiency quantities were compared across stiffness levels. Differences in GRF, joint angle and moment, and bilateral iEMG quantities were compared using two-factor (prosthetic foot, leg) ANOVAs. Differences in unilateral iEMG and prosthetic energy quantities were

compared using one-factor (prosthetic foot) ANOVAs. The prosthetic foot factor consisted of three levels (nominal, compliant and stiff) and the leg factor consisted of two levels (residual and intact). If an ANOVA had a significant main or interaction effect, pairwise comparisons were evaluated using a Bonferroni adjustment for multiple comparisons, which reduced the statistical significance level from $\alpha=0.05$. For presentation of these pairwise results, SPSS adjusted individual p-values were used for comparison to $\alpha=0.05$. Leg main effects and pairwise differences between legs (i.e., residual leg compared to the intact leg) were not reported.

RESULTS

Ground Reaction Forces

Altering prosthetic foot stiffness influenced the resulting peak GRF quantities in both residual and intact legs (Fig. 2.2, Table 2.2). Peak braking GRFs were larger in the compliant condition compared to the nominal and stiff conditions (prosthetic effect, $p<0.001$; compliant to nominal, $p\leq0.033$; compliant to stiff, $p\leq0.036$), while intact leg V1 GRF was larger in the stiff condition compared to the nominal condition (leg*prosthetic effect, $p=0.016$; stiff to nominal, $p=0.002$). In contrast, residual leg V2 GRF was reduced in the compliant condition relative to both the stiff and nominal conditions (Fig. 2.2, Table 2.2; prosthetic effect, $p<0.001$; leg*prosthetic effect, $p<0.001$; compliant to nominal, $p<0.001$; compliant to stiff, $p=0.001$).

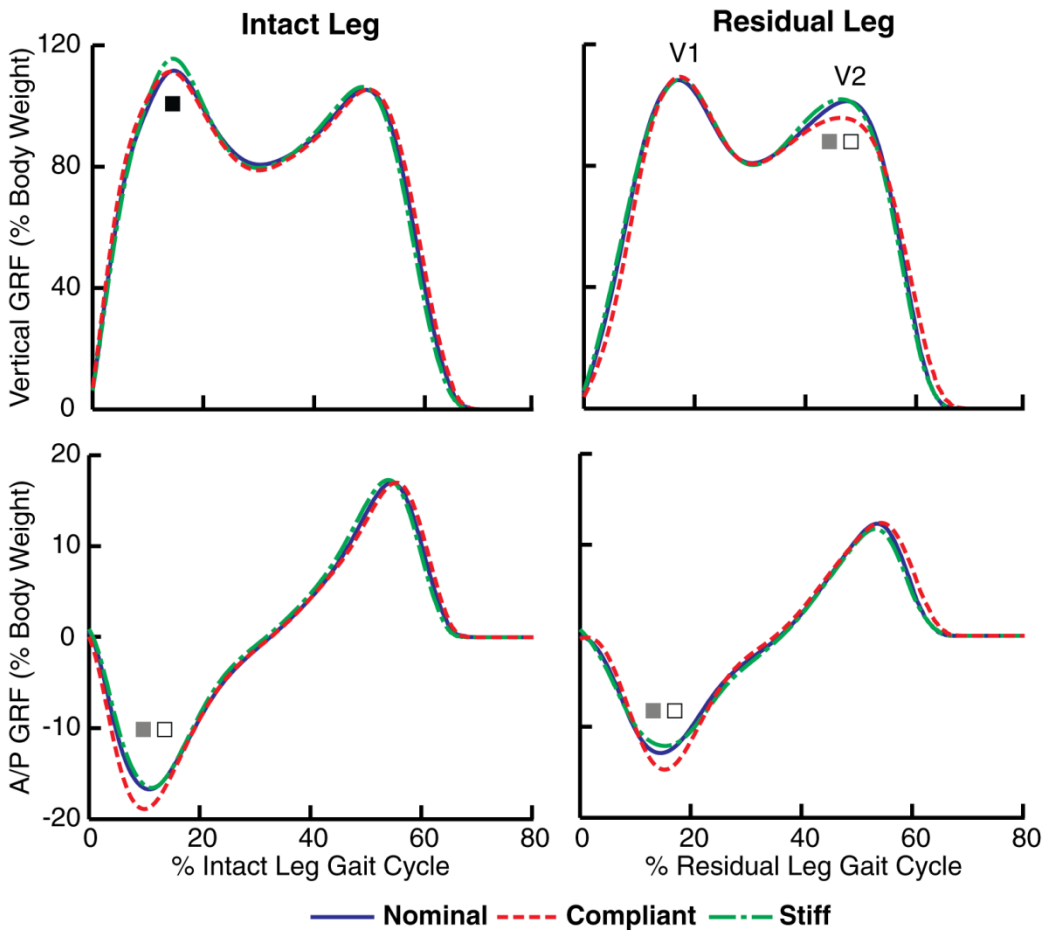

Figure 2.2: Group average ground reaction force (GRF) data. GRF data of the residual and intact legs were normalized in time to their respective gait cycles. Indicated on the figure are vertical V1 and V2 GRFs. Significant differences associated with each peak quantity between nominal and compliant (■), compliant and stiff (□), and nominal and stiff (■) conditions are also indicated.

Table 2.2: Mean (standard deviation) GRFs, joint angles, and joint moments of the residual and intact leg for each prosthetic foot condition.

▲ denotes a significant prosthetic main effect
○ denotes a significant leg*prosthetic interaction effect
■ denotes a significant nominal to compliant pairwise comparison
□ denotes a significant compliant to stiff pairwise comparison
■ denotes a significant nominal to stiff pairwise comparison

		Compliant	Nominal	Stiff
GRFs (% Body Weight)				
V1 ○	Residual	112.0 (3.6)	110.3 (4.8)	109.7 (5.8)
	Intact ■	113.0 (5.6)	**113.1 (8.2)**	**117.4 (8.3)**
V2 ▲○	Residual ■□	**96.5 (4.3)**	**102.1 (5.0)**	**103.4 (4.6)**
	Intact	106.2 (5.3)	105.9 (5.8)	107.0 (5.1)
Braking ▲	Residual ■□	**-15.8 (3.1)**	**-13.9 (3.2)**	**-13.4 (2.5)**
	Intact ■□	**-19.3 (3.1)**	**-17.3 (2.6)**	**-17.3 (2.5)**
Propulsion	Residual	12.6 (1.8)	12.7 (1.6)	12.4 (1.8)
	Intact	17.2 (2.2)	17.0 (2.2)	17.4 (2.0)
Joint Angles (°)				
Plantarflexion ▲○	Residual ■□	**-14.4 (3.5)**	**-12.2 (3.0)**	**-11.6 (3.0)**
	Intact	-12.4 (2.9)	-12.3 (2.1)	-12.3 (2.4)
Dorsiflexion ▲○	Residual ■□■	**13.1 (2.9)**	**8.6 (2.5)**	**5.7 (2.4)**
	Intact □	**11.0 (2.4)**	10.2 (2.3)	**9.2 (3.0)**
Knee flexion ▲	Residual □	**-58.8 (6.2)**	-57.2 (6.4)	**-56.7 (5.8)**
	Intact	-60.4 (5.4)	-60.3 (5.9)	-59.5 (6.2)
Hip extension	Residual	-13.2 (4.3)	-13.5 (4.0)	-13.1 (3.4)
	Intact	-11.0 (3.8)	-10.8 (3.8)	-10.3 (3.4)
Joint Moments (Nm/kg)				
Dorsiflexion ▲○	Residual ■	0.35 (0.14)	**0.36 (0.12)**	**0.42 (0.10)**
	Intact	0.29 (0.12)	0.27 (0.11)	0.27 (0.12)
Plantarflexion ▲○	Residual ■□	**-0.85 (0.15)**	**-1.05 (0.17)**	**-1.04 (0.13)**
	Intact	-1.33 (0.13)	-1.32 (0.13)	-1.34 (0.13)
K1 ▲○	Residual □■	**0.24 (0.25)**	**0.27 (0.24)**	**0.33 (0.24)**
	Intact ■	**0.56 (0.19)**	**0.44 (0.17)**	0.48 (0.17)
K2 ▲○	Residual ■□■	**0.05 (0.15)**	**-0.10 (0.15)**	**-0.14 (0.16)**
	Intact □	**-0.16 (0.17)**	-0.20 (0.15)	**-0.21 (0.14)**
K3 ▲○	Residual ■□	**0.34 (0.12)**	**0.28 (0.10)**	**0.27 (0.11)**
	Intact	0.30 (0.11)	0.28 (0.09)	0.29 (0.09)
H1 ▲	Residual	-0.68 (0.21)	-0.67 (0.18)	-0.65 (0.18)
	Intact □	**-0.60 (0.20)**	-0.58 (0.19)	**-0.54 (0.19)**
H2	Residual	0.78 (0.22)	0.83 (0.24)	0.82 (0.25)
	Intact	0.92 (0.15)	0.94 (0.14)	0.95 (0.15)

Joint Kinematics and Kinetics

The most notable change in joint kinematics was residual leg dorsiflexion angle (Table 2.2), which systematically increased as stiffness decreased. Relative to nominal, residual leg dorsiflexion angle increased and decreased by 52% and 34% in the compliant and stiff conditions, respectively (prosthetic effect, $p<0.001$; leg*prosthetic effect, $p<0.001$; compliant to nominal, $p<0.001$; nominal to stiff, $p<0.001$; compliant to stiff, $p<0.001$).

Intact leg dorsiflexion angle was larger in the compliant condition relative to the stiff condition (Table 2.2; prosthetic effect, $p<0.001$; leg*prosthetic effect, $p<0.001$; compliant to stiff, $p=0.006$). Residual leg plantarflexion angle in the compliant condition was also larger compared to the nominal and stiff conditions (Table 2.2; prosthetic effect, $p=0.004$; compliant to nominal, $p=0.002$; compliant to stiff, $p=0.001$). During swing, residual knee flexion angle was larger in the compliant condition compared to the stiff condition (Table 2.2; prosthetic effect, $p=0.006$; compliant to stiff, $p=0.023$).

Residual leg ankle plantarflexion moment and knee moments in the residual (K2, K3) and intact (K1) legs showed the largest differences across stiffnesses (Fig. 2.3, Table 2.2). Residual leg plantarflexion moment in the compliant condition was reduced by 19% compared to the nominal and stiff conditions (Fig. 2.3, Table 2.2; prosthetic effect, $p<0.001$; leg*prosthetic effect, $p<0.001$; compliant to nominal, $p<0.001$; compliant to stiff, $p<0.001$). Compared to the nominal condition, residual leg K2 moment increased (became more flexor) in the stiff condition and decreased (became extensor) in the compliant condition, which represented 43% and 147% net changes, respectively (Fig. 2.3, Table 2.2; prosthetic effect, $p<0.001$; leg*prosthetic effect, $p<0.001$; compliant to nominal, $p<0.001$; nominal to stiff, $p=0.014$; compliant to stiff, $p<0.001$). In addition, residual leg K3 moment was 25% larger in the compliant condition compared to nominal

and stiff conditions (prosthetic effect, $p<0.001$; leg*prosthetic effect; $p<0.001$; compliant to nominal, $p=0.002$; compliant to stiff, $p<0.001$). The increased residual leg K3 extensor moment in the compliant condition corresponded with a 29% larger intact leg K1 moment in the compliant condition compared to nominal (Fig. 2.3, Table 2.2; prosthetic effect, $p=0.008$; leg*prosthetic effect, $p<0.001$; compliant to nominal, $p=0.001$).

Intact leg K2 moment was reduced (prosthetic effect, $p<0.001$; leg*prosthetic effect, $p<0.001$; compliant to stiff, $p=0.048$) and H1 moment was larger (prosthetic effect, $p=0.035$; compliant to stiff, $p=0.010$) in the compliant condition compared to stiff (Fig. 2.3, Table 2.2). Finally, residual leg K1 moment was larger in the stiff condition compared to nominal and compliant conditions (Fig. 2.3, Table 2.2; prosthetic effect, $p=0.008$; leg*prosthetic effect, $p<0.001$; stiff to nominal, $p=0.011$; stiff to compliant, $p=0.012$) and residual leg dorsiflexion moment was larger in the stiff condition compared to nominal (prosthetic effect, $p=0.035$; leg*prosthetic, $p=0.006$; stiff compared to nominal, $p=0.016$).

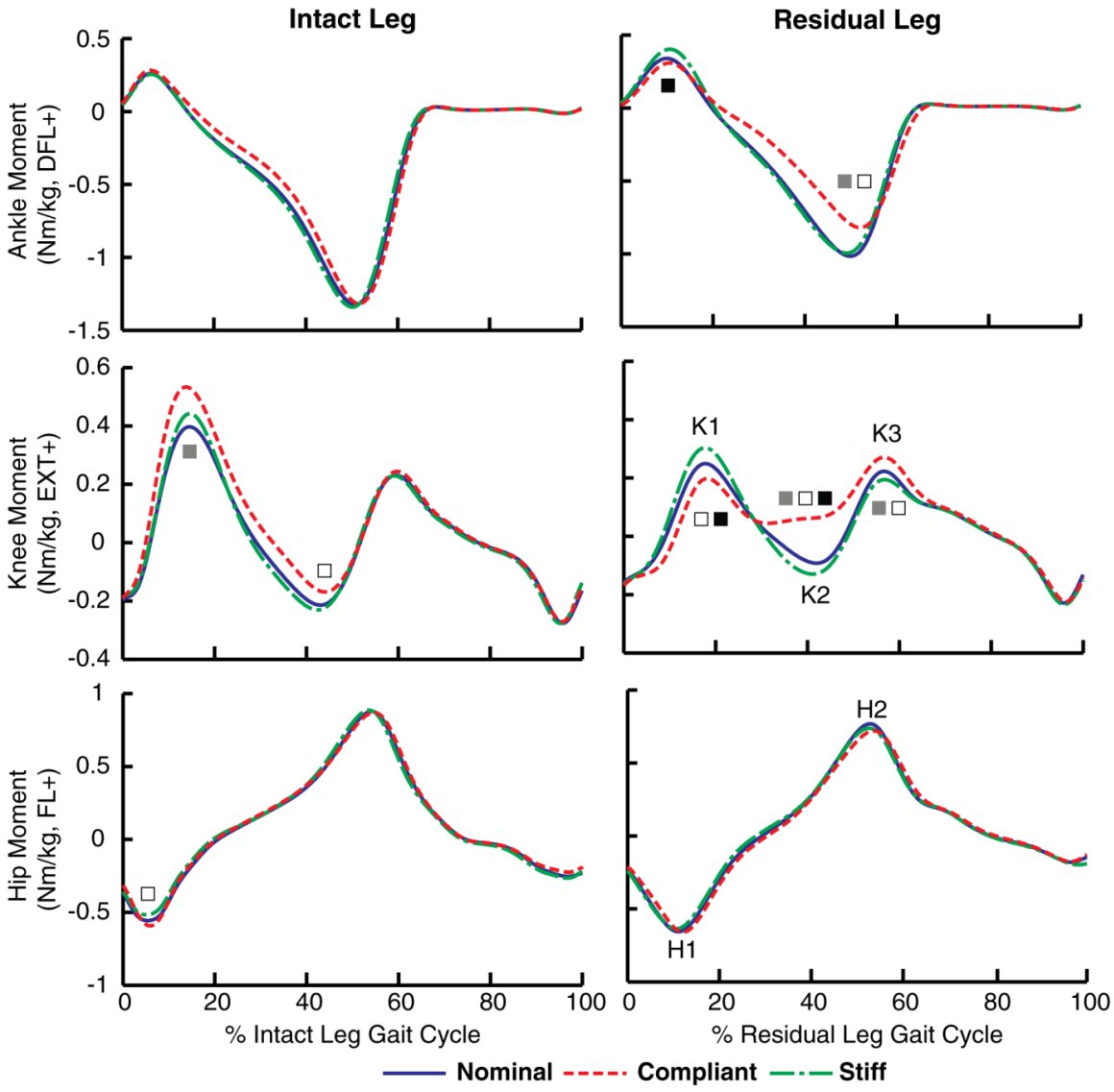

Figure 2.3: Group average joint moment data of the residual and intact legs. Data for each leg (residual and intact) were normalized in time to their respective gait cycles. Indicated in the figure are knee K1, K2, and K3 moments and hip H1 and H2 moments. Significant differences associated with each peak quantity between nominal and compliant (■), compliant and stiff (□), and nominal and stiff (■) conditions are also indicated.

Electromyography

No differences in muscle activity were found during the swing phase across all conditions (Fig. 2.4). However, differences in iEMG magnitudes were observed during stance in both residual and intact leg muscles, which generally increased activity as stiffness decreased.

From 0-30% of the gait cycle, the most apparent changes in muscle activity were observed in the residual leg GMED (prosthetic effect, $p=0.013$; leg*prosthetic effect, $p=0.006$; compliant to stiff, $p=0.003$) and intact leg VAS (prosthetic effect, $p=0.001$; compliant to nominal, $p=0.015$) and RF (prosthetic effect, $p=0.048$; compliant to nominal, $p=0.026$), which all increased in activity in the compliant condition as stiffness decreased (Fig. 2.4). Other differences were seen in GAS (prosthetic effect, $p=0.002$; compliant to nominal, $p=0.005$, compliant to stiff, $p=0.030$) and TA (prosthetic effect, $p=0.012$; compliant to nominal, $p=0.015$), which had lower and higher muscle activities in the compliant condition, respectively (Fig. 2.4).

From 30-60% of the gait cycle, changes in muscle activity were observed in the residual leg GMED (prosthetic effect, $p<0.001$; leg*prosthetic effect, $p=0.031$; compliant to nominal, $p=0.037$; compliant to stiff, $p=0.007$) and VAS (prosthetic effect, $p=0.028$; compliant to nominal, $p=0.030$), which increased activity as stiffness decreased (Fig. 2.4). BF excitation also decreased as stiffness decreased (leg*prosthetic effect, $p<0.001$; compliant to stiff, $p=0.016$). Also, from 30-60% of the gait cycle, GMAX activity had a prosthetic main effect ($p=0.006$) and appeared to increase as stiffness decreased. Pairwise differences of residual leg GMAX activity during this region approached significance (compliant to nominal, $p=0.070$). In addition, increased residual leg RF activity approached significance as stiffness decreased (Fig. 2.4; prosthetic effect, $p=0.054$), although it was highly variable across subjects.

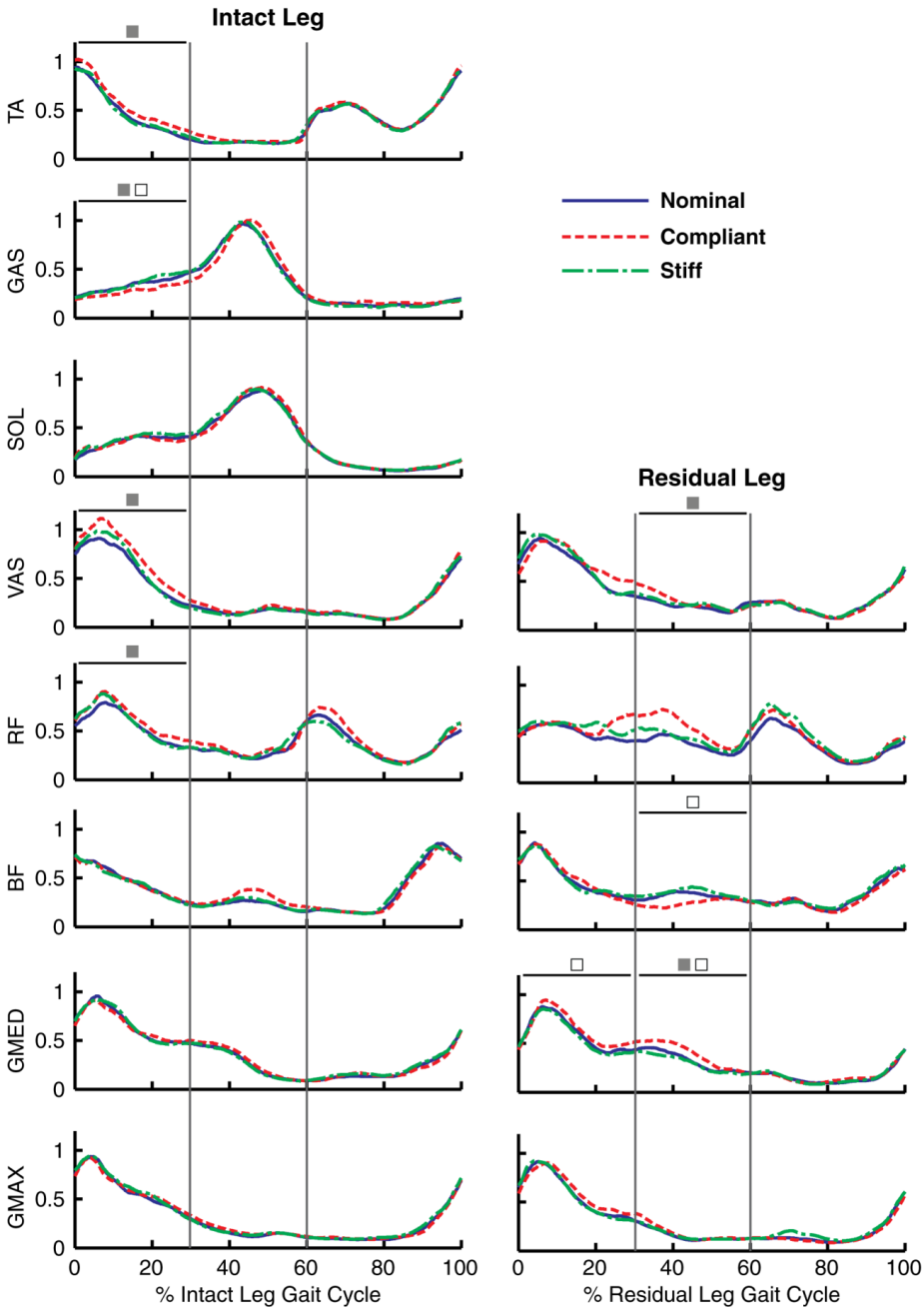

Figure 2.4: Group average smoothed EMG data of the intact and residual legs. Regions of the gait cycle representing loading response and mid-stance (0-30% gait cycle), terminal stance and pre-swing (30-60% gait cycle), and swing (60-100% gait cycle) are shown by vertical lines. In each region, significant differences associated with integrated EMG magnitude between nominal and compliant (■), compliant and stiff (□), and nominal and stiff (■) conditions are indicated.

Prosthetic Energy Storage and Return and Mechanical Efficiency

Energy stored, returned and efficiency values followed consistent trends as stiffness was altered (Fig. 2.5). Energy stored showed a significant prosthetic effect ($p<0.001$), with energy values increasing as stiffness decreased (nominal compared to stiff, $p<0.001$; compliant to stiff, $p<0.001$). Energy returned also increased as stiffness decreased (prosthetic effect, $p=0.003$; nominal to stiff, $p=0.001$; compliant to stiff, $p=0.014$). Energy stored values were all larger than their respective energy returned values such that efficiency ranged between 49-59%. In contrast to energy stored and returned, mechanical efficiency decreased as stiffness decreased (Fig. 2.5).

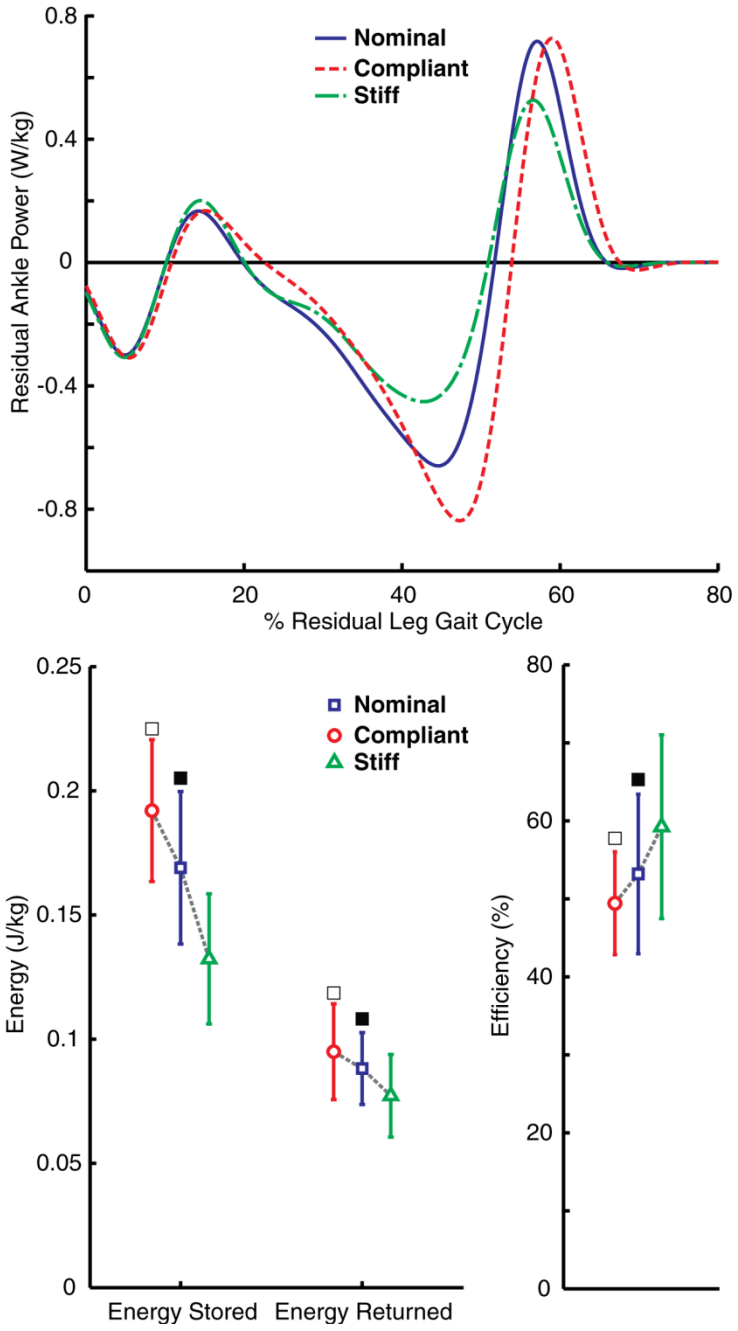

Figure 2.5: Group average residual leg ankle power curves and group average (+/- standard deviation) prosthetic energy stored, energy returned and efficiency quantities. Significant differences associated with each quantity between nominal and compliant (■), compliant and stiff (□), and nominal and stiff (■) conditions are indicated.

DISCUSSION

As a result of the changes in foot stiffness, significant differences in gait mechanics and muscle activity were observed in both the residual and intact legs, which primarily occurred in the muscle contributions to body support and forward propulsion. In terms of body support as stiffness decreased, the residual leg plantarflexion moment and V2 GRF were reduced (Figs. 2.2 and 2.3), and changes in joint kinematics were most apparent during single-leg support and terminal double-leg support of the residual leg stance and consistent with a more flexed body posture (Table 2.2). At the knee, the residual leg K2 and K3 moments became more extensor (Fig. 2.3, Table 2.2), which corresponded with increased VAS and reduced BF activity during the second half of stance (Fig. 2.4). At the hip, residual leg GMED activity increased throughout stance (Fig. 2.4). The changes in residual leg GMED and VAS were consistent with their functional roles to provide body support (Anderson and Pandy, 2003; Liu et al., 2006; McGowan et al., 2009; Neptune et al., 2004). Thus, as less support was provided by the prosthetic feet as stiffness decreased, these muscles appeared to compensate by increasing their activity to provide additional body support. Previously, increased residual VAS activity during the first half of stance had been identified in below-knee amputee walking using clinically prescribed prostheses (e.g., Fey et al., 2010; Powers et al., 1998). The present results suggest that decreased stiffness prolongs this compensatory mechanism into the second half of residual leg stance.

The changes in joint moments and muscle activity to provide additional support as stiffness decreased were not limited to the residual leg. During late stance of the residual leg (early stance of the intact leg), intact leg K1 extensor moment increased (Fig. 2.3, Table 2.2), consistent with its role to provide support during this region in non-amputee

walking (Kepple et al., 1997). The increase in intact leg knee extensor moment appears to be a result of knee extensor muscles (VAS and RF) increasing their activity (Fig. 2.4), which is consistent with their roles to provide support in non-amputee walking (Anderson and Pandy, 2003; Liu et al., 2006; McGowan et al., 2009; Neptune et al., 2004). In addition, during early stance of the intact leg, the increased intact leg hip extensor moment is consistent with the role of hip extensor muscles (Anderson and Pandy, 2003; Kepple et al., 1997; Liu et al., 2006; Neptune et al., 2004) to provide body support in non-amputee walking.

Changes in the residual and intact leg VAS and intact leg RF muscles as stiffness decreased (Fig. 2.4) may have contributed to the increased braking GRFs observed in the compliant condition in both legs (Fig. 2.2, Table 2.2). VAS and RF have been shown in non-amputee walking to contribute to braking during the first half of stance (Liu et al., 2006; Neptune et al., 2004). During amputee walking using their clinically prescribed prostheses, reduced residual leg braking has been shown to increase net propulsion in the absence of the ankle muscles (Silverman et al., 2008). Therefore, an overly compliant prosthetic foot may limit the ability of amputees to make use of this mechanism due to an increased need for body support.

The energy stored in the ESAR feet is primarily returned in late stance of the residual leg (Hafner et al., 2002b). As foot stiffness decreased, the energy returned during this region increased (Fig. 2.5). In non-amputee walking, the primary roles of the ankle plantar flexor muscles during late stance is to provide forward propulsion and swing initiation by delivering energy to the trunk and leg, respectively (Neptune et al., 2001). Since the energy returned increased as stiffness decreased, the contributions of the prosthetic feet to forward propulsion and swing initiation may have increased. Since BF has been shown to contribute to propulsion throughout stance in non-amputee walking

(Neptune et al., 2004), the reduced hamstring activity in the compliant condition (Fig. 2.4) suggests that the compliant prosthetic foot may be providing more propulsion during the second half of stance. However, the increased energy returned in late stance occurred as a consequence of substantially greater energy storage (negative work) from mid to late stance and decreased mechanical efficiency (Fig. 2.5). These trends were consistent with previous studies of amputee walking and running that compared energy characteristics of high (Flex foot) and low (Seattle foot) ESAR feet to SACH prosthetic feet (Czerniecki et al., 1991; Gitter et al., 1991). These studies found that in order for the Flex and Seattle feet to return more energy in late stance compared to SACH, they also required greater than normal energy storage (negative work) in mid stance.

Like the plantar flexor muscles, the hip flexors have also been shown to be primary contributors to swing initiation in non-amputee walking during late stance (e.g., Neptune et al., 2001; Neptune et al., 2004). However, the residual hip flexion moment did not change across stiffness conditions. Therefore, the residual hip flexor contributions to swing initiation appear consistent across conditions. Despite a reduced plantarflexion moment in the compliant condition, prosthetic energy returned increased as stiffness decreased. As previously noted, the contributions of the prosthetic feet to swing initiation may have increased as stiffness decreased. However, the total contribution of the hip flexors and prosthetic foot to swing initiation appear to have been insufficient since a kinematic adaptation to increase residual knee flexion angle during swing was observed (Table 2.2). This adaptation may have been needed to achieve toe clearance since a more flexed posture was observed as stiffness decreased from mid through late stance and at toe-off of the residual leg.

ESAR efficiency decreased as stiffness decreased (Fig. 2.5). However, a higher intact leg V1 GRF was observed in the stiff condition (Fig. 2.2, Table 2.2). As stiffness

decreased, the decrease in intact leg V1 GRF and increase in residual leg dorsiflexion angle were consistent with a previous study that modified prosthetic foot rollover shape and found that residual leg dorsiflexion angle influences intact leg vertical GRF magnitude in the same manner (Hansen et al., 2006). Our results suggest an important tradeoff exists between ESAR prosthetic foot efficiency and intact leg loading.

Other studies have mechanically tested different commercially available prosthetic feet of varying designs and stiffness levels and shown that in general energy lost through loading and unloading increased as stiffness decreased (Geil, 2001). Although these feet were not clinically tested on amputees, their results were consistent with our study since we found that mechanical efficiency decreased as stiffness decreased. Studies that have clinically tested carbon fiber ESAR prosthetic feet on amputees have reported similar magnitudes of mechanical efficiency (~57%) as those calculated in this study (e.g., Barr et al., 1992). Thus, the ESAR properties of the SLS feet manufactured for this study behaved similarly.

Although the results of this study highlight the influence of prosthetic foot stiffness on gait characteristics of amputees, there are some potential limitations. First, rigid body and fixed axis of rotation assumptions were made when defining the prosthetic foot segment and residual leg ankle joint for inverse dynamics calculations. These assumptions may have influenced energy stored and returned calculations. However, our goal was to observe relative differences in these estimated quantities as stiffness was altered. We expect that if a bias exists in these energy quantities across conditions, the same relative differences would be observed. Future work should consider including a deformable ESAR prosthetic foot model to account for its deflection and a possible moving axis of rotation. Another potential limitation is the same prosthetic feet were used on subjects of varying weight, which in some cases may have been substantially different

than their prescribed prosthetic foot. However, we expect the same relative trends would be observed for similar percentage changes in foot stiffness. Lastly, only male below-knee amputee patients were tested. Altering foot stiffness may result in different changes in walking mechanics and muscle activity for other classifications of amputees such as female or above-knee amputees.

In summary, changes in foot stiffness influenced the peak joint angles of both the residual and intact leg ankles during stance and residual leg knee flexion angle during swing. These quantities generally increased as stiffness decreased. Decreasing foot stiffness also resulted in increased braking GRFs in both the residual and intact legs and a decreased V2 GRF in the residual leg. During the same regions of residual leg stance, knee moments became more extensor in the residual (K2 and K3) and intact (K1) legs as stiffness decreased. These fluctuations in knee moments were consistent with the increased intact leg VAS and RF activity during the first half of stance; and in the residual leg, were consistent with the increased VAS activity and decreased BF activity during the second half of stance. The most apparent change in muscle activity was observed by residual leg GMED, which increased its activity throughout all of stance as stiffness decreased, consistent with its functional role to provide body support (Anderson and Pandy, 2003). All of these observed changes suggest a need for muscles to provide increased body support as prosthetic foot stiffness decreased. The results also suggest that the increased energy returned from the prosthetic feet during the second half of stance as stiffness decreased may have resulted in lower residual BF activity, which has previously been shown to contribute to body propulsion. Therefore, a tradeoff may exist between providing greater body support as stiffness increased and providing additional forward propulsion as stiffness decreased. In addition, as stiffness increased, the intact leg V1 GRF increased, which may be detrimental in amputee gait as below-knee amputees have

a greater prevalence of knee joint disorders in the intact leg (Burke et al., 1978; Lemaire and Fisher, 1994).

These relationships between prosthetic foot stiffness and resulting gait mechanics and muscle activity should be considered when assessing the mobility needs of amputees and suggest that important tradeoffs exist between identifying appropriate stiffness levels to provide needed body support and forward propulsion and its potential influence on ESAR efficiency and intact leg loading.

Aim 3: The Effect of Altering Stiffness on Prosthetic Foot and Muscle Function during Below-Knee Amputee Walking

INTRODUCTION

Below-knee amputees commonly develop asymmetrical gait patterns and comorbidities in their intact and residual legs (Burke et al., 1978; Sanderson and Martin, 1997; Winter and Sienko, 1988). Prosthetic feet have been developed to minimize these asymmetries by utilizing elastic energy storage and return (ESAR) to help provide the important walking subtasks of body support, forward propulsion and leg swing initiation, which are normally provided by the ankle plantar flexors in non-amputee walking (Neptune et al., 2001). However, the influence of ESAR prosthetic foot stiffness on walking characteristics is not well-understood (for review, see Hafner et al., 2002a). One challenge to acquiring needed biomechanical data to identify this influence is the complexity of manufacturing custom ESAR prosthetic feet with specific stiffness levels.

In order to overcome this challenge, we recently developed a manufacturing framework integrating selective laser sintering (SLS) to systematically vary prosthetic foot design to assess the influence of foot stiffness on experimental kinematics, kinetics and muscle activity during amputee walking (Fey et al., 2011). We found that decreasing foot stiffness increases the prosthesis range of motion, mid-stance energy storage and late-stance energy return that results in reduced residual leg hamstring activity. Thus, decreasing stiffness may enable ESAR prosthetic feet to provide additional forward propulsion and reduce the compensatory action of the hamstring muscles (Neptune et al., 2004). However, as stiffness decreased, a reduced residual leg vertical ground reactions force (GRF) and increased muscle activity of the residual leg vastus and gluteus medius, and intact leg vastus and rectus femoris were observed, which appear necessary to provide needed body support (Anderson and Pandy, 2003; Liu et al., 2006; Neptune et

al., 2004) in the absence of prosthetic foot support. These muscles not only provide body support, but they also contribute to the braking GRF (decreased forward propulsion) in early stance (Liu et al., 2006; Neptune et al., 2004). Thus, forward propulsion provided by the prosthetic feet during late-stance may be offset by needed muscle adaptations to provide body support in early stance that also act to decrease forward propulsion.

Identifying the causal relationships between foot stiffness and muscle and prosthetic foot contributions to walking subtasks would help develop quantitative rationale for prosthetic foot prescription and improve amputee mobility. In previous analyses of human locomotion, musculoskeletal models and forward dynamics simulations have provided much insight into muscle function (e.g., Anderson and Pandy, 2003; Liu et al., 2006; McGowan et al., 2009; Neptune et al., 2004). The purpose of this study was to develop forward dynamics simulations of below-knee amputee walking using a range of prosthetic foot stiffness levels to identify how foot stiffness influences muscle and prosthetic foot function.

We hypothesized that as stiffness decreases, prosthetic foot contributions to forward propulsion and leg swing initiation would increase, and therefore needed muscle contributions to these walking subtasks would decrease. Also as stiffness decreases, we expected that prosthetic foot contributions to body support would decrease, and therefore needed muscle contributions to body support would increase.

METHODS

Description of the development of the musculoskeletal and prosthetic foot models, analyses of the simulations, and collection of experimental tracking data are provided below. Further details are described in Appendix A.

Musculoskeletal Model

A planar bipedal musculoskeletal model was used to develop the forward dynamics simulations of unilateral below-knee amputee walking. The model was developed in SIMM/Dynamics Pipeline (MusculoGraphics, Inc.) and was similar to previous studies of amputee and non-amputee walking (e.g., Neptune et al., 2001; Zmitrewicz et al., 2007) (Fig. 3.1).

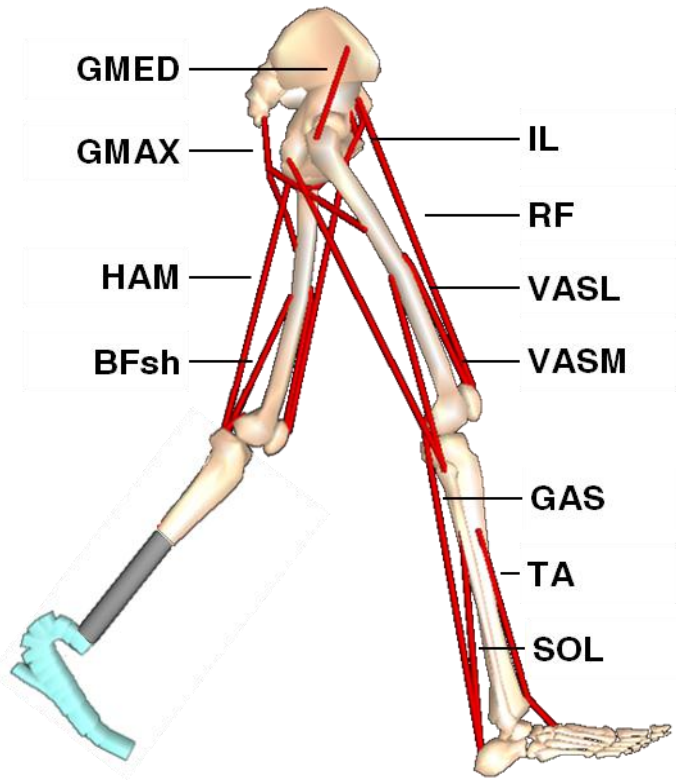

Figure 3.1: Amputee musculoskeletal model. The amputee model was actuated by 25 individual Hill-type musculotendon actuators in the intact leg. The individual actuators were grouped into 14 muscle groups based on anatomical classification. Muscles in each group received the same excitation pattern. The muscle groups consisted of GMED (anterior and posterior compartments of the gluteus medius), GMAX (gluteus maximus, adductor magnus), HAM (biceps femoris long head, medial hamstrings), BFsh (biceps femoris short head), IL (psoas, iliacus), RF (rectus femoris), VASL (vastus lateralis, vastus intermedius), VASM (vastus medialis), GAS (medial and lateral gastrocnemius), SOL (soleus, tibialis posterior), TA (tibialis anterior, peroneus tertius), PR (peroneus longus, peroneus brevis), FLXDG (flexor digitorum longus, flexor hallucis longus) and EXTDG (extensor digitorum longus, extensor hallucis longus). For figure clarify, the smaller muscle groups that actuated the foot (PR, FLXDG and EXTDG) are not illustrated. In the amputee residual leg, the same muscle groups were included except for the muscles crossing the ankle joint (GAS, SOL, TA, PR, FLXDG and EXTDG).

Rigid segments represented the trunk (head, arms and torso) in addition to the thigh and shank segments of both legs. In the intact leg foot, rigid segments also represented the talus, calcaneus, mid-foot and toes. The musculoskeletal geometry was based on Delp et al. (1990). The inertial properties of the residual leg shank segment were adjusted (Mattes et al., 2000; Silverman and Neptune, 2011). The trunk had 3 degrees of freedom (2 translations and 1 rotation). Single degree of freedom revolute joints modeled the hip flexion/extension. A planar joint was used to model the knee joint, with a flexion/extension rotation and the two translational degrees of freedom being prescribed as a function of knee flexion angle. In the intact leg, revolute joints modeled flexion/extension of the ankle, subtalar and metatarsophalangeal joints. Therefore, not including the residual leg prosthetic foot, the musculoskeletal model had a total of 10 degrees of freedom.

Foot-ground contact was modeled using 31 visco-elastic elements with coulomb friction on each foot (Neptune et al., 2000) (for additional details, see Appendix A). Passive torques at each joint representing ligaments, passive tissue, and joint structures were applied (Anderson and Pandy, 1999; Davy and Audu, 1987). Equations of motion were generated using SD/FAST (PTC).

Musculotendon Actuators

Each actuator was made up of a contractile element representing the active muscle fiber, series elastic element representing the tendon, and parallel elastic element representing the passive fiber stiffness (for additional details, see Appendix A). Similar to previous work (Hall et al., 2011), excitation patterns of each actuator were defined using a bimodal pattern:

$$e(t) = \sum_{i=1}^{2} \begin{cases} \frac{a_i}{2}\left[1 - \cos\left(\frac{2\pi(t-onset_i)}{offset_i - onset_i}\right)\right], onset_i \le t \le offset_i \\ 0 \qquad\qquad\qquad\qquad , otherwise \end{cases}$$

Excitation magnitude e(t) was a function of time (t) and amplitude (a_i), onset ($onset_i$), and offset ($offset_i$) of each mode (i). Thus, six parameters (two onsets, offsets and magnitudes) defined the excitation pattern of each muscle group. Muscle contraction dynamics were governed by force-length, force-velocity, and tendon force-strain relationships (Zajac, 1989). Activation-deactivation dynamics were modeled by a first-order differential equation (Raasch et al., 1997). Most muscle activation and deactivation time constants were derived from Winters and Stark (1988). For those muscles not included in Winters and Stark (1988), nominal activation and deactivation time constants of 12 and 48 ms were used.

Energy Storage and Return Prosthetic Foot Model

The prosthetic foot model consisted of 22 rigid segments. Each segment and the overall prosthetic shape were defined by two spline curves which represented the keel and heel sections (Fig. 3.2, for additional details, see Appendix A). The keel and heel shapes were defined using 15 and 9 spline points, respectively. This shape was used since it closely matched the shape of a widely prescribed commercial carbon fiber ESAR foot (Highlander^{TM}, FS 3000, Freedom Innovations, LLC) and was previously used to generate prototypes of SLS ESAR feet (South et al., 2010). The prosthetic foot model had a total of 18 degrees of freedom (13 keel and 5 heel single degree of freedom revolute joints, Fig. 3.2).

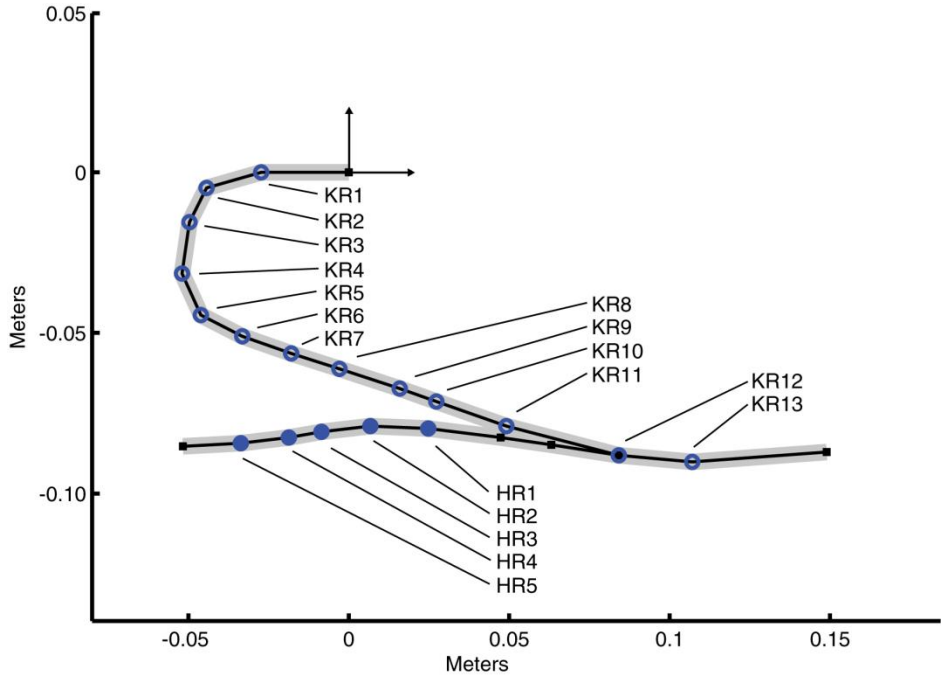

Figure 3.2: Schematic of prosthetic foot model consisting of 22 rigid segments connected in series. The prosthetic foot model had 13 keel (KR1-KR13, ○) and 5 heel (HR1-HR5, ●) rotational degrees of freedom.

Prosthetic Foot Stiffness

There was a viscoelastic element at each rotational degree of freedom in the prosthetic foot model that applied a passive torque:

$$\tau_i = -k_i \cdot \theta_i - b \cdot \dot{\theta}_i$$

The passive torque (τ_i) applied at each rotational degree of freedom (i) was a function of element stiffness (k_i), angular displacement (θ_i) and angular velocity ($\dot{\theta}_i$). A damping value b=5.73 N*m*s (for derivation, see Appendix A) was used.

Three different prosthetic foot stiffness distributions that encompassed a range of stiffness levels were used in the amputee simulations. These distributions (Fig. 3.3) were

calculated from the previously developed nominal, compliant and stiff SLS ESAR prosthetic feet (Fey et al., 2011) based on material properties and measured geometry. Each prosthetic foot segment was assumed to be a prismatic beam element and made from sintered Nylon 11 powder using SLS. Rotational stiffness of each element (KR1-KR13 and HR1-HR5) was calculated as follows:

$$k_i = \frac{E \cdot I_i}{L_i}$$

The rotational stiffness (k_i) was a function of the Young's modulus of the sintered Nylon 11 powder used to manufacture the SLS ESAR prosthetic feet (E=1.4 GPa), segment length (L_i) and area moment of inertia for a rectangular cross-section (I_i).

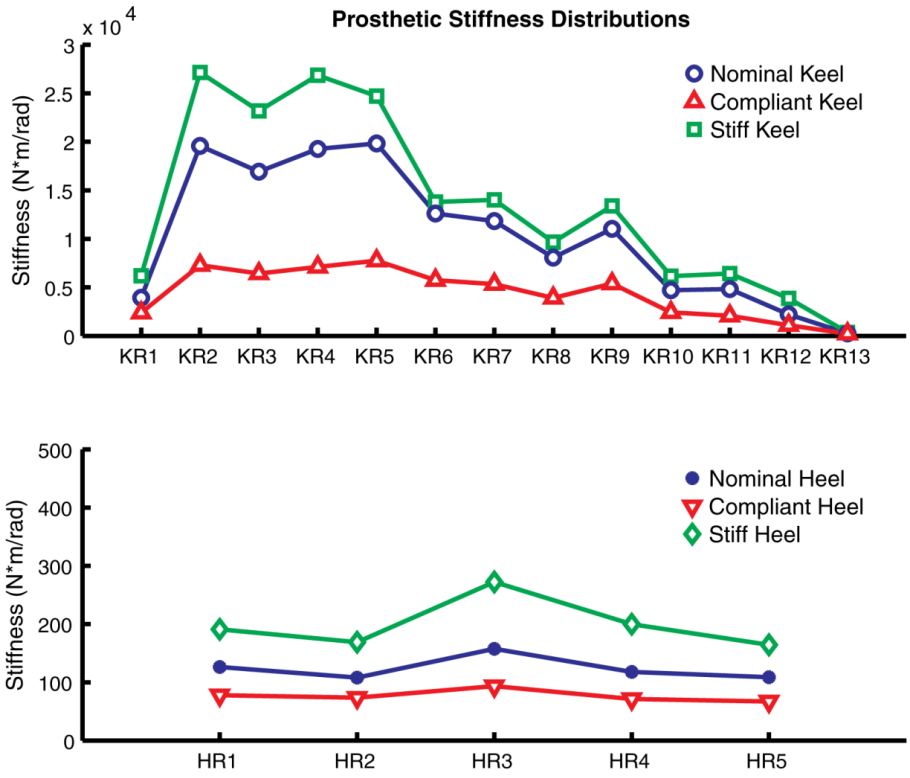

Figure 3.3: Nominal, compliant and stiff prosthetic foot stiffness distributions calculated from the three SLS ESAR feet. These stiffness distributions were used in simulations of amputee walking.

Dynamic Optimization

A simulated annealing optimization algorithm (Goffe et al., 1994) within a dynamic optimization framework (Fig. 3.4) was used to generate simulations of amputee walking.

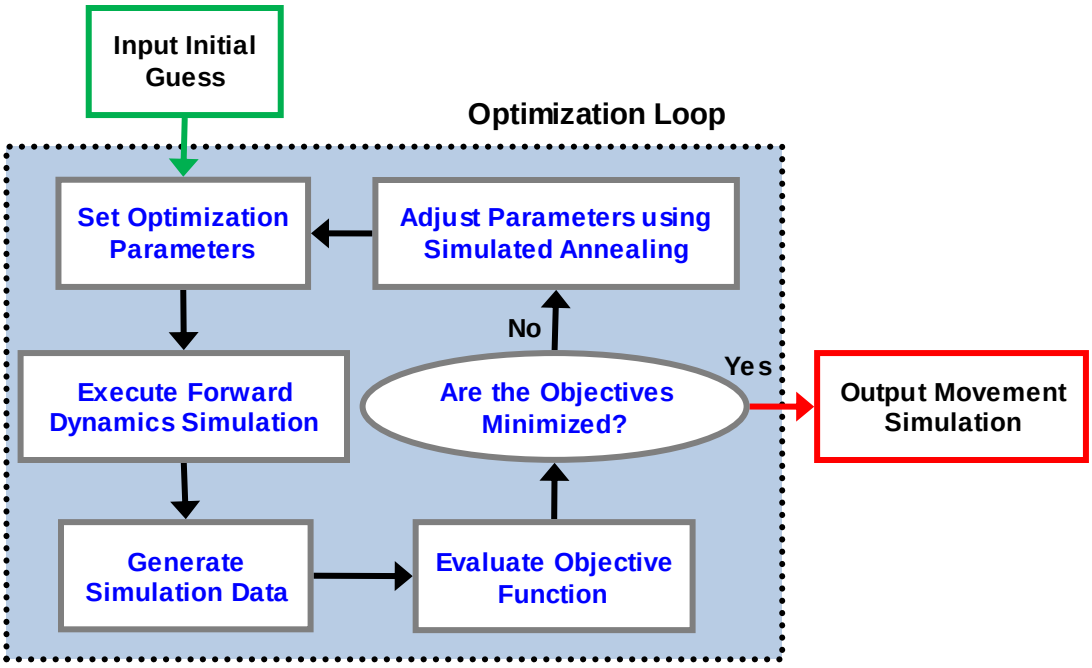

Figure 3.4: Optimization framework used to generate simulations of amputee walking.

Three simulations were generated for the nominal, compliant and stiff foot conditions. The objective functions used in the optimization sought to reproduce group average experimental data of the amputee subjects, while also minimizing the sum of squared individual muscle stresses. Optimization parameters for each simulation included the bimodal muscle excitation parameters of each muscle group and initial generalized velocities.

Muscle and Prosthetic Foot Function

To test the hypotheses that altering stiffness would change prosthetic foot and muscle contributions to important walking subtasks, individual muscle and prosthetic foot contributions to forward propulsion, support and leg swing initiation (Neptune et al., 2001; Neptune et al., 2004; Neptune et al., 2008) between the walking simulations were compared using a muscle-induced acceleration and segment power analysis (Fregly and

Zajac, 1996) (for additional details, see Appendix A). To quantify each muscle's contribution and the contribution of the prosthetic foot to forward propulsion, their contributions to the horizontal propulsion/braking of the body (i.e., anterior/posterior (A/P) acceleration of the center-of-mass or A/P GRF) and horizontal power of the trunk segment were calculated. Similarly for support, their contributions to the vertical support of the body (i.e., vertical GRF) and vertical power of the trunk segment were calculated. Both body and trunk braking/propulsion and support were examined because muscular contributions of the ankle plantar flexors (e.g., SOL and GAS) to these subtasks have been shown to differ (Neptune et al., 2001). To quantify each muscle's contribution and the contribution of the prosthetic foot to swing initiation, the induced power delivered to the residual leg was determined.

Experimental Tracking Data

To provide desired tracking data for the dynamic optimization, experimental data of amputees walking with the three SLS ESAR feet of varying stiffness levels were collected. Subjects provided informed consent to an Institutional Review Board approved protocol and included 12 unilateral, below-knee amputees (10 traumatic, 2 secondary illness; 12 males; 52 ± 17 years; 183.0 ± 34.9 lbs; 70.2 ± 2.5 in.). Each subject walked along a 10-m walkway at 1.2 (±0.06) m/s. Bilateral kinematic marker data (Silverman et al., 2008) were measured at 120 Hz using motion capture systems (Vicon, Oxford Metrics, Inc.), and GRF data were measured at 1200 Hz using four embedded force plates (Advanced Mechanical Technology, Inc. and Bertec Corporation). Amputee subjects walked with three previously developed custom SLS ESAR prosthetic feet (Fey et al. 2011) in a randomized order (Fig. 3.5). These three SLS ESAR feet were previously manufactured from Rilsan^{TM} D80 (Nylon 11, Arkema, Inc.) using a Vanguard HiQ

Sinterstation (3D Systems, Inc.) and encompassed a range of stiffness levels. Repeated trials were collected until at least five step-to-step force plate contacts per foot (left and right) were measured at each stiffness condition. Surface EMG were recorded from the intact leg tibialis anterior, soleus, medial gastrocnemius, and bilaterally from the vastus medialis, rectus femoris, biceps femoris long head, gluteus maximus and gluteus medius (2, 10-mm disposable self-adhesive Ag/AgCl sensor contacts, 16-mm interelectrode distance; TeleMyo 900, Noraxon U.S.A., Inc.). For additional details regarding the collection of experimental tracking data, see Appendix A.

Figure 3.5: ESAR prosthetic feet fabricated using SLS additive manufacturing technology that encompassed a wide range of stiffness levels. The linear stiffness of these feet were previously evaluated in toe-only, foot-flat and heel-only loading configurations (South et al., 2010), and closely matched the nominal stiffness of a widely prescribed carbon fiber foot (Nominal), and were 50% more stiff (Stiff) and 50% more compliant (Compliant).

RESULTS

Experimental Tracking Data

The amputee walking simulations exhibited movements that emulated the collected experimental data (Fig. 3.6). Across simulations, average root-mean-square kinematic joint angle and ground reaction force tracking deviations were 10.0 degrees and 0.09 GRF/BW, respectively. These deviations were nearly within 2 standard

deviations of the experimental data, which were 9.1 degrees and 0.08 GRF/BW. For the muscle groups in which experimental EMG data were collected, the optimal simulation excitation patterns were active during regions of the gait cycle when these muscles were found to have EMG activity (Fig. 3.7).

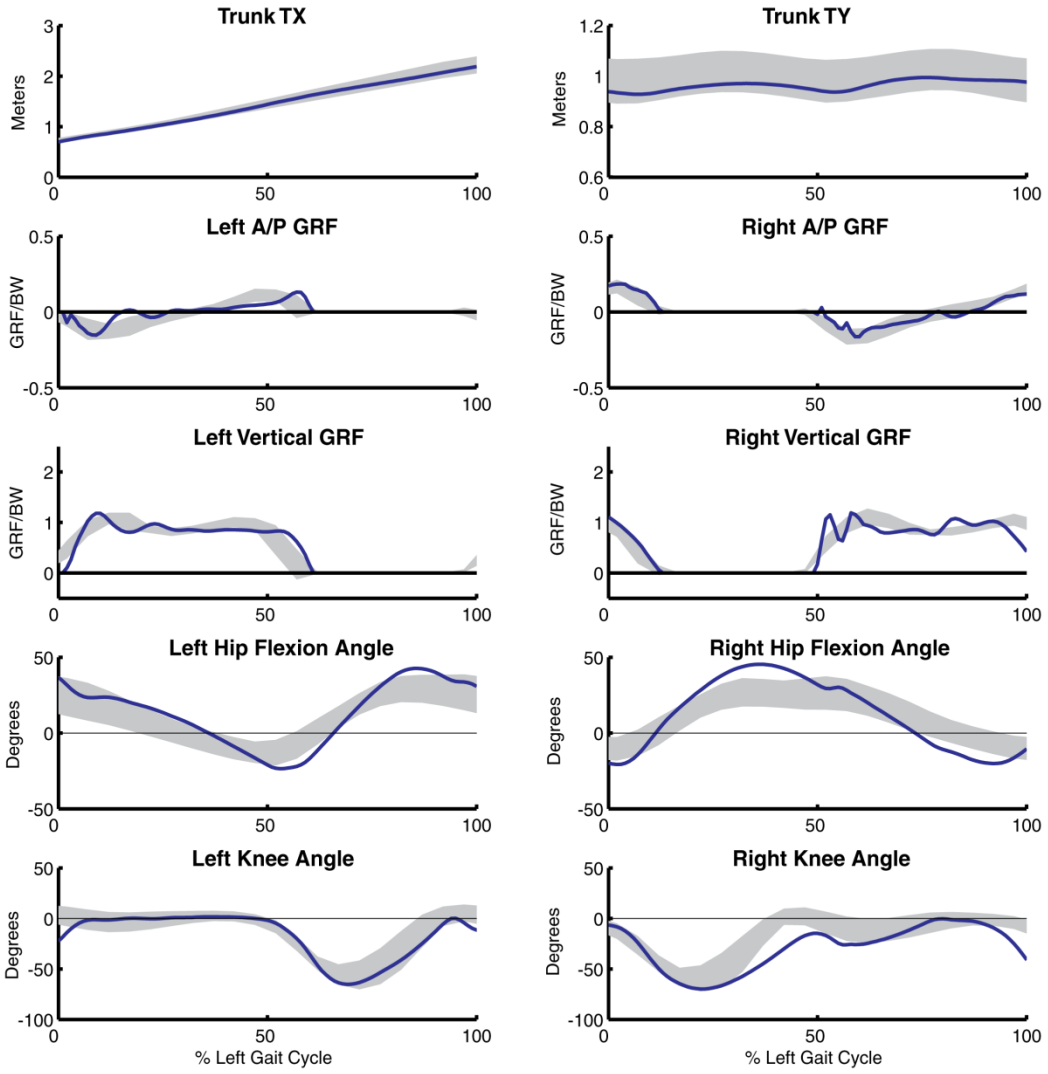

Figure 3.6: Representative simulation tracking comparison from the nominal amputee walking simulation. Simulated (blue) and experimental (gray, ± 2 SD) data are plotted. For tracking comparisons of the other amputee walking simulations see Appendix B.

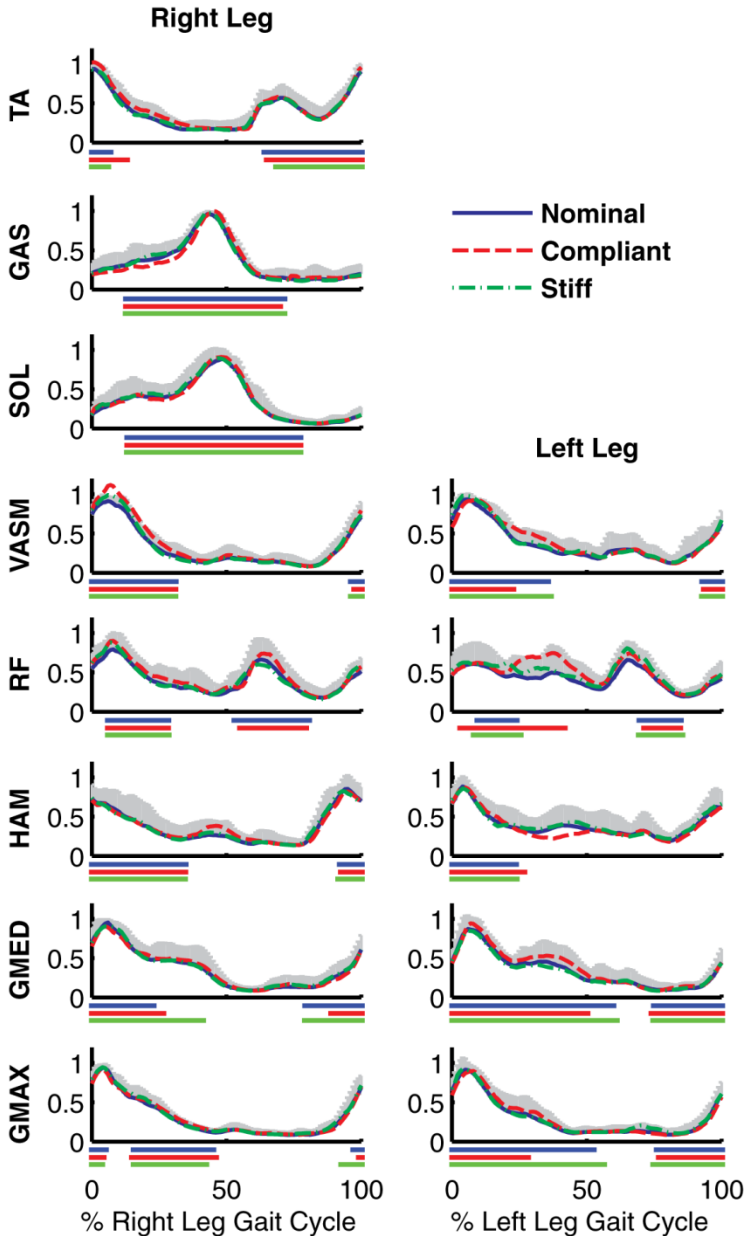

Figure 3.7: Comparison of excitation timing with group average experimental EMG data of amputee subjects (for only those muscles in which EMG data were collected). Group average experimental EMG data were normalized to the peak magnitude in the nominal condition prior to group averaging. Nominal EMG +1 SD are also plotted using vertical error bars. Excitation timing in the three amputee walking simulations are plotted below each x-axis and correspond in color with the plotted EMG timing for each condition.

Prosthetic Foot Deflections, Torques and Energy Storage and Return

The individual prosthetic foot element deflections, torques and energy storage return followed similar trends in all of the simulations (e.g., Fig. 3.8). In early stance, the heel elements (HR1-HR5) and keel elements closest to the attachment of the heel (KR11 and KR12) experienced negative (plantarflexion) angular deflections. From mid to late stance, the keel elements all experienced positive (dorsiflexion) angular deflections. Predictably, as stiffness decreased, the deformation of the prosthetic foot increased (Fig. 3.9). In early stance, the heel elements produced positive dorsiflexion moments, which increased in the elements closest to the attachment of the keel (Fig. 3.8). Also in early stance, dorsiflexion torques were produced by most keel elements, and increased in the elements closest to the attachment of the heel (KR11 and KR12). From mid to late stance, the keel elements produced plantarflexion moments that typically increased as the element location moved from the toe to the ankle. The heel elements stored energy (negative power) in early stance and returned a small amount of energy (positive power) in mid stance, and the keel elements typically stored energy in mid stance and returned energy during late stance. However, the keel elements closest to the attachment of the heel (e.g., KR12) stored and returned energy during the first and second halves of stance due to their dynamic interaction with the heel during the first half of stance and the ground during the second half of stance. As stiffness decreased, the largest changes of the total prosthetic foot energy storage and return (Fig. 3.10) were the keel energy storage during early and mid stance and keel energy return in late stance.

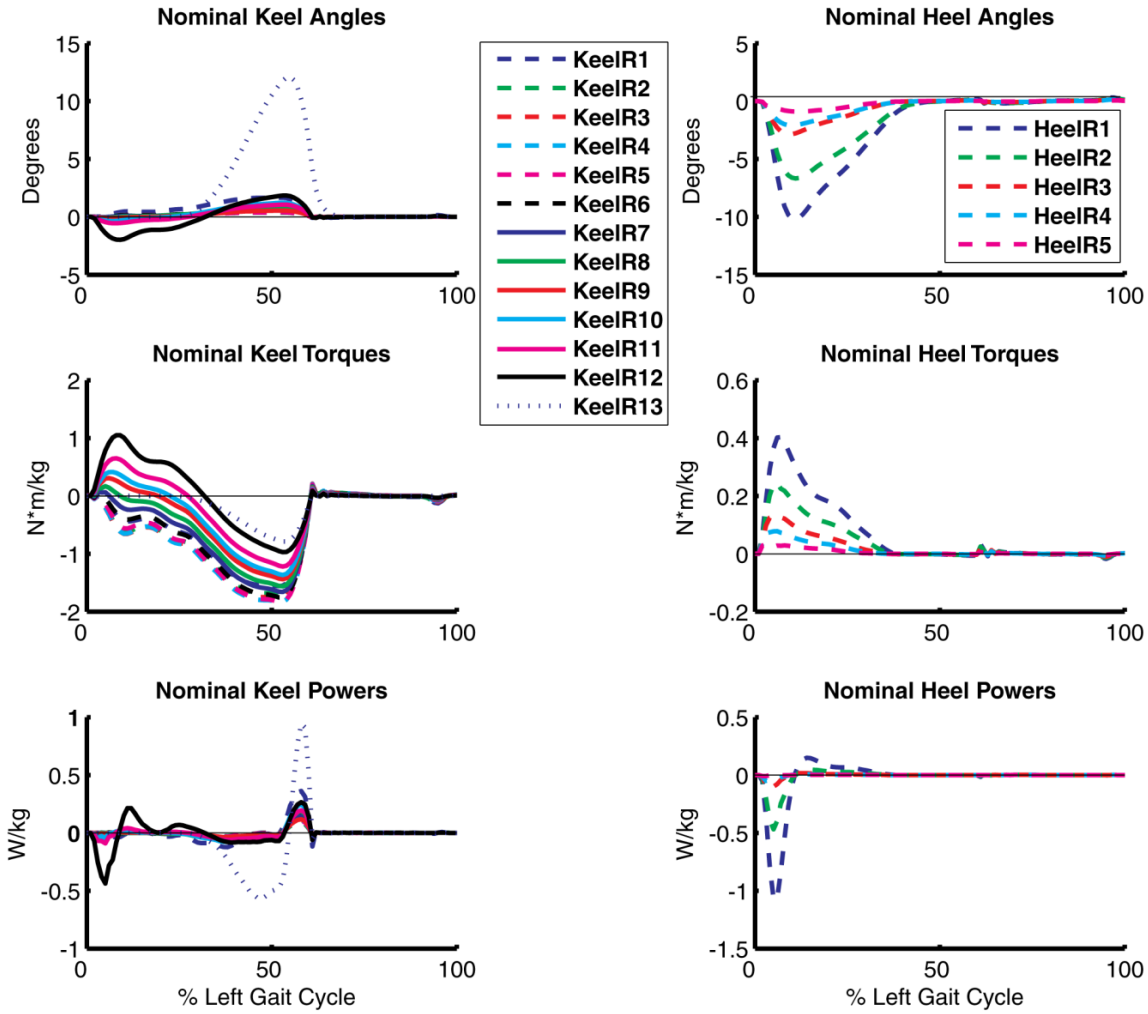

Figure 3.8: Representative keel (left column, KR1-KR13) and heel (right column, HR1-HR5) rotational element angular deflections (top row), torques (middle row) and powers (bottom row) in the nominal amputee walking simulation. Torque and power curves are normalized by body mass. Positive angular deflection and torque indicate dorsiflexion. See Appendix B for the data from the compliant and stiff simulations.

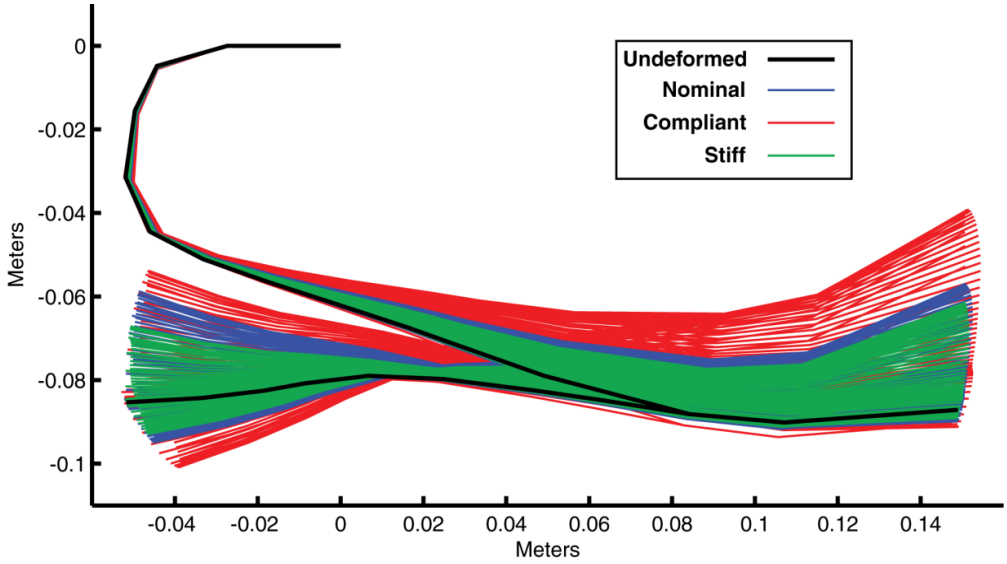

Figure 3.9: Prosthetic foot shape deformations during the nominal, compliant and stiff amputee walking simulations. The undeformed shape is plotted on top of the shapes of the prosthetic feet at each time step in the simulations.

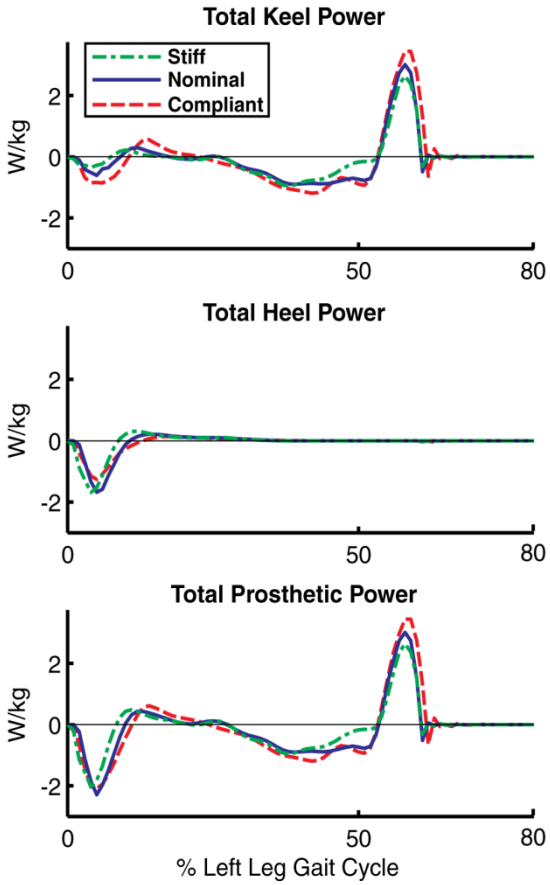

Figure 3.10: Keel (KR1-KR13), heel (HR1-HR5) and total (keel + heel) power curves in the nominal, compliant and stiff simulations. Keel and heel powers were calculated by summing the power across rotational elements within each region of the foot and were normalized by body mass.

Contributions to Walking Ground Reaction Forces

The contributions of gravity, muscles and the prosthetic foot to the A/P and vertical ground reaction forces of the residual leg were similar across simulations (Fig. 3.11). During the first half of stance, gravity and the prosthetic foot acted to brake the body (negative A/P GRF) and muscles produced propulsion (positive A/P GRF) (Fig. 3.11A). These contributions from the prosthetic keel and muscles increased as stiffness

decreased, while gravity contributions decreased. Also, the prosthetic keel contributions to body support (positive vertical GRF) increased, while the prosthetic heel and gravity contributions decreased (Fig. 3.11C).

During the second half of residual leg stance, keel contributions to propulsion decreased as stiffness decreased (Fig. 3.11B). In the compliant condition, gravity contributed to propulsion and muscles contributed to braking, which differed from the nominal and stiff conditions (Fig. 3.11B). In addition, the keel contributions to body support increased as stiffness decreased (Fig. 3.11D).

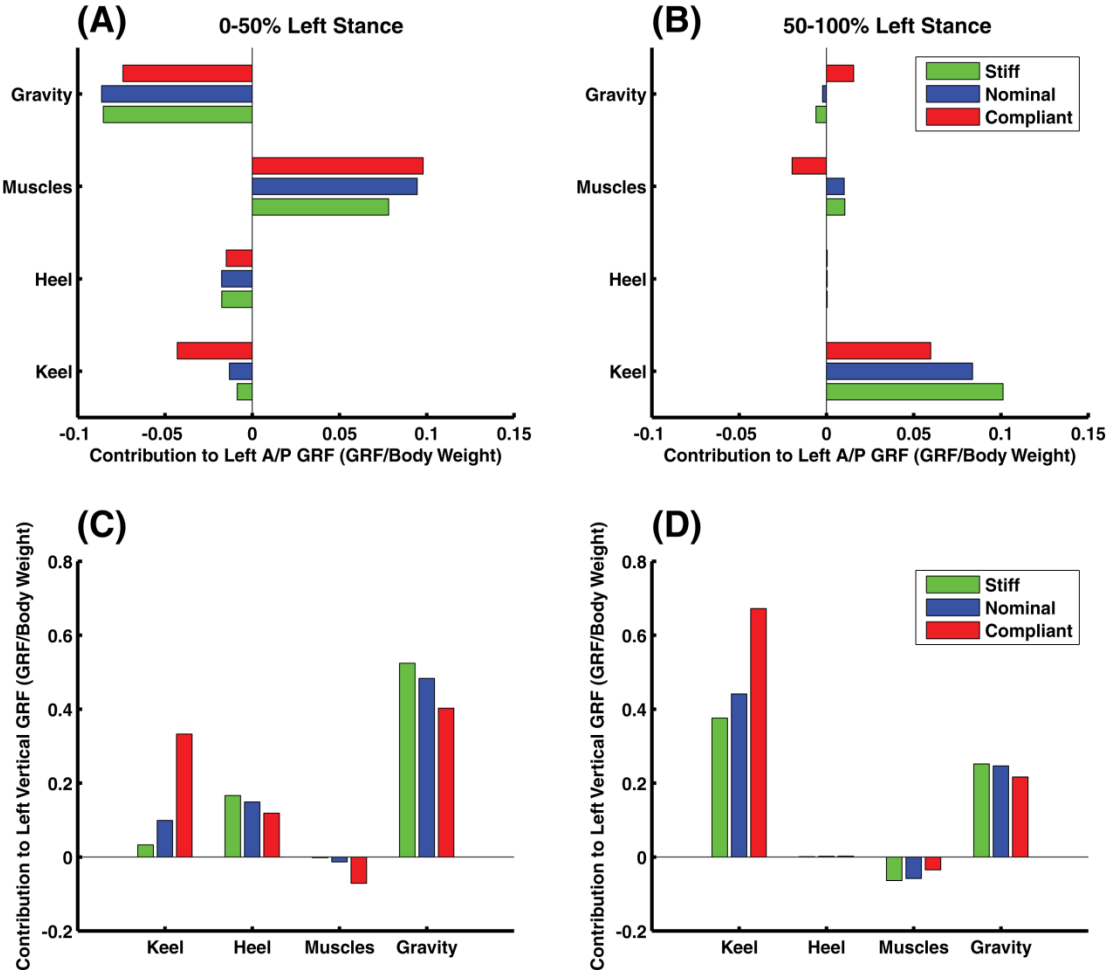

Figure 3.11: Mean contributions of the prosthetic foot, residual (left leg) and intact (right leg) muscles, and gravity to A/P and vertical GRF of the residual leg. Data were averaged during the first (left column) and second (right column) halves of the residual (left leg) stance phase.

Individual muscle contributions to body support and propulsion were also influence by stiffness (Figs. 3.12 and 3.13). During the first half of residual leg stance, residual GMAX, GMED and HAM contributed to propulsion, and their contributions increased as stiffness decreased (Fig. 3.12A). Also, residual RF and VAS contributed to braking (Fig. 3.12A), and the RF contributions to braking during all of stance increased in the compliant condition (Figs. 3.12A and 3.12B).

Contrary to the first half of stance, the residual leg GMAX and GMED provided increased propulsion in the nominal and stiff simulations (as stiffness *increased*) during the second half of stance (Fig. 3.12B). Most residual leg muscle contributions to body support were small during stance compared to the intact leg (compare Figs. 3.12C and 3.12D to Figs. 3.13C and 3.13D) because these functions were performed by the prosthetic foot and gravity (Figs. 3.11C and 3.11D). However, the residual HAM had a substantial contribution to body support during the first half of stance, and decreased its contribution as stiffness decreased (Fig. 3.12C).

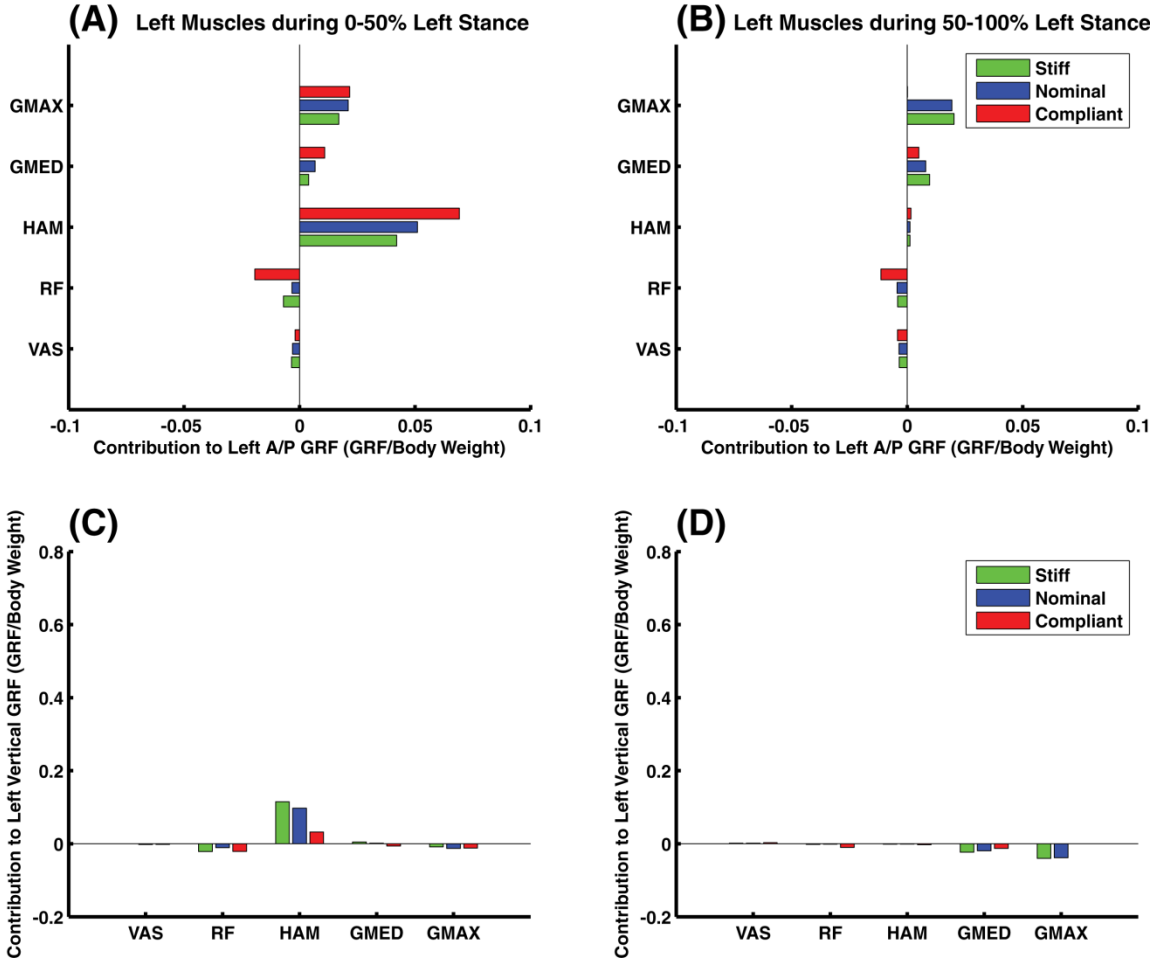

Figure 3.12: Mean individual residual (left leg) muscle contributions to A/P and vertical GRF of the residual leg. Data were averaged during the first (left column) and second (right column) halves of the residual (left leg) stance phase. Contributions of VASL and VASM were summed (VAS) for these analyses.

During the first half of intact leg stance, intact leg RF, VAS, SOL and GAS contributed to body braking and HAM contributed to propulsion (Figs. 3.13A and 3.13C). All of these intact leg muscles provided body support, with the contributions of VAS to support being the largest. During the second half of intact leg stance, intact leg RF and VAS provided small amounts of braking and support, while SOL and GAS were the primary contributors to propulsion and support (Figs. 3.13B and 3.13D). The largest

observed changes across stiffness were the increased VAS contributions to braking and support during the first half of stance as stiffness decreased (Figs. 3.13A and 3.13C).

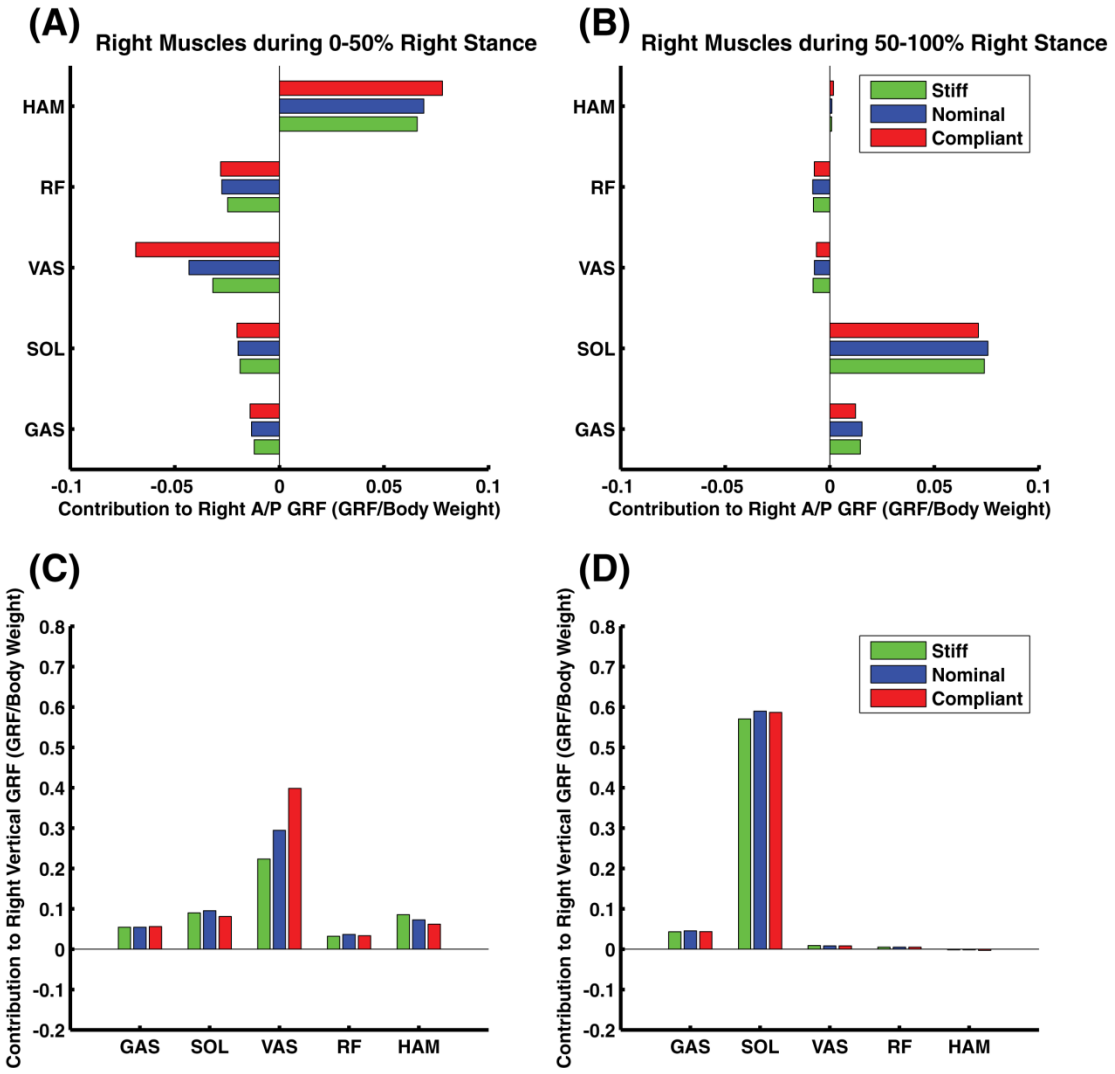

Figure 3.13: Mean individual intact (right leg) muscle contributions to A/P and vertical GRF of the intact leg. Data were averaged during the first (left column) and second (right column) halves of the intact (right leg) stance phase. Contributions of VASL and VASM were summed (VAS) for these analyses.

Contributions to Trunk Power

During the first half of residual leg stance, the prosthetic keel and heel acted to absorb horizontal energy from the trunk (trunk braking), while the muscles of the residual and intact legs delivered horizontal energy to the trunk (trunk propulsion) (Fig. 3.14A). As stiffness decreased, the keel absorbed less horizontal energy, while the residual leg GMED and RF and intact leg TA delivered increased horizontal trunk energy. In the nominal and stiff simulations, the intact leg SOL delivered increased horizontal trunk energy. In addition, the keel provided greater vertical energy to the trunk (trunk support), while the residual leg HAM delivered less vertical energy (Fig. 3.14D).

The largest change in individual contributions to trunk energy occurred during the second half of residual leg stance as stiffness decreased (Figs. 3.14B and 3.14E). The prosthetic keel delivered the largest horizontal energy to the trunk and absorbed the largest vertical energy from the trunk, which decreased and increased, respectively as stiffness decreased. Similar to its behavior during the first half of stance, the residual leg RF delivered increased horizontal energy to the trunk (Fig. 3.14B). The intact leg VAS absorbed increased horizontal energy from the trunk and delivered increased vertical energy to the trunk (Figs. 3.14B and 3.14E). The intact leg TA also delivered increased vertical trunk energy (Fig. 3.14E). Lastly, the intact leg VAS also delivered increased vertical energy during swing of the residual leg (Fig. 3.14F).

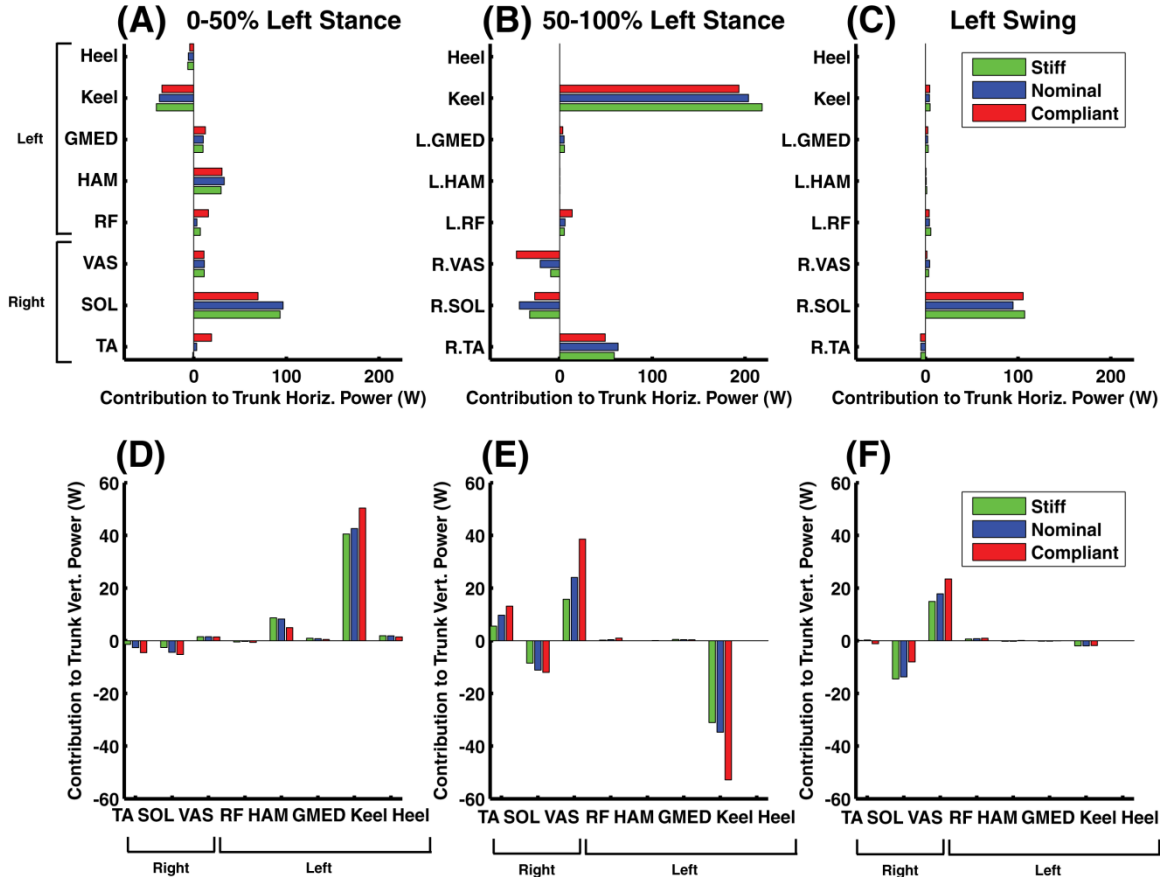

Figure 3.14: Mean prosthetic foot and residual (left leg) and intact (right leg) muscle contributions to horizontal (top row) and vertical (bottom row) trunk power. Data were averaged during the first (left column) and second (middle column) halves of the residual (left leg) stance and swing phases (right column).

Contributions to Residual Leg Power

During the first half of residual leg stance, the residual leg muscles and prosthetic foot primarily absorbed energy from the leg (Fig. 3.15A). As stiffness decreased, the keel absorbed more energy from the leg. Also, the residual leg RF absorbed more energy from the leg in the compliant simulation. Similarly during the second half of residual leg stance, the residual RF absorbed more energy from the leg (Fig. 3.15B). Unlike the trends

observed during the first half of stance, the prosthetic keel absorbed less energy from the leg as stiffness decreased (Fig. 3.15B). During swing, the residual IL delivered more energy to the leg as stiffness *increased*, and the residual GMAX and HAM absorbed more and less energy from the leg, respectively (Fig. 3.15C).

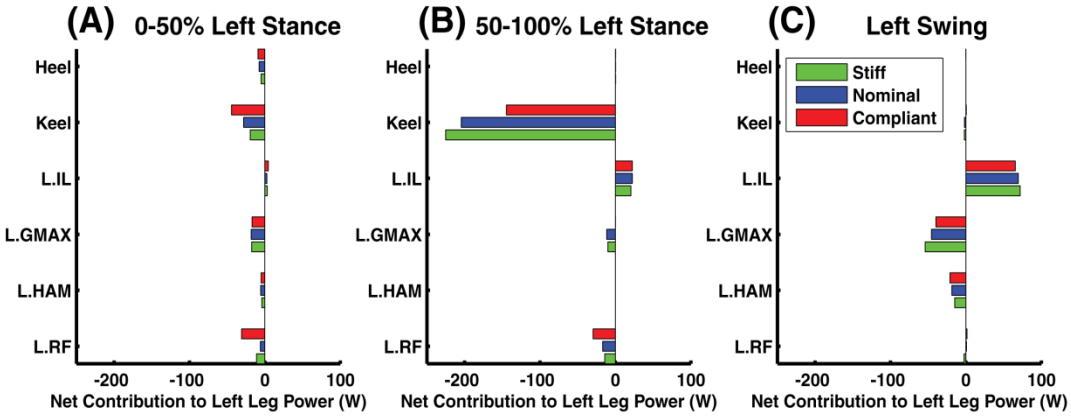

Figure 3.15: Mean prosthetic foot and individual muscle contributions to total residual leg power. Data are averaged during the first (left column) and second (middle column) halves of residual (left leg) stance and swing (right column).

DISCUSSION

The purpose of this study was to develop forward dynamics simulations of below-knee amputee walking using a range of prosthetic foot stiffness levels to identify how foot stiffness influences muscle and prosthetic foot function. We hypothesized that as stiffness decreased, prosthetic foot contributions to forward propulsion and leg swing initiation would increase, and therefore muscle contributions to these walking subtasks would decrease. We also expected that prosthetic foot contributions to body support would decrease as stiffness decreased, and therefore muscle contributions to body support

would increase to compensate. These hypotheses were only partially supported due to complex interactions between the prosthetic foot, muscles and body segments, and functional differences in the contributions of muscles and the prosthetic foot to walking subtasks throughout the gait cycle.

Prosthetic Foot Function is Influenced by Stiffness

During the first half of residual leg stance as stiffness decreased, the prosthetic keel provided increased body braking, but reduced braking of the trunk. Also, support provided by the keel to both the body and trunk increased, and were much larger than the support provided by the heel, which decreased. Therefore with the exception of the heel providing decreased support and the keel providing decreased braking of the trunk, these findings did not support our hypotheses. However, the increased contributions of the keel to body braking was consistent experimentally with the increased residual leg braking GRF observed in these amputee subjects (Fey et al., 2011). The current study suggests that the increased residual leg braking GRF observed experimentally was the result of increased prosthetic keel contributions as stiffness decreased.

During the second half of residual leg stance as stiffness decreased, the prosthetic keel provided decreased body and trunk propulsion. Also, the keel provided increased body support, but an increased negative contribution to trunk support. Therefore, with the exception of the keel providing decreased support of the trunk, these findings were not consistent with our hypotheses. However, a smaller residual leg vertical ground reaction force was observed experimentally in the amputee subjects walking with the compliant foot (Fey et al., 2011). Thus, despite higher keel contributions to body support, the total vertical acceleration of the body was less, suggesting that vertical support of both the trunk and body by the prosthetic feet may be limited during the second half of residual

leg stance as stiffness decreased. These observed functions of the prosthetic keel to body and trunk support and braking during the first and second halves of stance are consistent with the function role of the SOL in non-amputee walking (Neptune et al., 2001).

During the first half of stance, the prosthetic keel and heel absorbed increased energy from the leg as stiffness decreased. However, for swing initiation (i.e., energy delivered to the residual leg prior to swing during the second half of stance), the prosthetic keel's absorption of leg energy decreased. Therefore, despite acting to absorb energy from the leg during this region, the keel absorbed less energy as stiffness decreased, thus contributing more to swing initiation. These results during the second half of residual leg stance were consistent with our hypotheses. The function of the prosthetic keel to absorb energy from the leg during the second half of stance is again consistent with the functional role of SOL in non-amputee walking, and not with the role of GAS which delivers energy to the leg for swing initiation (Neptune et al., 2001).

Individual Compensations in Response to Altered Prosthetic Foot Function

To compensate for increased body braking of the prosthetic keel as stiffness decreased during the first half of residual leg stance, the residual leg HAM, GMAX and GMED increased their contributions to body propulsion. In addition, HAM provided less body support as the prosthetic keel contribution to support increased since the prosthetic keel had increased contributions to this subtask.

As stiffness decreased during the second half of residual leg stance, gravity contributed more to body propulsion and less to body support to compensate for a reduced contribution of the prosthetic keel to propulsion, increased RF contribution to braking, and increased contribution of the keel to support. In the nominal and stiff conditions (*increased* stiffness), increased contributions of residual GMED and GMAX

to body propulsion were observed, perhaps in response to less contribution of gravity to this task as stiffness increased. In these amputee subjects, reduced residual leg BF muscle activity was observed experimentally in the compliant condition during the second half of residual leg stance (Fey et al., 2011), which can act co-functionally with GMED and GMAX to provide propulsion during mid stance (Lin et al., 2011; Liu et al., 2006; Neptune et al., 2004). Therefore, although not observed in these simulations, the reduced activity of the biceps femoris longhead observed experimentally in the compliant condition may be related to higher contributions of gravity to body propulsion. The contributions of RF to body braking and HAM, GMED, GMAX and gravity to body propulsion during stance is consistent with their ability to perform these functions in previous modeling and simulation studies of non-amputee walking (Lin et al., 2011; Liu et al., 2006; Neptune et al., 2004)

During the first half of intact leg stance, intact HAM increased its contribution to body propulsion as stiffness decreased. Compensation of the intact HAM may have occurred as a result of the increased intact VAS contributions to braking. These intact leg compensations in the horizontal (A/P) direction appear necessary due to the large increases body support contributions of the intact VAS. The compensation of intact VAS as stiffness decreased is consistent with increased intact knee extensor moments, VAS muscle activity, and intact leg braking GRF that were observed experimentally in the amputee subjects (Fey et al., 2011). The contribution of VAS to body support and braking is consistent with its function in previous modeling and simulation studies of non-amputee walking (Anderson and Pandy, 2003; Liu et al., 2006; Neptune et al., 2004). In addition, modulation of VAS contributions to body support has been shown in previous work when the mechanical demand for body weight support was augmented (McGowan et al., 2009). Thus, our results highlight the need for increased intact leg body

support during this region as stiffness decreased. During the second half of intact leg stance, intact SOL and GAS were the primary contributors to body support and propulsion, which was consistent with their roles in non-amputee walking (Neptune et al., 2001).

Similar to the keel providing less braking of the trunk during the first half of residual leg stance as stiffness decreased, the residual leg RF and GMED increased their contributions to trunk propulsion. Therefore, even though RF contributed more to body braking, it delivered more propulsion to the trunk. These increased compensations of the residual leg RF and GMED are consistent with increased activity of these muscles that were observed experimentally as stiffness decreased (Fey et al., 2011). Although it was postulated from the experimental results that these increases in activity would provide added support as stiffness decreased, these simulation results suggest that their contributions to trunk propulsion are increased by altered stiffness. Our results also suggest that as stiffness *increased* and the prosthetic keel provided increased trunk braking, the intact leg SOL provided additional trunk propulsion. The function of the residual RF and intact SOL to deliver energy to the trunk for forward propulsion is consistent with previous modeling work of non-amputee walking (Neptune et al., 2001; Neptune et al., 2004).

During the second half of residual leg stance as stiffness decreased, the keel provided less trunk propulsion and an increased negative contribution to trunk support. These keel contributions are consistent with the increased mid stance energy storage of the keel as stiffness decreased that was observed as well as experimentally with these amputee subjects (Fey et al., 2011). These results suggest the primary compensation to these changes in keel function was increased intact leg VAS contributions to trunk support. However, a consequence of increased VAS contribution to trunk support, was an

increase in its contribution to trunk braking. As a result, an increased contribution to trunk propulsion was needed by the residual RF. The contributions of VAS to trunk braking and support are consistent with previous modeling studies of non-amputee walking (Neptune et al., 2004). Other compensations in response to decreased stiffness included an increased intact leg TA contribution to trunk support, which was consistent with increased EMG activity of this muscle observed experimentally in the amputee subjects (Fey et al., 2011). Therefore, due to altered prosthetic keel contributions to trunk propulsion and support during the second half of stance, residual leg muscles needed to modulate their contributions to trunk propulsion, while the intact muscles modulated their contributions to trunk support.

Lastly, in terms of the residual leg power during both the first and second halves of residual leg stance, the residual leg RF acted to absorb increased energy from the leg, and increased trunk propulsion as stiffness decreased. Thus, the residual RF transferred more energy from the leg to the trunk as stiffness decreased, and is consistent with the functional role of RF in non-amputee walking, acting primarily to transfer energy from the leg to the trunk (Neptune et al., 2004). As noted above, the keel contributed more to swing initiation during the second half of stance as stiffness decreased. These keel contributions are consistent with increased late stance energy return that was observed and experimentally in the amputee subjects (Fey et al., 2011). Our results suggest reduced swing initiation as stiffness *increased* was compensated for by increased contributions of residual leg IL to leg power during swing, consistent with the role of IL in non-amputee walking (Neptune et al., 2004) and symmetric amputee walking (Zmitrewicz et al., 2007).

Comparison of Energy Storage and Return

The patterns of total energy storage and return in the prosthetic feet calculated (Fig. 3.10) were similar to patterns of energy storage and return calculated experimentally using an inverse dynamics model which assumed a fixed axis of rotation for the prosthetic foot located at the ankle and a rigid foot segment (Fig. 3.16) (Fey et al., 2011). The experimentally calculated values of mid stance energy return and mid stance energy storage were similar in magnitude and followed a similar trend as stiffness was altered. However, the experimental values of early stance energy storage and late stance energy return were much less than those calculated in this study. The underestimation of early stance energy storage is likely due to not accounting for heel energy that is stored, and the underestimation of energy return is likely due to not accounting for the toe energy that is returned. The experimental estimates of energy storage and return most closely resemble the calculated keel energy storage and return pattern, but with reduced late stance energy return. However, estimating the keel energy storage and return pattern experimentally may be more functionally relevant since we found that prosthetic foot function is largely performed by the keel rather than the heel, and keel function was most influence by altered foot stiffness.

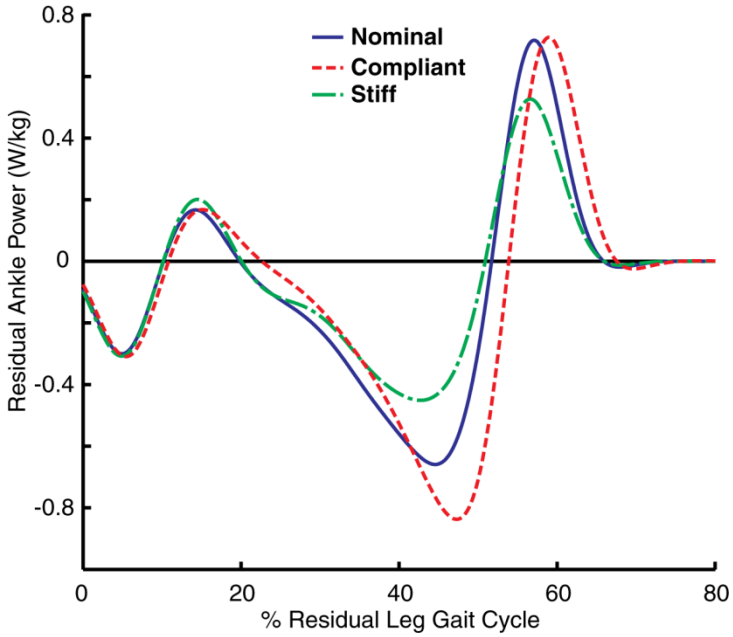

Figure 3.16: Amputee group average residual leg ankle power curves which were calculated experimentally to estimate the prosthetic foot energy storage and return characteristics of the prosthetic feet.

Conclusions and Limitations

In summary, altering ESAR prosthetic foot stiffness can significantly influence prosthetic foot and muscle function of both the residual and intact legs during multiple regions of the gait cycle. Thus, given an amputee's functional deficits, the prescription of ESAR prosthetic feet with appropriate stiffness levels is important and may substantially influence their ability to walk. This study provided much insight into the influence of prosthetic foot stiffness on muscle and prosthetic foot function, and the approach used enabled us to examine the dynamic interactions between the prosthetic foot and musculoskeletal system. These abilities may also prove beneficial in future applications such as fine-tuning of prosthetic foot design characteristics or evaluating prosthetic foot prototypes prior to manufacture. For example, our results suggest that in terms of the

mechanical demand on the prosthetic foot, the highest torques were observed in the ankle region of the prosthetic foot during the second half of stance and nearest the attachment of the heel to the keel following heel-strike during the loading response. But in terms of energy storage and return, the ankle, midfoot nearest the attachment of the heel to the keel, and toe sections all substantially stored and returned energy throughout stance. A limitation of this study was that a 2D walking model was used to study unilateral amputee walking. Increased degrees of freedom may elucidate other compensations as prosthetic foot stiffness is altered or other functional roles of muscles and ESAR prosthetic feet. For example, added frontal plane and transverse plane rotational and translational degrees of freedom of the trunk may highlight other functional roles of increased residual leg GMED activity other than providing increased body and trunk propulsion since it has been shown in previous 3D studies of non-amputee walking that its primary role is to provide support (Anderson and Pandy, 2003). Thus, a promising area of future work is to examine the influence of prosthetic foot stiffness using a 3D model to assess these contributions.

Aim 4: Optimization of Prosthetic Foot Stiffness to Reduce Metabolic Cost and Intact Knee Loading of Below-Knee Amputee Walking

INTRODUCTION

Unilateral below-knee amputees have distinct gait characteristics compared to non-amputees, including bilateral asymmetries (e.g., Sanderson and Martin, 1997), altered residual leg muscle activity (e.g., Winter and Sienko, 1988), increased metabolic cost (e.g., Waters et al., 1976) and reduced walking speed (e.g., Robinson et al., 1977). Amputees also develop disorders such as chronic leg and back pain (Burke et al., 1978; Ephraim et al., 2005; Kulkarni et al., 2005; Smith et al., 1999). Sustained prosthetic use has been linked to joint pain in the intact leg knee that is often associated with osteoarthritis (for review, see Gailey et al., 2008). Of these biomechanical factors that can adversely affect amputee mobility, two of the most prominent are an elevated metabolic cost during walking and the development of joint disorders in the intact knee.

Differences in gait characteristics between amputees and non-amputees are often attributed to the functional loss of the residual leg ankle muscles, which perform important walking subtasks such as generating body support, forward propulsion and leg swing initiation (Neptune et al., 2001). Passive prosthetic devices such as energy storage and return (ESAR) feet have been developed to help improve amputee gait by storing and releasing elastic energy during stance (Hafner et al., 2002a). However, selection of the appropriate prosthetic foot design (e.g., stiffness characteristics) is not well-defined since its influence on prosthetic foot function and biomechanical quantities such as metabolic cost and joint loading (e.g., knee contact forces) are not well-understood. The design of prosthetic feet that reduce metabolic cost and joint loading could provide a considerable advancement in amputee care.

A promising strategy to achieve this goal is to combine design optimization with advanced manufacturing techniques such as selective laser sintering (SLS) to develop novel designs that focus on these important biomechanical quantities. However, an important element to include is the dynamic interactions between the musculoskeletal system and design characteristics of the prosthetic foot to assess how they influence walking performance. One method that includes this element is to use detailed musculoskeletal models and forward dynamics simulations, which have been effective in assessing individual muscle function (e.g., Liu et al., 2006; Neptune et al., 2004) and estimating difficult to measure *in vivo* quantities such as muscle work, metabolic cost and joint contact forces (Neptune and Kautz, 2000; Sasaki et al., 2009; Sasaki and Neptune; Shelburne et al., 2005; Umberger, 2010) during human movement.

The purpose of this study was to couple design optimization of ESAR prosthetic feet with forward dynamics simulations of amputee walking to identify the optimal prosthetic foot designs that improve metabolic cost and joint loading for below-knee amputees. Previously, we showed that altering prosthetic foot stiffness influences the walking mechanics and muscle activity of below-knee amputees (Fey et al., 2011). Therefore, altering prosthetic foot stiffness likely influences the *in vivo* quantities of metabolic cost and joint contact forces. In this study, we focused on optimizing the stiffness characteristics of ESAR prosthetic feet to satisfy specific biomechanical objectives. We hypothesized that optimal prosthetic foot stiffness characteristics exist that minimize metabolic cost and intact knee joint contact forces during amputee walking. To help interpret how changes in these measures influence muscle and prosthetic foot function, an induced acceleration and segment power analysis was performed.

METHODS

Description of the development of the musculoskeletal and prosthetic foot models, simulation analyses, and collection of experimental tracking data are provided below. Further details are described in Appendix A.

Musculoskeletal Model

A planar bipedal musculoskeletal model was used to develop the forward dynamics simulations of unilateral below-knee amputee walking. The model was developed in SIMM/Dynamics Pipeline (MusculoGraphics, Inc.) and was similar to previous studies of amputee and non-amputee walking (e.g., Neptune et al., 2001; Zmitrewicz et al., 2007) (Fig. 4.1).

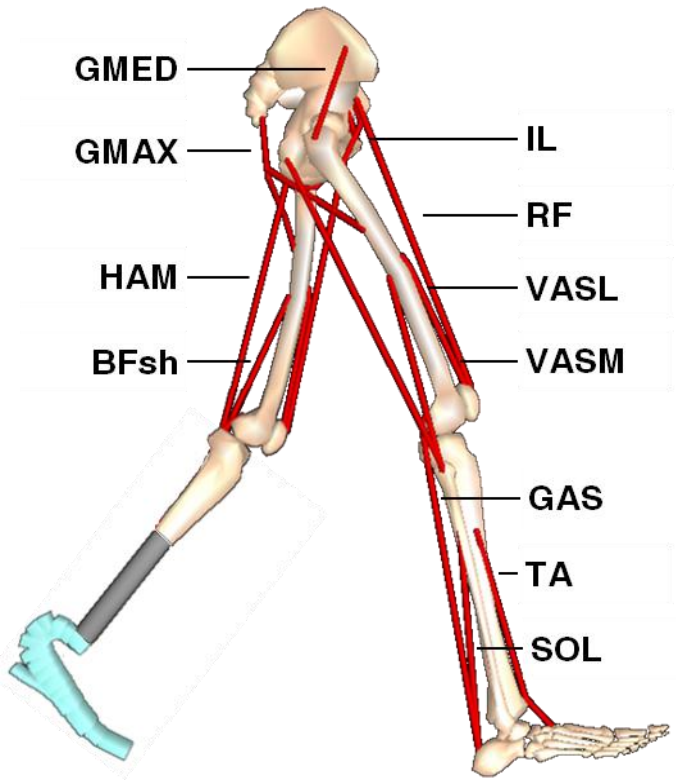

Figure 4.1: Amputee musculoskeletal model. The intact leg was actuated by 25 individual Hill-type musculotendon actuators. These individual actuators were grouped into 14 muscle groups based on anatomical classification with muscles in each group receiving the same excitation pattern. The 14 muscle groups consisted of GMED (anterior and posterior compartments of the gluteus medius), GMAX (gluteus maximus, adductor magnus), HAM (biceps femoris long head, medial hamstrings), BFsh (biceps femoris short head), IL (psoas, iliacus), RF (rectus femoris), VASL (vastus lateralis, vastus intermedius), VASM (vastus medialis), GAS (medial and lateral gastrocnemius), SOL (soleus, tibialis posterior), TA (tibialis anterior, peroneus tertius), PR (peroneus longus, peroneus brevis), FLXDG (flexor digitorum longus, flexor hallucis longus) and EXTDG (extensor digitorum longus, extensor hallucis longus). To improve model visualization, the smaller muscle groups that actuated the foot (PR, FLXDG and EXTDG) are not illustrated. In the amputee residual leg, the same muscle groups were included except for those lost due to modeling a unilateral below-knee amputation (GAS, SOL, TA, PR, FLXDG and EXTDG).

Rigid segments represented the trunk (head, arms and torso) and thigh and shank segments of both legs. In the intact leg foot, rigid segments also represented the talus, calcaneus, mid-foot and toes. The musculoskeletal geometry was based on Delp et al. (1990). The inertial properties of the residual leg shank segment were adjusted (Mattes et al., 2000; Silverman and Neptune, 2011). The trunk had 3 degrees of freedom (2 translations and 1 rotation). In both legs, hip flexion/extension was modeled using revolute joints. A planar joint was used to model the knee joint, with a flexion/extension rotation and the two translational degrees of freedom being prescribed as a function of knee flexion angle. In the intact leg, revolute joints modeled the ankle, subtalar and metatarsophalangeal joints. In the amputated leg, a prosthetic foot model was used (see below). Therefore, excluding the prosthetic foot, the musculoskeletal model had a total of 10 degrees of freedom

Foot-ground contact was modeled using 31 viscoelastic elements with coulomb friction on each foot (Neptune et al., 2000) (for additional details, see Appendix A). Passive torques were applied at each joint representing ligaments, passive tissue, and joint structures (Anderson and Pandy, 1999; Davy and Audu, 1987). Equations of motion were generated using SD/FAST (PTC).

Musculotendon Actuators

Each Hill-type actuator consisted of a contractile element representing the active muscle fiber, series elastic element representing the tendon, and parallel elastic element representing the passive fiber stiffness (for additional details, see Appendix A). Similar to previous work (Hall et al., 2011), excitation patterns of each actuator were defined using a bimodal pattern defined as:

$$e(t) = \sum_{i=1}^{2} \begin{cases} \frac{a_i}{2}\left[1 - \cos\left(\frac{2\pi(t-onset_i)}{offset_i - onset_i}\right)\right], onset_i \le t \le offset_i \\ 0 \qquad\qquad\qquad\qquad , otherwise \end{cases}$$

where excitation magnitude e(t) was a function of time (t) and amplitude (a_i), onset ($onset_i$), and offset ($offset_i$) of each mode (i). Thus, six parameters (two onsets, offsets and magnitudes) defined the excitation pattern of each muscle group. Muscle contraction dynamics were governed by force-length, force-velocity, and tendon force-strain relationships (Zajac, 1989). Activation-deactivation dynamics were modeled by a first-order differential equation (Raasch et al., 1997). Muscle activation and deactivation time constants were derived from Winters and Stark (1988). For those muscles not included in Winters and Stark (1988), nominal activation and deactivation time constants of 12 and 48 ms were used.

Energy Storage and Return Prosthetic Foot Model

The prosthetic foot model consisted of 22 rigid segments. Each segment and the overall prosthetic shape were defined by two spline curves which represented the keel and heel sections (Fig. 4.2, for additional details, see Appendix A). The keel and heel shapes were defined using 15 and 9 spline points, respectively. This shape was used since it closely matched the shape of the widely prescribed commercial carbon fiber ESAR foot and was previously used to generate prototypes of the SLS ESAR foot (South et al., 2010). The prosthetic foot model had a total of 18 degrees of freedom (13 keel and 5 heel single degree of freedom revolute joints, Fig. 4.2).

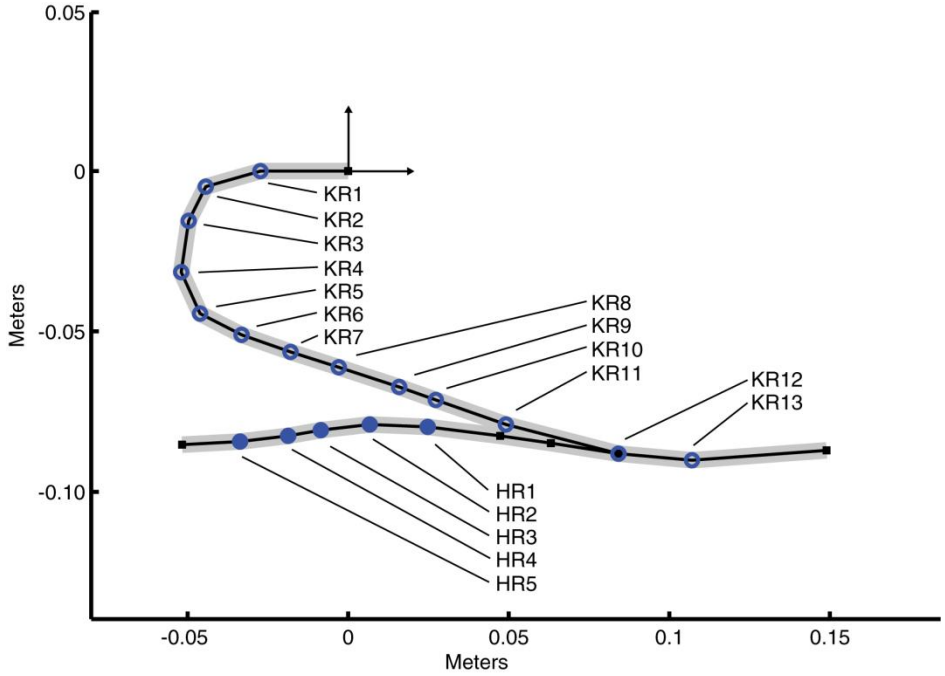

Figure 4.2: Schematic of prosthetic foot model consisting of 22 rigid segments connected in series. The prosthetic foot model had 13 keel (KR1-KR13, ○) and 5 heel (HR1-HR5, ●) rotational degrees of freedom.

Prosthetic Foot Stiffness

Foot stiffness was modeled using viscoelastic elements at each rotational degree of freedom in the prosthetic foot model that applied a passive torque:

$$\tau_i = -k_i \cdot \theta_i - b \cdot \dot{\theta}_i$$

The passive torque (τ_i) applied at each rotational degree of freedom (i) was a function of element stiffness (k_i), angular displacement (θ_i) and angular velocity ($\dot{\theta}_i$). A damping value b=5.73 N*m*s (for derivation, see Appendix A) was used.

Metabolic Cost and Joint Contact Forces

The metabolic cost model was based on previous work (Umberger et al., 2003; Umberger, 2010) and included both mechanical and thermal energy expenditures. The rate of energy liberated for a given muscle ($\dot{E}$) was computed as the sum of activation heat rate ($\dot{h}_A$), maintenance heat rate ($\dot{h}_M$), shortening/lengthening heat rate ($\dot{h}_{SL}$), and mechanical work rate ($\dot{w}_{CE}$) of the contractile element in the Hill-type muscle model. Activation heat rate represents energy expended when a muscle is activated. Maintenance heat rate represents energy expended to maintain a contraction. Shortening/lengthening heat rate represents the heat produced during a muscle's shortening and lengthening. Mechanical work rate ($\dot{w}_{CE}$) was calculated as the product of the contractile element's force and velocity. Total energy consumption during the simulations was calculated by the time integral of the rate of energy liberated over the gait cycle as:

$$\dot{E} = \dot{h}_A + \dot{h}_M + \dot{h}_{SL} + \dot{w}_{CE}$$

In addition, knee tibio-femoral and hip contact forces were calculated based on the intersegmental forces and compressive forces due to muscles spanning the joint by SD/FAST.

Dynamic Optimization

A simulated annealing optimization algorithm (Goffe et al., 1994) within a dynamic optimization framework (Fig. 4.3) was used to generate simulations of amputee walking. Three simulations were performed in which prosthetic foot stiffness, muscle excitation parameters and initial generalized velocities were optimized to reproduce group average amputee experimental data while 1) minimizing metabolic cost, 2)

minimizing intact knee loading (peak axial knee contact force and axial knee contact force impulse), and 3) minimizing metabolic cost and intact knee loading.

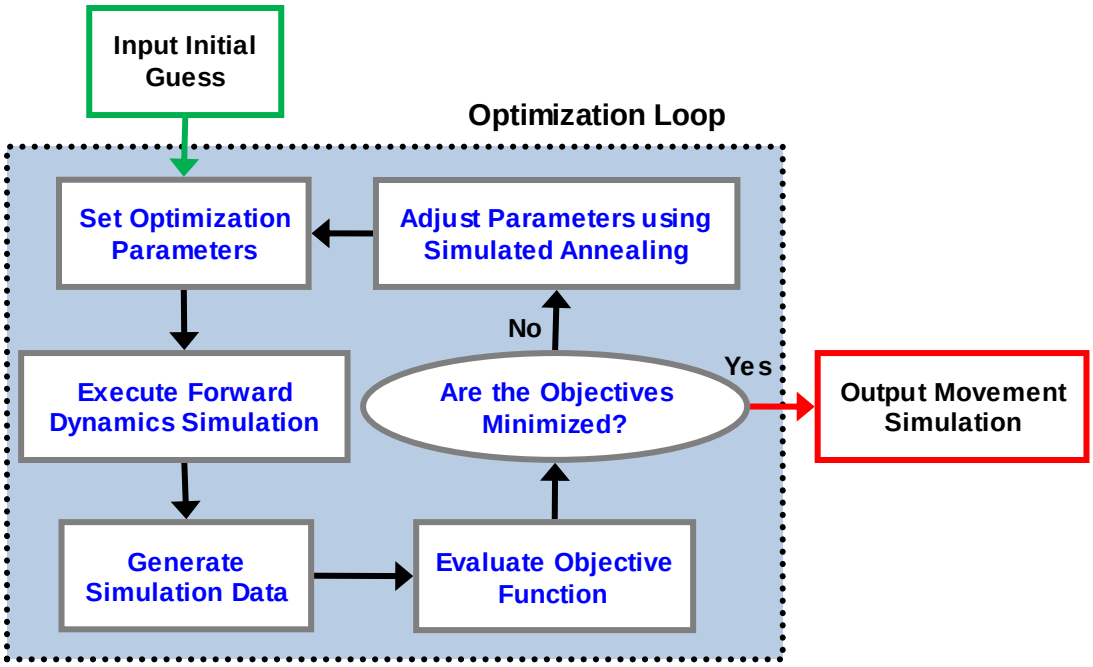

Figure 4.3: Optimization framework used to generate simulations of amputee walking.

To use as an initial guess for prosthetic foot stiffness, a nominal stiffness distribution was calculated based on the SLS ESAR foot. Each prosthetic foot segment was assumed to be a prismatic beam element and made from sintered Nylon 11 powder using SLS. The rotational stiffness of each element (KR1-KR13 and HR1-HR5, Fig. 4.4) was calculated as follows:

$$k_i = \frac{E \cdot I_i}{L_i}$$

The rotational stiffness (k_i) was a function of the Young's modulus of the sintered Nylon 11 powder used to manufacture the SLS ESAR prosthetic foot (E=1.4 GPa), segment length (L_i) and area moment of inertia for a rectangular cross-section (I_i). In the optimization framework, prosthetic foot stiffness distribution was altered by four scale factors, which independently scaled the ankle (KR2-KR7), mid-foot (KR8–KR11) and toe (KR12 and KR13) sections of the keel in addition to the heel (HR1-HR5). Initial guesses for each prosthetic scale factor (ankle, mid-foot, toe and heel sections) were set to 1.0.

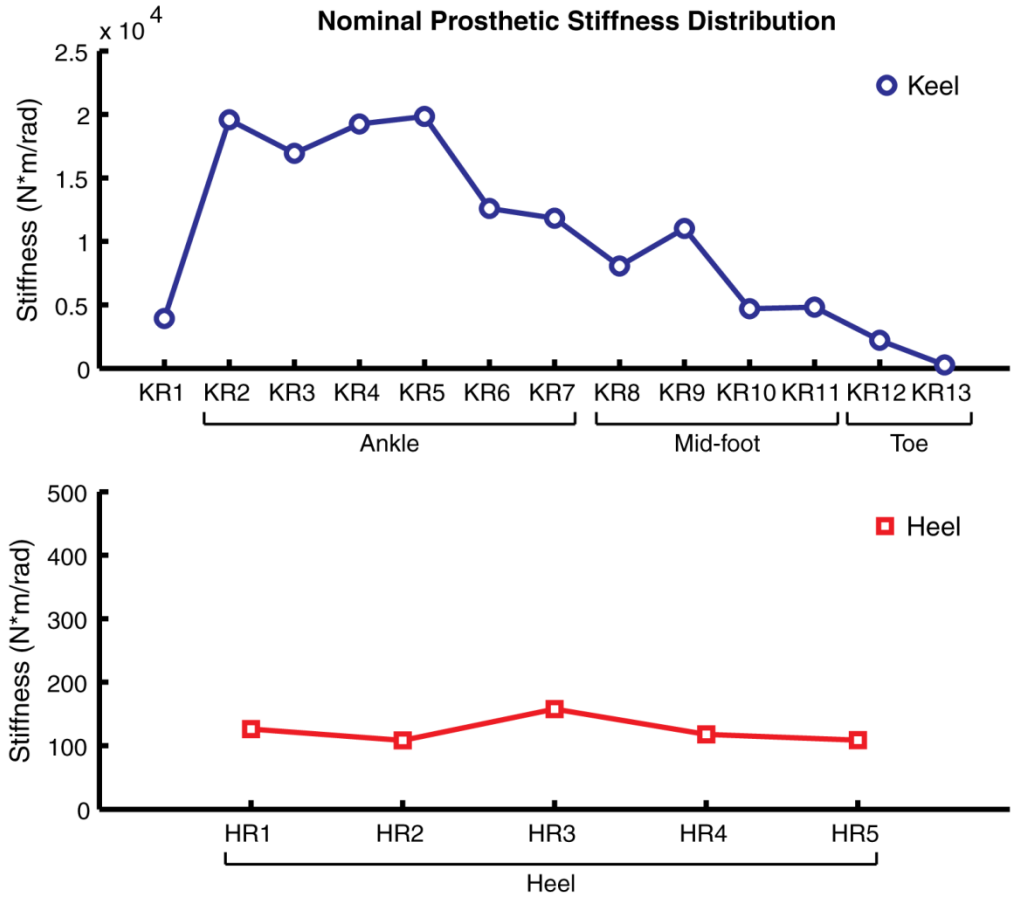

Figure 4.4: Nominal prosthetic foot stiffness distribution calculated from the SLS ESAR foot. The stiffness distribution was optimized using four scale factors which modified the ankle, mid-foot, toe and heel stiffnesses, independently. KR1 stiffness was constant to model constant geometry of the two proximal prosthetic foot segments, which are required to attach to the pylon.

Muscle and Prosthetic Foot Function

To compare differences in muscle and prosthetic foot function between the simulations, individual muscle and prosthetic foot contributions to the walking subtasks of forward propulsion, support and leg swing initiation (Neptune et al., 2001; Neptune et al., 2004; Neptune et al., 2008) were calculated using an induced acceleration and segment power analysis (Fregly and Zajac, 1996) (for additional details, see Appendix

A). To quantify each muscle's contribution and the contribution of the prosthetic foot to forward propulsion, their contributions to the horizontal propulsion/braking of the body (i.e., acceleration of the center-of-mass, anterior/posterior, A/P, GRF) and horizontal power of the trunk segment were calculated. Similarly for support, their contributions to the vertical support of the body (i.e., vertical GRF) and vertical power of the trunk segment were calculated. Both body and trunk braking/propulsion and support were examined because muscular contributions to these subtasks can differ (e.g., SOL and GAS) (Neptune et al., 2001). Thus, altering stiffness may influence the prosthetic foot contributions to these subtasks in different ways. To quantify each muscle's contribution and the contribution of the prosthetic foot to swing initiation, the induced power delivered to the residual leg was calculated.

Experimental Tracking Data

To provide tracking data for the dynamic optimization, experimental data of amputees walking with the SLS ESAR foot were collected. Subjects provided informed consent to an Institutional Review Board approved protocol and included 12 unilateral, below-knee amputees (10 traumatic, 2 secondary illness; 12 males; 52 ± 17 years; 183.0 ± 34.9 lbs; 70.2 ± 2.5 in.). Each subject walked along a 10-m walkway at 1.2 (±0.06) m/s. Bilateral kinematic marker data (Silverman et al., 2008) were measured at 120 Hz using an eight-camera motion capture system (Vicon, Oxford Metrics, Inc.), and GRF data were measured at 1200 Hz using four embedded force plates (Advanced Mechanical Technology, Inc.). Subjects walked with a previously developed custom SLS ESAR prosthetic foot (South et al., 2010) that closely matched the stiffness and response of a widely prescribed commercial carbon fiber ESAR foot (Highlander^{TM}, FS 3000, Freedom Innovations, LLC). The SLS ESAR foot (Fig. 4.5) was manufactured from Rilsan^{TM} D80

(Nylon 11, Arkema, Inc.) using a Vanguard HiQ Sinterstation (3D Systems, Inc.). Repeated trials were collected until at least five step-to-step force plate contacts per foot were measured. Surface EMG were recorded from the intact leg tibialis anterior, soleus, medial gastrocnemius, and bilaterally from the vastus medialis, rectus femoris, biceps femoris long head, gluteus maximus and gluteus medius (2, 10-mm disposable self-adhesive Ag/AgCl sensor contacts, 16-mm interelectrode distance; TeleMyo 900, Noraxon U.S.A., Inc.). For additional details regarding the collection of experimental tracking data, see Appendix A.

Figure 4.5: ESAR prosthetic foot fabricated using SLS additive manufacturing technology that was worn during the amputee walking trials.

RESULTS

Minimization of Metabolic Cost and Intact Knee Contact Force

The optimizations for minimizing only metabolic cost (MetE) and only intact knee contact force (JCont) successfully reduced each objective (Table 4.1) and the combined optimization for minimizing both metabolic cost and intact knee contact force (JCont+MetE) reduced both objectives, which were comparable in magnitude to the other two optimizations that individually-minimized their magnitudes. While the optimized

stiffness scale factors varied, there were notable similarities in the stiffness scale factors for optimizations that consisted of reducing the same objective (Table 4.1). Optimizations to reduce metabolic cost reduced ankle stiffness by approximately the same amount, and all optimizations increased mid-foot stiffness. However, mid-foot stiffness was increased less when reducing metabolic cost and increased most when minimizing intact knee contact force. Minimizing only metabolic cost reduced toe stiffness, while minimizing intact knee contact force increased toe stiffness. All optimizations reduced heel stiffness. Across all simulations, the prosthetic deflections observed in the simulations were similar, but were also consistent with the optimized stiffness distributions (Fig. 4.6). For example, the simulation for minimizing metabolic cost experienced the largest toe deflections due to its reduced stiffness compared to the other two simulations.

Table 4.1: Metabolic cost and intact knee (right knee) contact force objectives. Minimizing intact knee contact force sought to minimize the peak magnitude and impulse (computed over the entire gait cycle) of the axial component of the right knee contact force. Also included in this table are the optimized scale factors which varied the prosthetic foot stiffness distribution. Shaded regions in the table highlight similarities in metabolic cost and intact knee contact force objectives as well as optimized scale factors.

	Min(MetE)	Min(JCont+MetE)	Min(JCont)
Metabolic Cost (J)	307	315	481
Intact Knee Imp. (N*s)	1389	1130	1062
Intact Knee Peak (N)	3473	2424	2480
Prosthetic Ankle Scale	0.81	0.83	1.07
Prosthetic Mid-Foot Scale	1.86	1.88	1.97
Prosthetic Toe Scale	0.5	1.99	1.83
Prosthetic Heel Scale	0.5	0.55	0.5

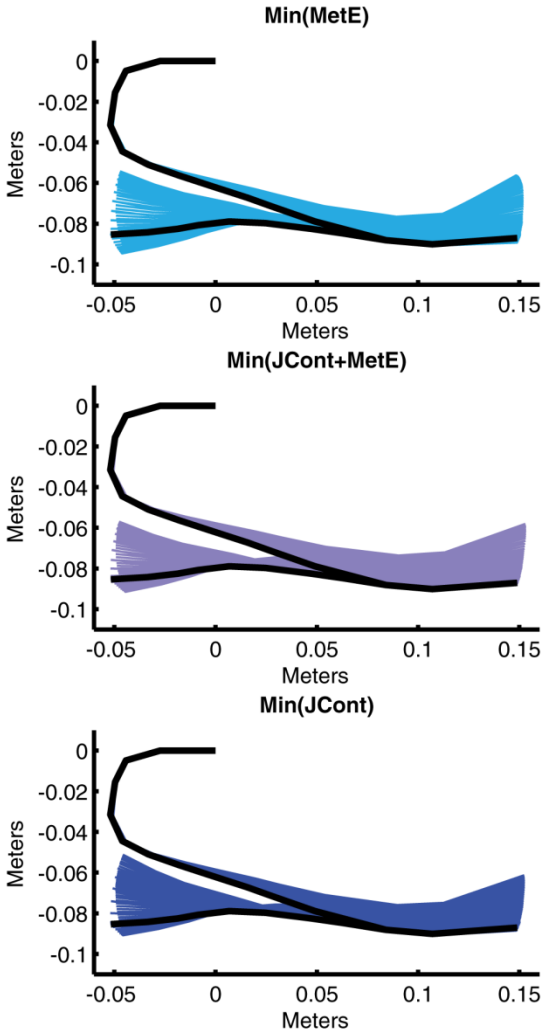

Figure 4.6: Prosthetic foot shape deformations throughout each of the three amputee walking simulations. The undeformed shape (solid black line) is plotted on top of the prosthetic foot shape for each time step of the simulations. Colored lines indicate the prosthetic foot shapes.

Experimental Tracking Data

Despite the altered stiffness distributions of the prosthetic feet, each simulation produced movements that were similar to the collected experimental data of the amputees walking with the nominal stiffness SLS ESAR prosthetic foot (Fig. 4.7). This was most

true of the optimization for minimizing only metabolic cost. Across simulations, average root-mean-square kinematic joint angle and ground reaction force tracking deviations were 8.9 degrees and 0.09 GRF/BW, respectively. These deviations were nearly within 2 standard deviations of the experimental data, which were 9.0 degrees and 0.08 GRF/BW. For the optimizations that minimized intact knee loading, reductions from the nominal tracking data of the intact leg vertical and A/P braking GRF were observed during the first half of intact leg stance, which were consistent with offloading the intact leg. For the muscle groups in which experimental EMG data were collected while using the nominal SLS ESAR prosthetic foot, the optimized excitation patterns were active during regions of the gait cycle when these muscles were shown to be active (Fig. 4.8).

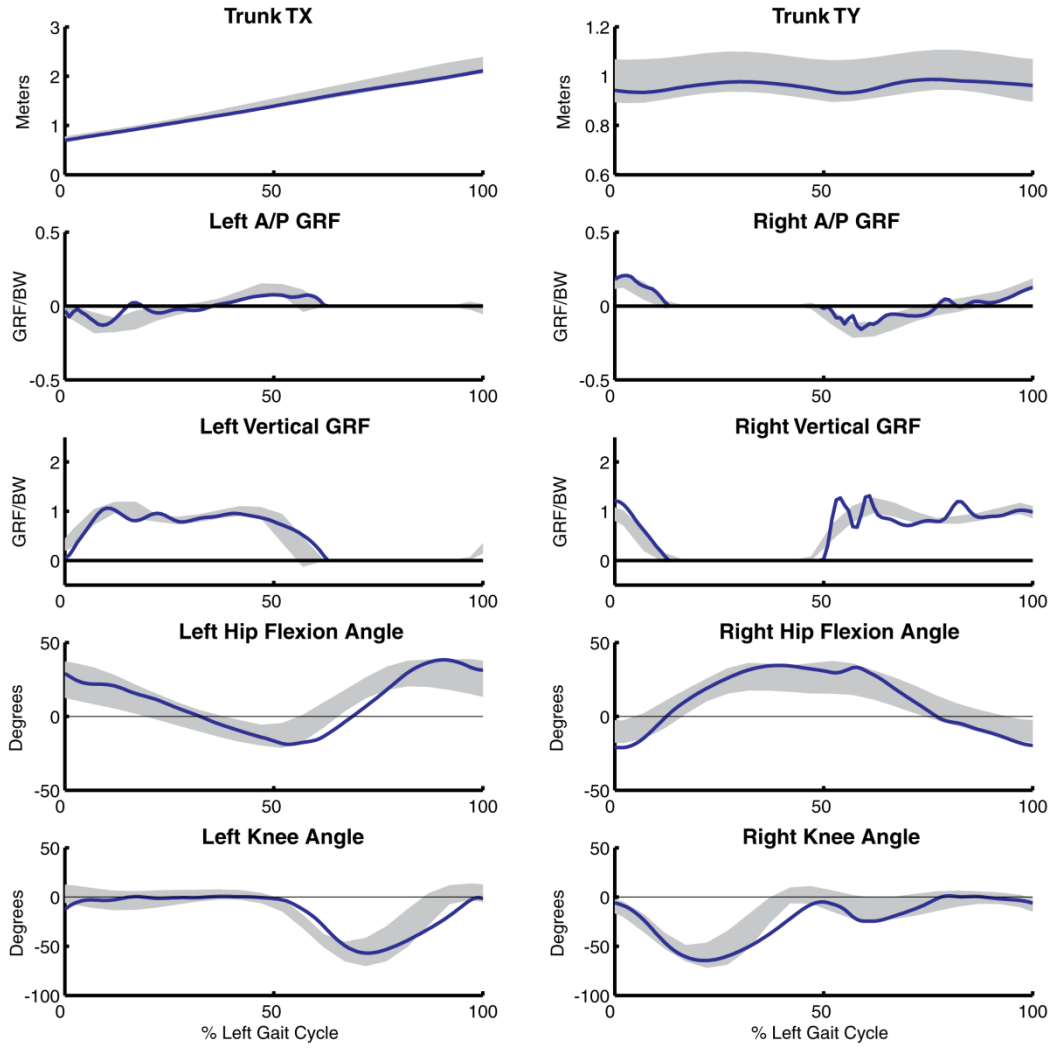

Figure 4.7: Representative simulation tracking comparison from the amputee walking simulation for minimizing metabolic cost. Simulated data (blue) are plotted with experimental tracking data of the amputees walking with the SLS ESAR foot (gray, ± 2 SD). For tracking comparisons of the other amputee walking simulations see Appendix C.

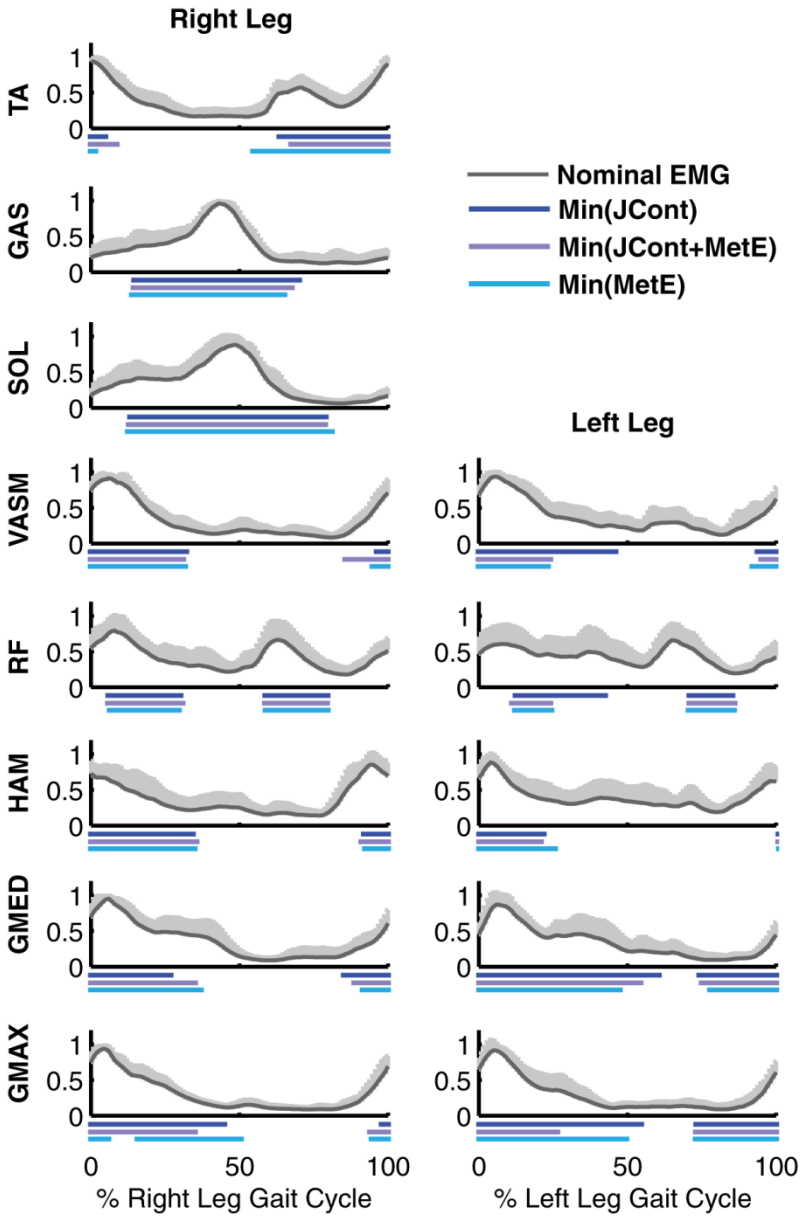

Figure 4.8: Comparison of simulation excitation timing (plotted below each x-axis) with group average experimental EMG data (+1 SD) of amputee subjects walking with the SLS ESAR foot (only those muscles in which EMG data were collected are plotted).

Individual Joint Contact Forces and Muscle Metabolic Cost

In the simulations for minimizing the intact (right leg) knee axial force, intact knee A/P contact force was reduced (Fig. 4.9). However, small increases of the intact hip axial and A/P contact force during the same region of the gait cycle were observed. In the simulation for minimizing only intact knee axial force, increased residual (left leg) knee and hip axial forces were observed. In the simulations for minimizing metabolic cost, several residual leg muscles showed decreases in metabolic cost (VAS, HAM, GMED, GMAX and IL, Fig. 4.10). However, there were also several muscles of the intact leg that experienced reductions of metabolic cost (TA, HAM, GMED, IL) in these simulations. Although, intact leg VAS and GMAX did not experience consistent increases or decreases in metabolic cost, these muscles also showed substantial changes in their metabolic cost profiles across simulations.

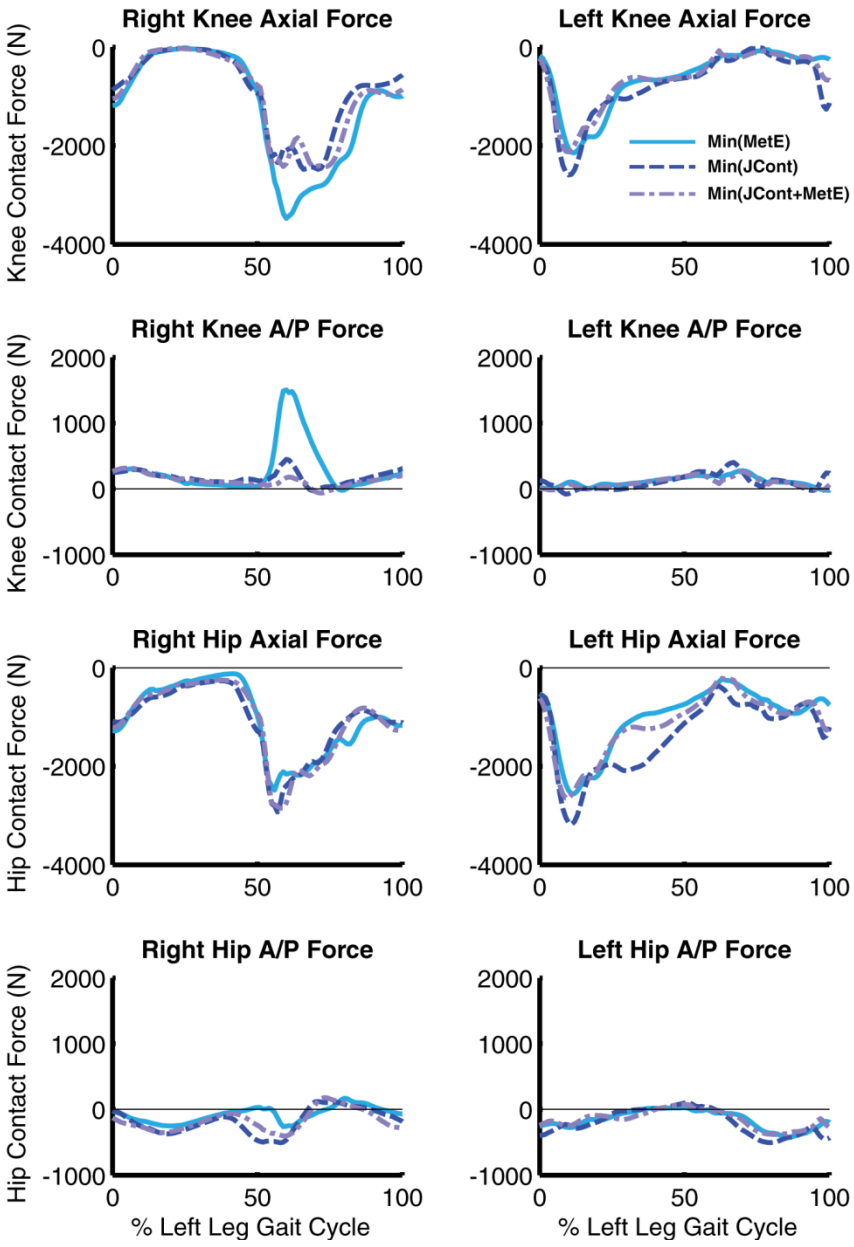

Figure 4.9: Intact (right leg) and residual (left leg) knee and hip contact forces for each walking simulation. For each joint, forces are expressed in the distal segment reference frame and represent the force of the proximal segment on the distal segment. For example, the right knee axial force is expressed in the right tibia reference frame and represents the force of the right femur on the right tibia. Segment reference frames are defined to be positive in the vertical axial direction and positive in the anterior horizontal direction. The total body weight of the model was 715 N.

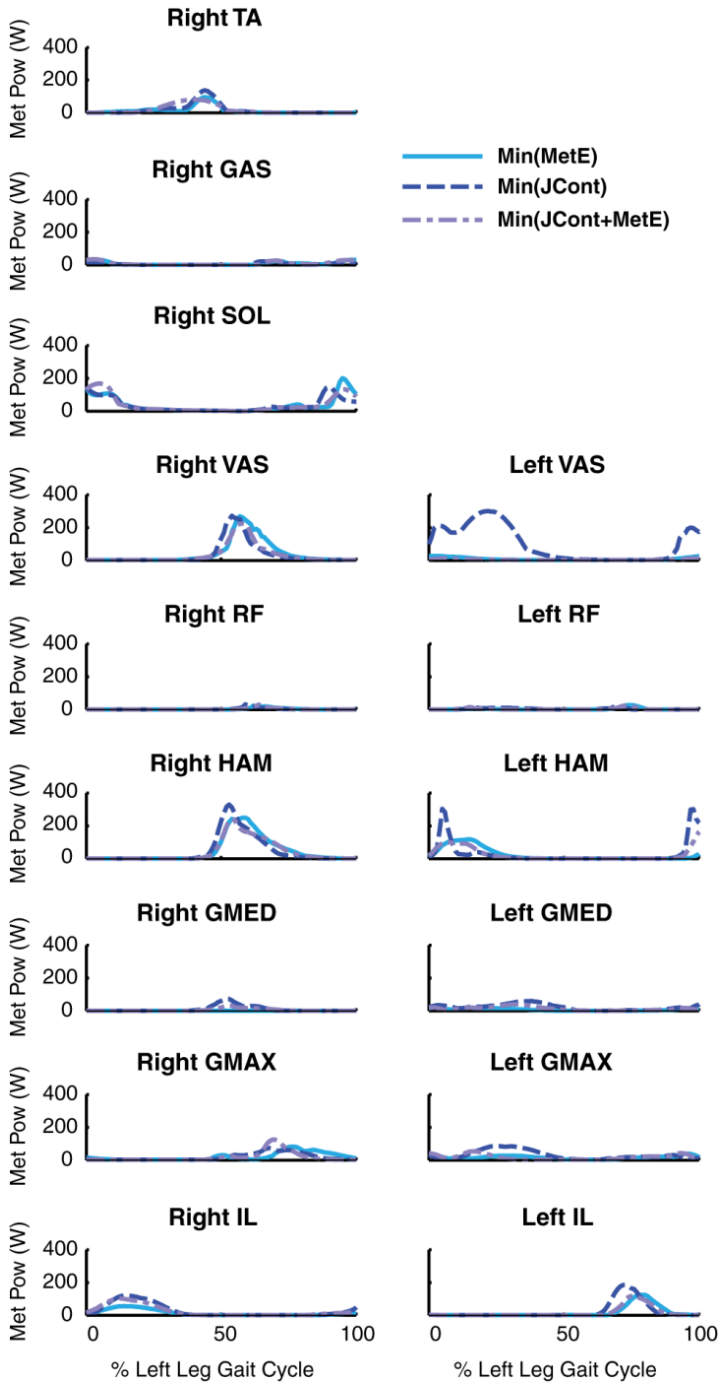

Figure 4.10: Individual muscle group metabolic cost profiles of intact (right leg) and residual (left leg) muscle groups. These data are limited to those muscle groups which had the largest metabolic costs. All others had minimal values. For analyses, metabolic cost of VASL and VASM muscles were summed (VAS). For the total metabolic cost profiles, see Appendix C.

Contributions to Residual Leg Walking Ground Reaction Forces

During the first half of residual leg stance, in the simulations for minimizing metabolic cost, the keel provided more braking and support of the body, and muscles provided less body propulsion (Figs. 4.11A and 4.11C). In contrast, in the simulation for minimizing only intact knee contact force, the keel provided less braking and support of the body, while the heel provided more braking and support (Figs. 4.11A and 4.11C).

During the second half of residual leg stance, for minimizing only metabolic cost, the keel provided less body propulsion, while gravity provided small increases in propulsion (Fig. 4.11B). For minimizing only intact knee contact force, the keel provided a moderate amount of propulsion and muscles provided more propulsion. For minimizing both objectives, the keel provided the most propulsion and support, while gravity and muscle contributions to these tasks were moderate (Figs. 4.11B and 4.11D).

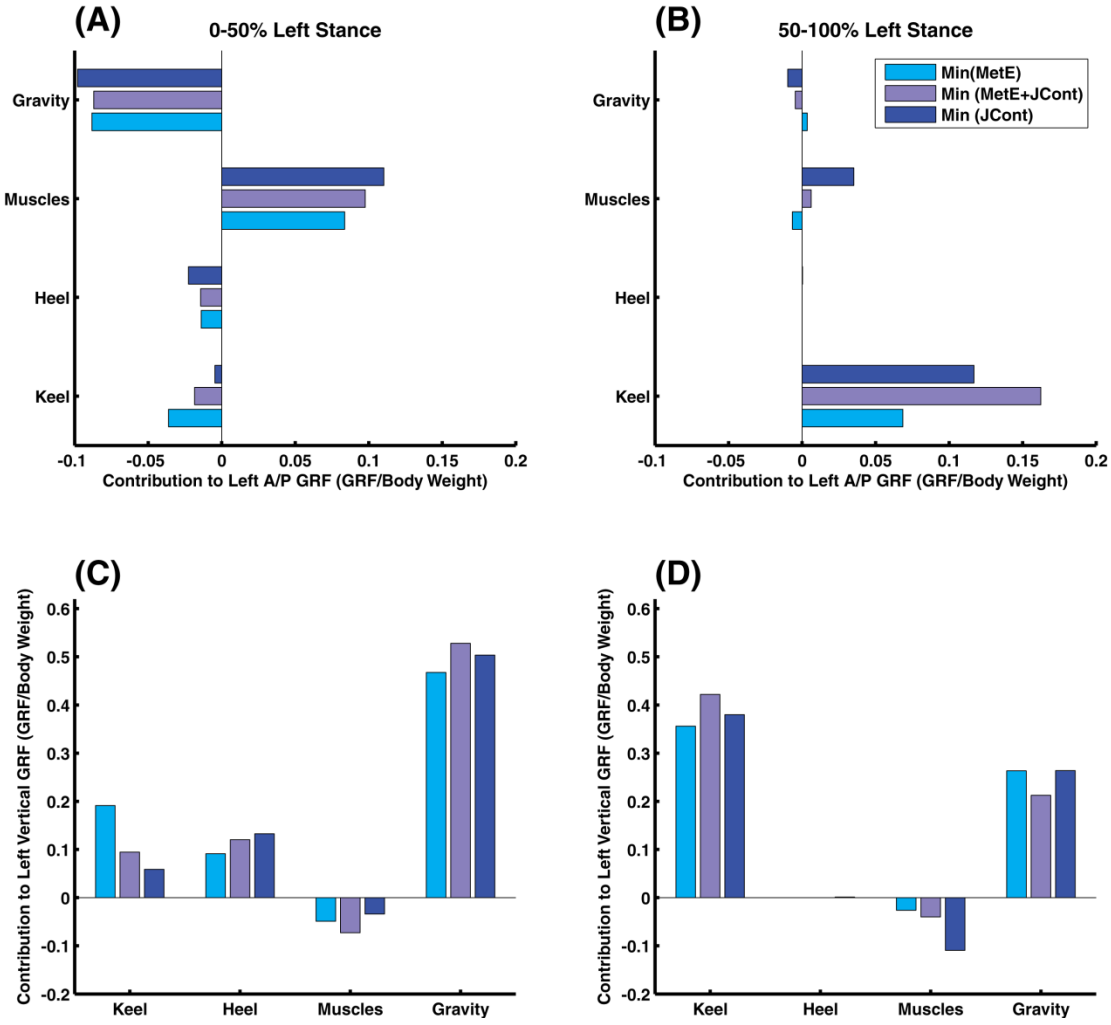

Figure 4.11: Contributions of the prosthetic keel and heel, muscles (left and right legs), and gravity to residual leg A/P and vertical ground reaction forces during the first (left column) and second (right column) halves of residual leg stance.

Individual Muscle Contributions to Walking Ground Reaction Forces

In the simulations for minimizing intact knee contact force during both halves of stance, the residual leg GMED and GMAX increased their contributions to body propulsion, while residual leg RF had small increases in its contribution to braking (Figs.

4.12A and 4.12B). In the simulation for minimizing only metabolic cost, during the first half of stance the residual HAM increased its contribution to propulsion and decreased its contribution to body support (Figs. 4.12A and 4.12C).

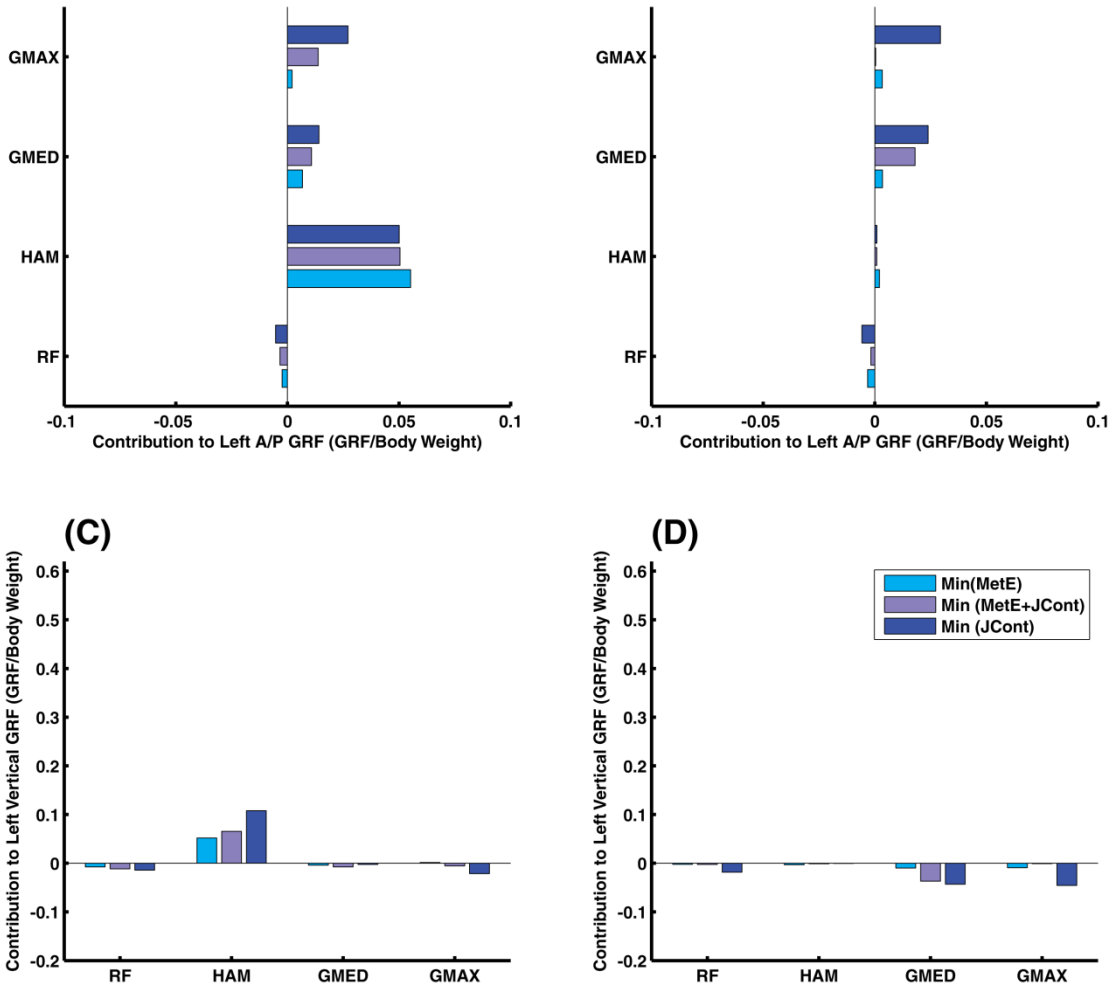

Figure 4.12: Mean individual residual (left leg) muscle contributions to A/P and vertical GRF of the residual leg. Data are averaged during the first (left column) and second (right column) halves of residual (left leg) stance.

During the first half of intact leg stance in all three simulations, the intact leg RF, VAS, GAS and SOL provided body braking, while HAM provided body propulsion (Fig. 4.13A). The intact leg RF, VAS and HAM contributions to body braking and propulsion during this region followed consistent trends in which the simulation for minimizing only metabolic cost had the largest contributions, the simulation for minimizing only intact knee contact force had the second largest contributions, and the simulation for minimizing both objectives had the smallest contributions (Fig. 4.13A). Also during the first half of intact leg stance in all three simulations, the intact leg GMED, HAM, VAS, GAS and SOL had the highest contributions to body support (Fig. 4.13C). In the simulations for minimizing intact knee contact force, GMED and SOL increased their contributions. In the simulation for minimizing both objectives, the contribution of VAS to body support was largely reduced, and the contribution of HAM was largely increased. In contrast, in the simulation for minimizing only metabolic cost, the contribution of intact VAS to body support was largely increased (Fig. 4.13C).

During the second half of intact leg stance, the primary contributors to body propulsion and support were SOL and GAS (Figs. 4.13B and 4.13D). For minimizing only intact knee contact force, GAS contributions to support and propulsion were reduced, while SOL contributions increased. For minimizing both objectives, SOL contributions to propulsion and support decreased.

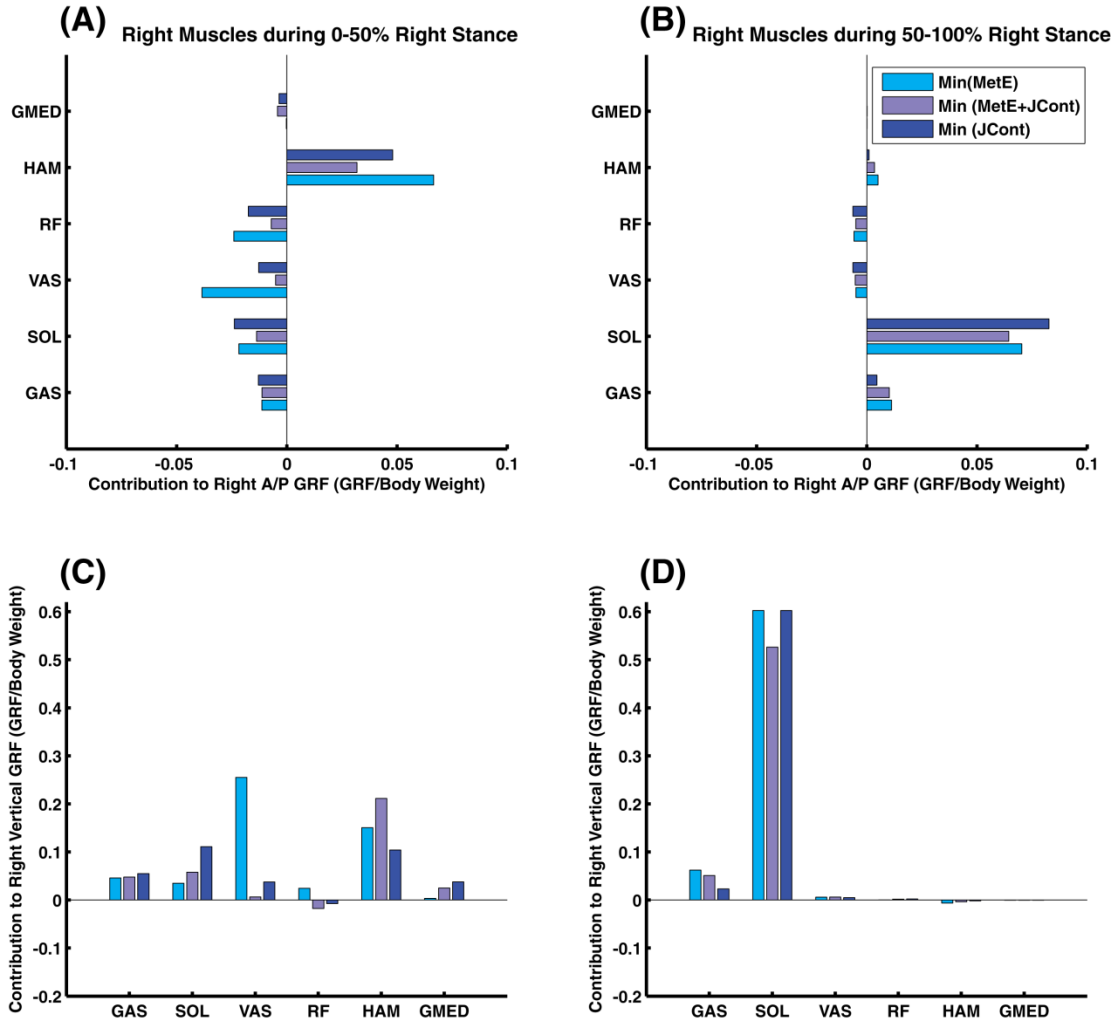

Figure 4.13: Mean individual intact (right leg) muscle contributions to A/P and vertical GRF of the intact leg. Data are averaged during the first (left column) and second (right column) halves of intact (right leg) stance. Contributions of VASL and VASM were summed (VAS) for these analyses.

Prosthetic and Muscular Contributions to Trunk Propulsion and Support

In all three walking simulations, the prosthetic heel had negligible contributions to trunk power. However, considerable differences were observed in the prosthetic keel (Fig. 4.14). During the first half of residual leg stance, the prosthetic keel decreased its

contributions to trunk braking and support in the simulation when minimizing both objectives (Figs. 4.14A and 4.14D). In contrast, during the second half of residual leg stance, the prosthetic keel increased its contributions to trunk propulsion and support when minimizing both objectives (Figs. 4.14B and 4.14E).

Also during the first half of residual leg stance, the intact leg SOL decreased its contribution to trunk propulsion when minimizing both objectives (Fig. 4.15A). In the simulations for minimizing intact knee contact forces, residual leg GMED, GMAX and RF had small increases in their contributions to trunk propulsion during both halves of stance (Figs. 4.14A and 4.14B).

For trunk support during the second half of residual leg stance and swing of the residual leg, the intact leg VAS and HAM showed the largest changes across simulations (Figs. 4.15E and 4.15F). For minimizing only metabolic cost, intact VAS largely increased its contribution to support. But for minimizing both objectives, VAS greatly decreased its contribution to support. In contrast, HAM decreased its contributions to support for minimizing only metabolic cost and greatly increased its contribution to support for minimizing both objectives. In the simulations for reducing intact knee contact force, small increases in the contributions of the intact GMED and GMAX to trunk support were observed during the second half of stance (Fig. 4.15E).

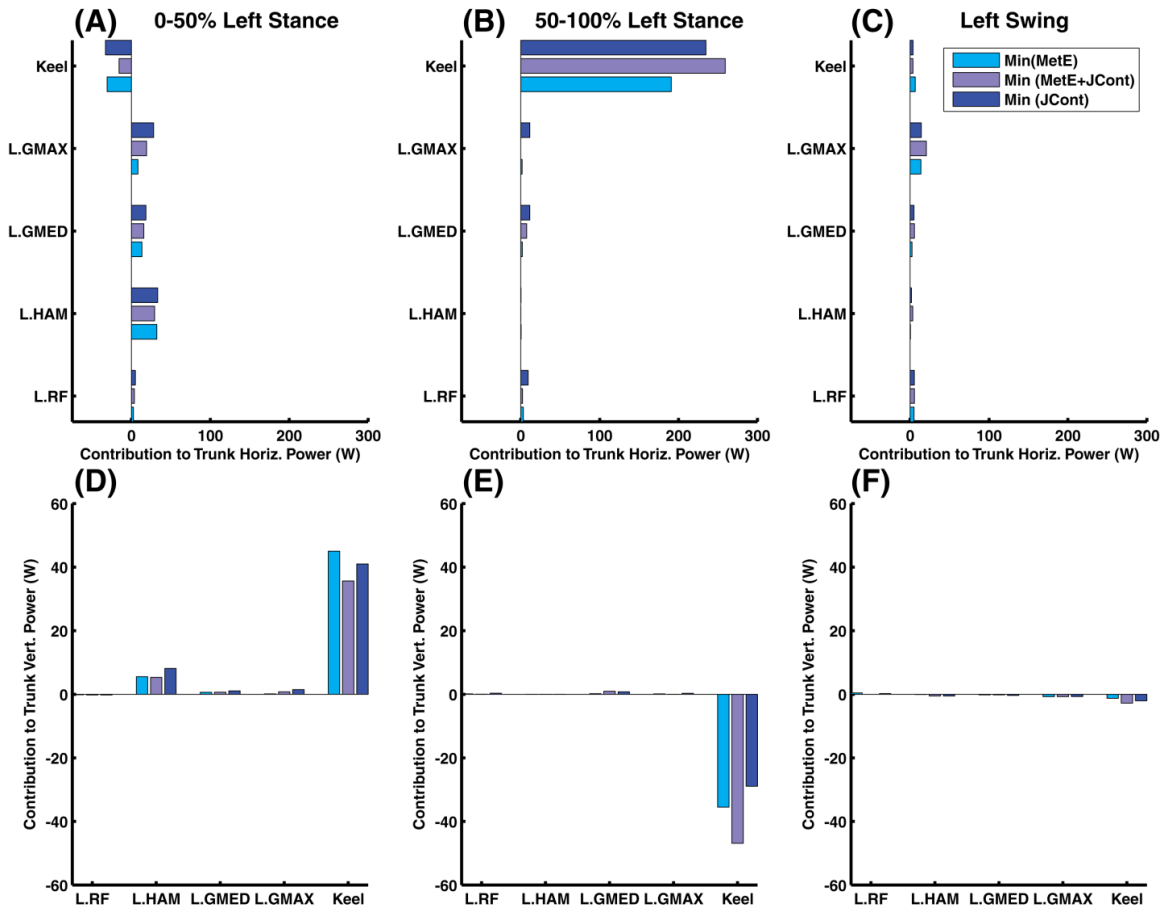

Figure 4.14: Mean prosthetic foot and residual (left leg) muscle contributions to horizontal (top row) and vertical (bottom row) power delivered to the trunk. Data are averaged during the first (left column) and second (middle column) halves of residual (left leg) stance and swing (right column).

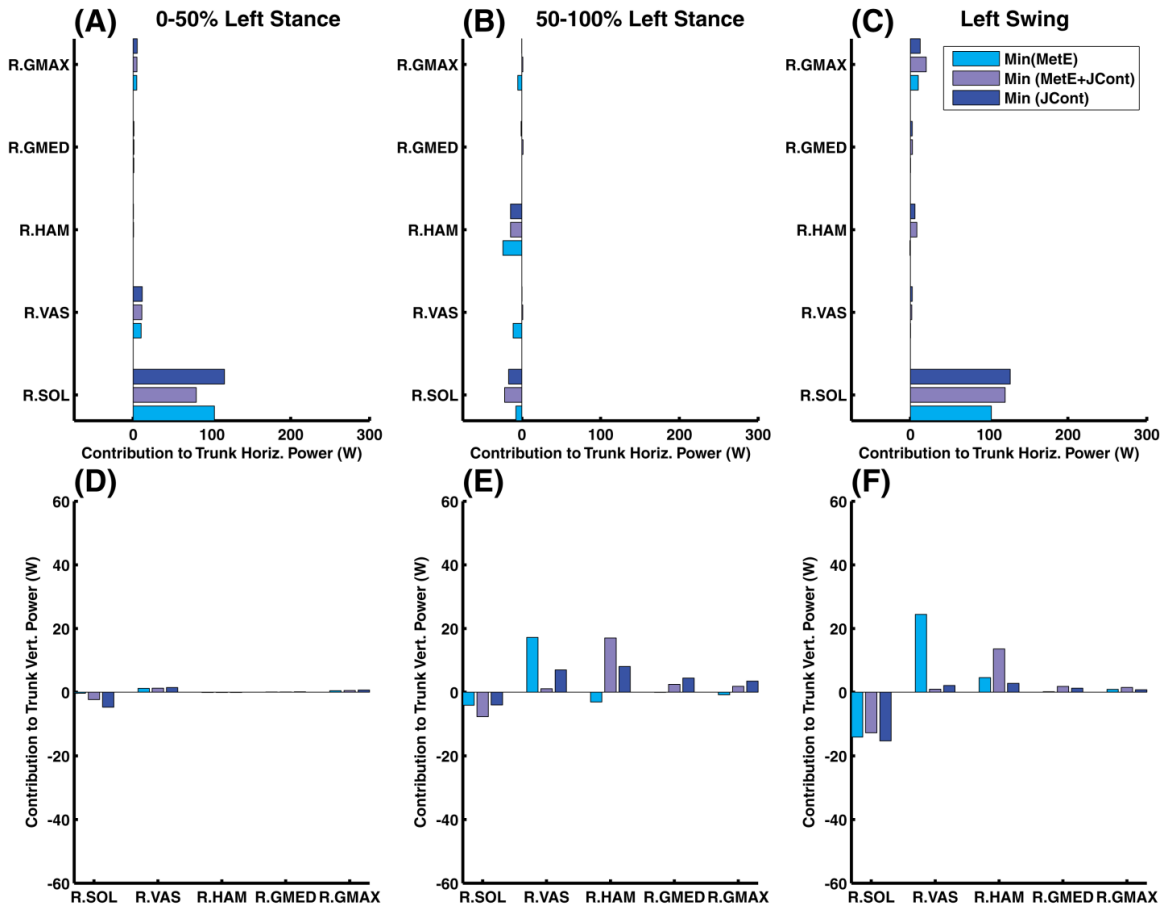

Figure 4.15: Mean intact (right leg) muscle contributions to horizontal (top row) and vertical (bottom row) power delivered to the trunk. Data are averaged during the first (left column) and second (middle column) halves of residual (left leg) stance and swing (right column).

Prosthetic and Muscular Contributions to Residual Leg Power

Across simulations, the largest differences in power delivered to the residual leg occurred during the second half of stance (Fig. 4.16B). In the simulation for minimizing only metabolic cost, the prosthetic keel absorbed much less energy from the residual leg. In the simulations for minimizing intact knee contact force, the keel absorbed much greater energy from the residual leg. In the simulation for reducing only intact knee

contact force, residual GMED, GMAX and RF absorbed more energy from the leg. For minimizing both objectives, the residual leg RF absorbed the least amount of energy from the leg. Lastly, in the simulation for minimizing only intact knee contact force during swing, the residual leg IL delivered more energy to the leg (Fig. 4.16C).

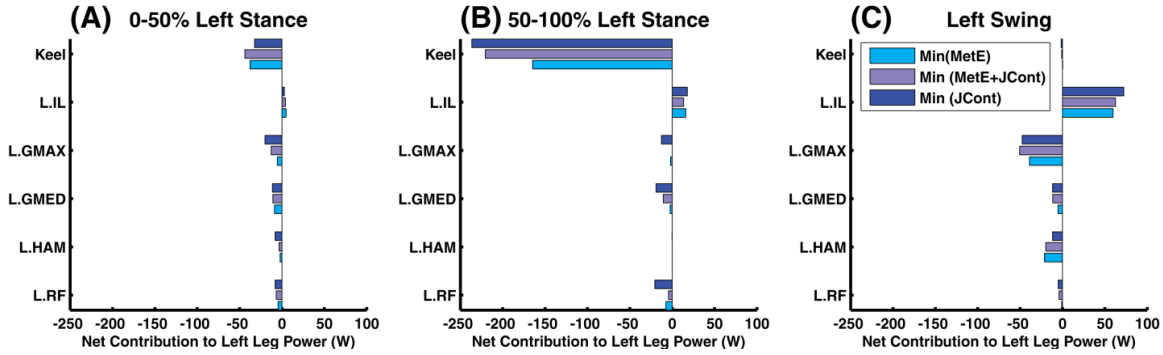

Figure 4.16: Mean prosthetic foot and individual muscle contributions to total power delivered to the leg. Data are averaged during the first (left column) and second (middle column) halves of residual (left leg) stance and swing (right column).

DISCUSSION

The purpose of this study was to couple design optimization of ESAR prosthetic feet with forward dynamics simulations of amputee walking in order to identify optimal prosthetic foot designs. We hypothesized that optimal prosthetic foot stiffness characteristics exist that minimize metabolic cost and intact knee joint contact forces. Integrating prosthetic foot design optimization with forward dynamics simulations enabled us to not only examine the performance of ESAR prosthetic foot designs, but also the interactions between prosthetic foot and muscle contributions to essential walking subtasks. The results of this study showed that there are optimal prosthetic foot stiffness characteristics for unilateral below-knee amputees that minimize metabolic cost

and intact knee contact forces. However, there were interesting tradeoffs in prosthetic foot and muscle function.

Reducing Metabolic Cost

When minimizing only metabolic cost, reducing ankle stiffness and toe stiffness while increasing mid-foot stiffness was the optimal prosthetic keel design. This decreased the total muscle contributions to residual leg body braking and propulsion throughout residual leg stance, decreased the prosthetic keel contribution to body and trunk propulsion during the second half of stance, and increased the contribution of gravity to body propulsion during the second half of stance. However, minimizing only metabolic cost increased the dependence on the prosthetic keel during the first half of residual leg stance for body support, and increased intact leg VAS contributions to body and trunk support during the second half of residual leg stance. Also, the prosthetic keel absorbed much less energy from the residual leg during the second half of stance, thus requiring less energy delivered to the leg by IL during swing. Therefore, this prosthetic keel design was successful in terms of reducing the overall metabolic demand from muscles of both legs.

However, this prosthetic keel design led to increased intact knee loading, primarily from the intact leg VAS. VAS has been shown to be the highest contributor to axial knee contact force during non-amputee walking (Sasaki and Neptune, 2010), and the highest intact knee axial and A/P contact forces were observed in this simulation. The peak axial intact knee force (~3500 N) was largely increased compared to the residual leg knee in this simulation (~2100 N) as well as compared to previous simulation analyses of non-amputee walking at the same speed (~2100 N) (Sasaki and Neptune, 2010) and other moderate speeds (~1600-2000 N) (Kim et al., 2009; Lin et al., 2010; Shelburne et al.,

2005). Also, in an experimental study of amputee walking, as overall ESAR prosthetic foot stiffness was decreased, increased activity of the intact leg VAS muscles have been observed (Fey et al., 2011). Therefore, reducing ankle or toe stiffness leads to increases in VAS muscle activity and a substantial increase in intact knee loading.

Reducing the Intact Knee Contact Force

When minimizing only intact knee contact force, maintaining the same ankle stiffness while increasing mid-foot and toe stiffness was the optimal prosthetic keel design. This enabled the keel to provide a moderate amount of body and trunk propulsion during the second half of residual leg stance, but increased the total muscle contributions to residual leg body propulsion throughout stance. Increased contributions to trunk propulsion of residual leg muscles such as GMAX, GMED and RF as well as the highest contributions of intact SOL to body and trunk propulsion throughout residual leg stance were observed. Minimizing only intact knee contact force also decreased the dependence on the prosthetic keel to residual leg body support and increased the dependence on residual HAM for this function during the first half of stance. Increased residual leg HAM activity during the first half of stance has been found to be one of the most consistent changes of muscle activity in unilateral below-knee amputee walking (e.g., Winter and Sienko, 1988). Therefore, increasing the demand on this muscle that is likely already compensating following an amputation may present an increased risk of overuse injury or an increase in an already elevated metabolic cost of amputee walking since large increases in the metabolic cost of residual HAM was observed (see Fig. 4.10). In this simulation during the second half of intact leg stance, the smallest contributions of intact GAS to body propulsion and support were shown, which were consistent with reducing the intact knee contact force since GAS has been shown to be the primary contributor to

axial knee contact force during the second half of stance (Sasaki and Neptune, 2010). This keel design also absorbed the largest energy from the leg during the second half of residual leg stance and required the highest contribution of IL to deliver energy to the leg during swing. These changes in prosthetic foot and muscle function resulted in a higher overall metabolic cost of walking. Thus, while this keel design successfully offloaded the intact knee (by reducing both axial and A/P contact forces in the intact knee), it required an increase in metabolic cost and resulted in higher contact forces of remaining lower limb joints (i.e., increased axial forces in the intact leg hip and residual leg knee and hip joints). This simulation produced axial knee forces that were similar in both the intact and residual legs (~2500 N). However, these values were still substantially higher than predicted peak knee axial forces during normal non-amputee walking at the same speed (~2100 N) (Sasaki and Neptune, 2010) and other moderate speeds (~1600-2000 N) (Kim et al., 2009; Lin et al., 2010; Shelburne et al., 2005).

Reducing Both Metabolic Cost and Intact Knee Contact Force

When minimizing both metabolic cost and intact knee contact force, the prosthetic keel design encompassed design aspects of the other optimal designs. Ankle stiffness was reduced (similar to when minimizing only metabolic cost), and toe stiffness was increased (similar to when minimizing only intact knee contact force). Mid-foot stiffness was also increased. This optimal keel design produced the most body propulsion and support during the second half of residual leg stance, as well as the least trunk braking and most trunk propulsion during the first and second halves of stance, respectively. This prosthetic keel also largely reduced the contributions of the intact SOL during the first half of residual leg stance for trunk propulsion and the second half of intact leg stance for intact leg body propulsion. In addition, contributions of the intact VAS to body support

during the first half of intact leg stance and trunk support during the second half of residual leg stance and residual leg swing were largely reduced. As previously noted, reducing VAS contributions to these tasks is consistent with reducing the intact knee axial force since it has been shown to be a primary contributor to the knee axial force during non-amputee walking (Sasaki and Neptune, 2010). To compensate for reduced intact VAS function, intact HAM contributions to body and trunk support were increased. HAM contributions to the knee axial force have been shown to be much less than VAS during walking (Sasaki and Neptune, 2010). Therefore, this keel design enabled the model to offload the intact leg knee and led to a reduced metabolic cost of walking. However, changes in both prosthetic keel and muscle function were essential. Offloading the intact leg knee by limiting the contributions of VAS is consistent with previous modeling work that suggested a quadriceps avoidance gait pattern may be used by non-amputee patients that experience knee osteoarthritis (Sasaki and Neptune, 2010). Osteoarthritic non-amputee patients typically experience decreased knee flexion angles and knee extensor torques during early stance (Astephen et al., 2008; Childs et al., 2004; Deluzio and Astephen, 2007; Zeni and Higginson, 2009). Other studies have suggested that an increased dependence on HAM over VAS may be an effective method to mitigate knee degeneration of non-amputees (Shelburne et al., 2005). Thus, this keel design may enable amputees who experience intact knee osteoarthritis to more effectively offload their intact knee.

Limitations and Future Work

Some limitations and areas of future work exist. First, this study optimized different prosthetic foot stiffness levels and produced promising design concepts that require further investigation. The observed compensations of the musculoskeletal model

when optimizing prosthetic foot stiffness for these specific biomechanical objectives need to be assessed in below-knee amputees. Future work should involve manufacturing these custom ESAR prosthetic feet and clinically testing them on amputees. In addition, it is unclear whether the biomechanical objectives optimized in this study may be utilized by the central nervous system of amputees to optimize walking in a similar manner. However, as previously described, reducing metabolic cost and intact knee contact forces are key clinically-relevant objectives that hold great promise for improving amputee mobility. While this framework is theoretical in nature, the simulated motions and muscle excitations emulated experimentally-collected data of amputee walking and the identified functions of intact and residual leg muscles in terms of their abilities to provide support, propulsion, and energy to the leg were consistent with what has been typically observed in modeling and simulation work of non-amputee walking (Anderson and Pandy, 2003; Liu et al., 2006; Neptune et al., 2001; Neptune et al., 2004). In addition, the observed functions of the prosthetic keel to body and trunk support and braking during the first and second halves of stance as well as energy absorbed from the leg are consistent with the function role of the SOL in non-amputee walking (Neptune et al., 2001). Thus, the optimized movements were realistic and the identified muscle and prosthetic foot functions were found to be consistent with previous work. Lastly, while the primary design variable of interest in this study was prosthetic foot stiffness, other design variables exist such as prosthetic foot shape and size that are promising areas of future work. These variables combined with prosthetic foot stiffness may be important to consider for prosthetic foot selection since they also have the potential to influence the walking mechanics, intact knee loading and metabolic cost of amputees.

Conclusions

In summary, fine-tuning the nominal SLS ESAR prosthetic foot design by stiffening the prosthetic toe and mid-foot while making the prosthetic ankle less stiff may improve prosthetic keel performance by offloading the intact knee during early to mid stance of the intact leg and reducing the metabolic cost of intact and residual leg muscles over the gait cycle. In this framework, optimizing foot stiffness for minimizing only metabolic cost or only intact knee contact force resulted in identified muscular and prosthetic foot compensations which adversely increased the opposing objective. Optimizing for both objectives simultaneously successfully reduced each objective while incorporating common prosthetic design aspects. Therefore, as an important first step in optimizing the stiffness characteristics of ESAR prosthetic feet to improve amputee mobility and care, this study has provided insight into the influence of prosthetic foot stiffness on prosthetic foot and muscle function and important *in vivo* biomechanical quantities of amputees.

Conclusions and Future Research

In order to improve amputee mobility and provide evidence-based biomechanical rationale for prosthetic foot selection, this research focused on identifying the influence of walking speed and prosthetic foot stiffness on the walking mechanics of unilateral below-knee amputees.

Specifically, the influence of walking speed on knee joint loading was examined for amputees walking with prescribed prosthetic feet. In this work, the mechanical loading of the intact knee was not greater than the control subjects across a wide range of speeds, which was surprising given the fact that the intact knee often develops overuse injuries. However, there were sagittal and transverse plane bilateral knee moment asymmetries, which were larger in the intact knee at multiple speeds. In addition, some sagittal plane residual knee loading impulses were insensitive to walking speed increases, while these quantities increased in the intact and control knees. Future studies are needed to determine if these bilateral asymmetries across speed lead to less favorable intact knee loading that may contribute to joint disorders over time. In addition, future studies should investigate knee loading during non-steady-state tasks that may also play an important role in developing joint disorders.

This research next investigated the influence of altering prosthetic foot stiffness using experimental and modeling techniques. The experimental work found that decreasing foot stiffness resulted in a more flexed posture, increased braking ground reaction forces in both the residual and intact legs, and decreased residual leg vertical ground reaction force. Knee moments also became more extensor in the residual and intact legs, consistent with increased intact leg quadriceps activity, increased residual leg quadriceps activity, and decreased residual leg hamstring activity. Residual leg gluteus medius activity also increased throughout all of stance as stiffness decreased. These

changes suggest a need for muscles to modulate their contributions to body support and forward propulsion as stiffness is altered. Also, increased energy storage and return was observed as stiffness decreased. Therefore, tradeoffs in prosthetic foot stiffness may exist between providing greater body support as stiffness increased and providing additional energy return as stiffness decreased. These relationships between prosthetic foot stiffness and resulting gait mechanics should be considered when prescribing specific prosthetic feet for a given amputee.

The modeling work found that altering stiffness changed the performance of the prosthetic foot and function of muscles of the both residual and intact legs during all regions of the gait cycle. Decreasing stiffness resulted in large increases in the contribution of the intact leg quadriceps to provide body and trunk support during the second half of residual leg stance and residual leg swing. However, these increases resulted in increased contribution of the quadriceps to braking of the intact leg. Decreasing foot stiffness also increased the contributions of the prosthetic foot to braking and support of the residual leg during the first half of stance, which required increases of several residual leg muscle contributions such as the quadriceps and glutei muscles to provide increased trunk propulsion throughout stance. However, as stiffness decreased, the prosthetic foot absorbed less power from the residual leg prior to swing which was beneficial for leg swing initiation.

The experimental and modeling studies were important steps in showing that the prescription of energy storage and return prosthetic feet with appropriate stiffness levels are critical as stiffness can significantly influence their walking performance. A promising area of future work would be to extend the 2D modeling studies to 3D to examine the influence of foot stiffness on out-of-plane motion. Frontal and transverse

plane motion may highlight other important influences of stiffness on muscle and prosthetic foot function that were not captured by the 2D analyses used.

The final study integrating design optimization of prosthetic foot stiffness with forward dynamics simulations of amputee walking provided a framework for investigating promising design concepts for improving clinically-relevant *in vivo* biomechanical quantities (i.e., metabolic cost and intact knee contact force). This design work found that fine-tuning a nominal prosthetic foot stiffness distribution by stiffening the prosthetic toe and mid-foot while making the prosthetic ankle less stiff may improve prosthetic keel performance by offloading the intact knee during early to mid stance of the intact leg and reducing the metabolic cost of intact and residual leg muscles. This study found that optimizing foot stiffness for minimizing only metabolic cost or only intact knee contact force resulted in identified muscle and prosthetic foot compensations that adversely increased the opposing objective. Optimizing both objectives successfully reduced both objectives and incorporated common prosthetic design features. Therefore, as an important first step to optimize the stiffness characteristics of energy storage and return prosthetic feet, this study provided insight into the influence of optimal prosthetic foot stiffness characteristics on prosthetic foot and muscle function and important *in vivo* biomechanical quantities of amputees. Future work will be directed at manufacturing these custom prosthetic feet and clinically testing them on amputees to see if amputees use the observed compensatory strategies and if metabolic cost is indeed reduced during amputee use. In addition, design variables other than prosthetic foot stiffness exist such as prosthetic foot shape and size. These variables along with foot stiffness are important to consider for prosthetic foot selection since they directly influence walking mechanics and *in vivo* biomechanical quantities. Thus, a promising area of future work would be to

use topology optimization to identify novel prosthetic foot designs that improve amputee gait.

Appendix A: Additional Aims 3 and 4 Methods

EXPERIMENTAL TRACKING DATA

Amputee subject time from amputation was ≥0.8 years (14 ± 14 years, average ± standard deviation). Prior to use of the custom SLS ESAR prosthetic feet, a certified and licensed prosthetist with 15 years clinical experience ensured proper fit and alignment. Amputee subjects were allowed as much time as needed until they felt comfortable with each foot, which did not exceed five minutes for any subject. All participants were free of any musculoskeletal disorders and pain.

Kinematic data were low-pass filtered using a 4^{th}-order Butterworth filter with a cut-off frequency of 6 Hz, and GRF data were low-pass filtered with a cut-off frequency of 20 Hz. Amputee EMG data common mode rejection and amplification characteristics included: effective 130 dB at DC (0 Hz), >100 dB at 50/60 Hz, and minimum 85 dB through 10-500 Hz operating range; <1.2 μV root-mean-square (RMS) noise level, 2000 fixed overall gain and >10 MΩ input impedance. Non-amputee EMG data detection mode and amplification characteristics included >100 dB at 65 Hz common-mode rejection, 20 to 500 Hz signal bandwidth, <1.2 μV root-mean-square (RMS) noise level, 20 ± 1% gain at 1 kHz and >100 MΩ input impedance. Electrodes were placed on the muscle belly along the line of action between the origin and insertion points based on guidelines provided by Perotto and Delagi (1994). Each electrode location was shaved and cleaned with alcohol prior to placing the electrodes. A ground electrode was placed on the sacrum. Electrodes were secured with tape and Coban (3M, Inc.) to minimize movement artifact. The raw EMG signals will be filtered and processed in MATLAB (MathWorks, Inc.). The EMG data were demeaned, and then smoothed using a moving, symmetric 80-ms (± 40 ms) RMS window.

MUSCULOTENDON ACTUATORS

Each actuator was made up of a contractile element (CE) representing the active muscle fiber, series elastic element (SEE) representing the tendon, and parallel elastic element (PEE) representing the passive fiber stiffness (Fig. A1).

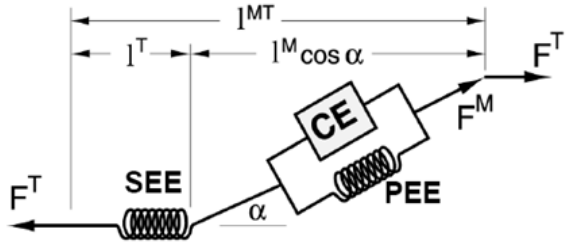

Figure A1: Schematic of Hill-type musculotendon actuator made up of a contractile element (CE), series elastic element (SEE) and parallel elastic element (PEE). Muscle force (F^M) and tendon force (F^T) were determined by muscle contraction dynamics. Total musculotendon length (l^{MT}) was a function of tendon length (l^T), muscle length (l^M) and pennation angle (α).

Muscle contraction dynamics were governed by force-length, force-velocity, and tendon force-strain relationships (Fig. A2), which were scaled by individual muscle parameters that include maximum isometric force ($F_o{}^M$), optimal fiber length ($l_o{}^M$) and tendon slack length ($l_S{}^T$) and maximum fiber shortening velocity ($v_{max}{}^M$).

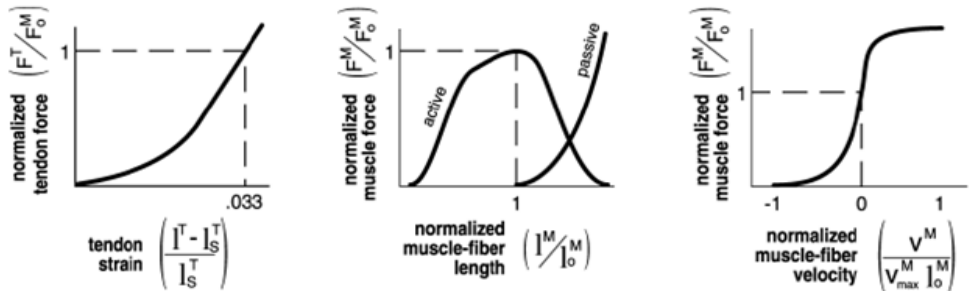

Figure A2: Musculotendon contraction dynamics included muscle force-length, muscle force-velocity, and tendon force-strain relationships.

ENERGY STORAGE AND RETURN PROSTHETIC FOOT MODEL

The attachment of the shank/pylon segment to the top of the keel was defined using a weld joint as well as 3 spline points which represented the rigid attachment of the heel to the keel (Fig. 3.2). Frontal plane depth and sagittal plane thickness dimensions were used to calculate prosthetic foot segment volume. The total prosthetic foot mass was equal to the total mass of the intact leg and control leg feet, and each individual prosthetic foot segment mass was calculated based on segment volume (Fig. A3, Table A1).

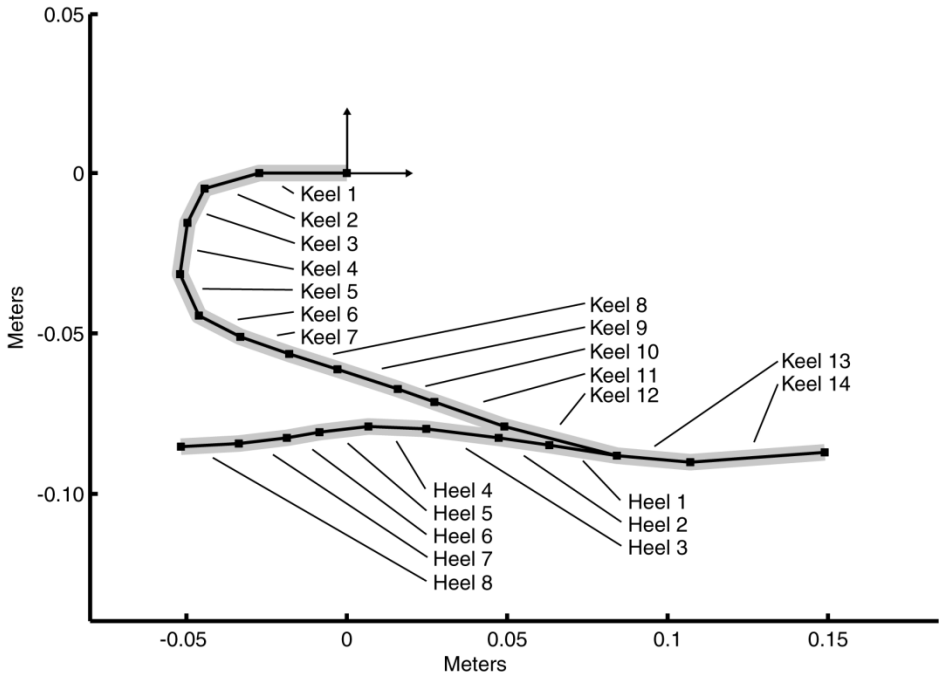

Figure A3: Prosthetic foot segment definitions. The prosthetic foot model consisted of 22 (14 keel and 8 heel) rigid segments connected in series.

Table A1: Prosthetic foot segment geometry (length, thickness and depth), which were used to calculate individual segment volumes and masses. Total prosthetic foot mass was equal to the total mass of the intact leg and non-amputee foot segments.

Segment		Length (m)	Thickness (m)			Depth (m)	Volume (m^3)			Mass (g)		
			Nominal	Compliant	Stiff		Nominal	Compliant	Stiff	Nominal	Compliant	Stiff
Keel	1	0.027	0.019	0.019	0.019	0.049	2.56E-05	2.56E-05	2.56E-05	64.5	80.0	58.4
	2	0.018	0.023	0.020	0.027	0.047	1.95E-05	1.66E-05	2.27E-05	49.3	51.8	51.9
	3	0.012	0.035	0.025	0.039	0.046	2.00E-05	1.44E-05	2.23E-05	50.5	45.0	51.0
	4	0.016	0.037	0.027	0.041	0.046	2.74E-05	1.98E-05	3.04E-05	69.1	62.1	69.5
	5	0.014	0.037	0.026	0.041	0.047	2.46E-05	1.77E-05	2.75E-05	62.1	55.2	62.8
	6	0.014	0.037	0.027	0.040	0.049	2.63E-05	1.92E-05	2.83E-05	66.3	60.1	64.6
	7	0.016	0.033	0.025	0.034	0.049	2.62E-05	2.01E-05	2.70E-05	66.0	63.0	61.7
	8	0.016	0.030	0.023	0.032	0.056	2.71E-05	2.08E-05	2.86E-05	68.3	64.9	65.5
	9	0.020	0.028	0.022	0.030	0.059	3.35E-05	2.63E-05	3.56E-05	84.5	82.4	81.3
	10	0.012	0.026	0.021	0.028	0.062	2.01E-05	1.59E-05	2.15E-05	50.8	49.6	49.1
	11	0.023	0.024	0.020	0.027	0.065	3.71E-05	2.97E-05	4.05E-05	93.5	93.0	92.6
	12	0.036	0.020	0.014	0.023	0.069	5.02E-05	3.62E-05	5.72E-05	126.6	113.3	130.6
	13	0.023	0.012	0.010	0.015	0.069	1.89E-05	1.61E-05	2.46E-05	47.7	50.4	56.1
	14	0.042	0.011	0.011	0.012	0.069	3.21E-05	3.07E-05	3.58E-05	81.0	95.9	81.7
Heel	1	0.021	0.006	0.006	0.007	0.069	9.29E-06	8.55E-06	1.04E-05	23.4	26.7	23.8
	2	0.016	0.007	0.007	0.008	0.068	7.93E-06	7.11E-06	8.75E-06	20.0	22.2	20.0
	3	0.023	0.008	0.007	0.008	0.068	1.18E-05	1.06E-05	1.26E-05	29.7	33.1	28.7
	4	0.018	0.007	0.006	0.008	0.060	7.48E-06	6.37E-06	8.58E-06	18.9	19.9	19.6
	5	0.015	0.006	0.006	0.007	0.056	5.52E-06	4.86E-06	6.41E-06	13.9	15.2	14.6
	6	0.010	0.006	0.005	0.008	0.054	3.46E-06	2.90E-06	4.15E-06	8.7	9.1	9.5
	7	0.015	0.007	0.006	0.008	0.053	5.20E-06	4.40E-06	6.20E-06	13.1	13.8	14.2
	8	0.018	0.007	0.006	0.008	0.052	6.44E-06	5.49E-06	7.39E-06	16.2	17.2	16.9
Total										**1124.1**	**1124.1**	**1124.1**

MUSCLE AND PROSTHETIC FOOT FUNCTION

To determine the function of the prosthetic foot and individual muscles, a ground reaction force decomposition and segment power analysis (Fregly and Zajac, 1996) was performed. First, the system equations of motion were expressed in the following form.

$$M(q)\ddot{q} = R(q) \cdot F^{mus} + F^{Ext}(q, \dot{q}) + G(q) + V(q, \dot{q})$$

In the equation, $q, \dot{q}$, and $\ddot{q}$ are vectors of the generalized coordinates, velocities and accelerations, respectively. $M(q)$ is the system mass matrix and $R(q) \cdot F^{mus}$ represent net muscle moments, which are the product of the moment arm matrix ($R(q)$) and the muscle forces (F^{mus}). The $F^{Ext}(q, \dot{q})$ term represents GRFs and passive torques applied in the prosthetic foot model (in the amputee simulations only) and at each joint. The $G(q)$ term represents the gravitational forces. The $V(q, \dot{q})$ term represents velocity-dependent forces and includes Coriolis and centripetal effects. Because the system mass matrix ($M(q)$) is not diagonal, individual muscle forces (F_j^{mus}) and external forces (F_j^{Ext}) could contribute to each generalized coordinate acceleration. Thus, individual muscle forces and external forces have the ability to contribute to the accelerations of all segments and joints.

The contribution of each muscle to the GRF was evaluated by first calculating the state of the system at a given time step i. Then after applying all of the muscle forces except for the muscle of interest to the system at time step i-1 and integrating forward to time step i, the GRF in the new perturbed state i was determined. The contribution of each muscle to the GRF is the difference between the original state i and the perturbed state i. The procedure was repeated for each muscle at every time step within the simulation. Similarly, the contribution of the prosthetic foot to the GRF was evaluated by

applying all of the forces except for the passive torques in the prosthetic model at time step i-1 and then integrating forward in time to state i.

The contribution of each muscle to the generalized accelerations, $\ddot{q}$, was determined by setting all the forces in the equations of motion to zero except the muscle force of interest and its corresponding contribution to the GRF and solving the equations of motion. Similarly, the contribution of the prosthetic foot to the generalized accelerations was determined by setting all of the forces in the equation of motion to zero except for the prosthetic foot passive torques and their contributions to the GRF.

To find the contribution of a muscle to the mechanical power of each segment, P_i, at each instant in time, the state of the system at each time step i was combined with a muscle's induced acceleration at the same time step as follows:

$$P_i = (m_i \cdot a_i)v_i + (I_i \cdot \alpha_i)\omega_i + (m_i \cdot G)v_i$$

where G is the gravitational acceleration vector, m_i is the segment mass, a_i is the muscle's induced linear acceleration, v_i is the segment linear velocity, I_i is the segment inertia matrix, α_i is the muscle's induced angular acceleration, ω_i is the segment angular velocity. A positive contribution to a segmental power means the muscle accelerates the segment in the same direction as its motion. Conversely, a negative contribution to a segmental power means the muscle decelerates the segment in its direction of motion. Similarly, the contribution of the prosthetic foot to the mechanical power of each segment was determined.

DISTRIBUTION OF GROUND CONTACT ELEMENTS

Shoe contact element distribution was adjusted for the residual foot due to differing distal foot segments (Fig. A4).

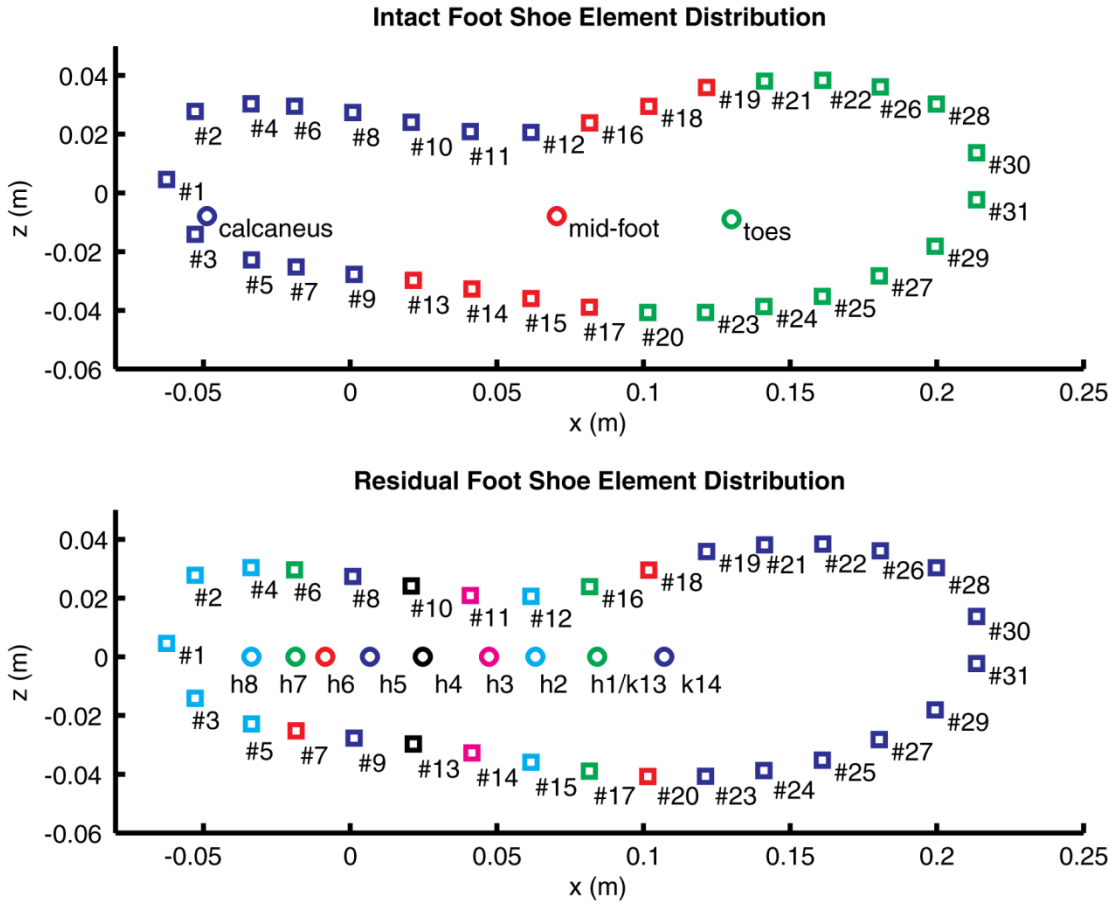

Figure A4: The distribution of 31 ground contact elements (indicated by square symbols) attached to the distal segments of the feet. The same shoe shape was used for the intact and residual legs. However, the foot segments to which each element was attached to differed between feet. Local reference frame origins of each foot segment are indicated by circular symbols. Reference frame and contact element color show which elements are attached to each foot segment. Segments h1-h8 denote heel segments 1-8, and segments k13 and k14 denote keel segments 13 and 14 (in Table A1 above). In the residual foot, h1 and k13 segment origins are coincident. But, elements #16 and #17 are attached to h1, while elements #18 and #20 are attached to k13. Each segment origin is located at the proximal end of each segment.

PROSTHETIC FOOT DAMPING

Damping constants for the prosthetic feet were estimated by developing regression equations to predict the experimentally-measured residual leg ankle torque from the residual leg ankle angle and angular velocity (Figs. A5-A7). Although, the computed stiffness varied among the prosthetic feet, a common damping value (b=5.73 N*m*s, 0.1 N*m*s/deg) was found predict the experimentally-measured residual leg ankle torque from ankle angle and velocity.

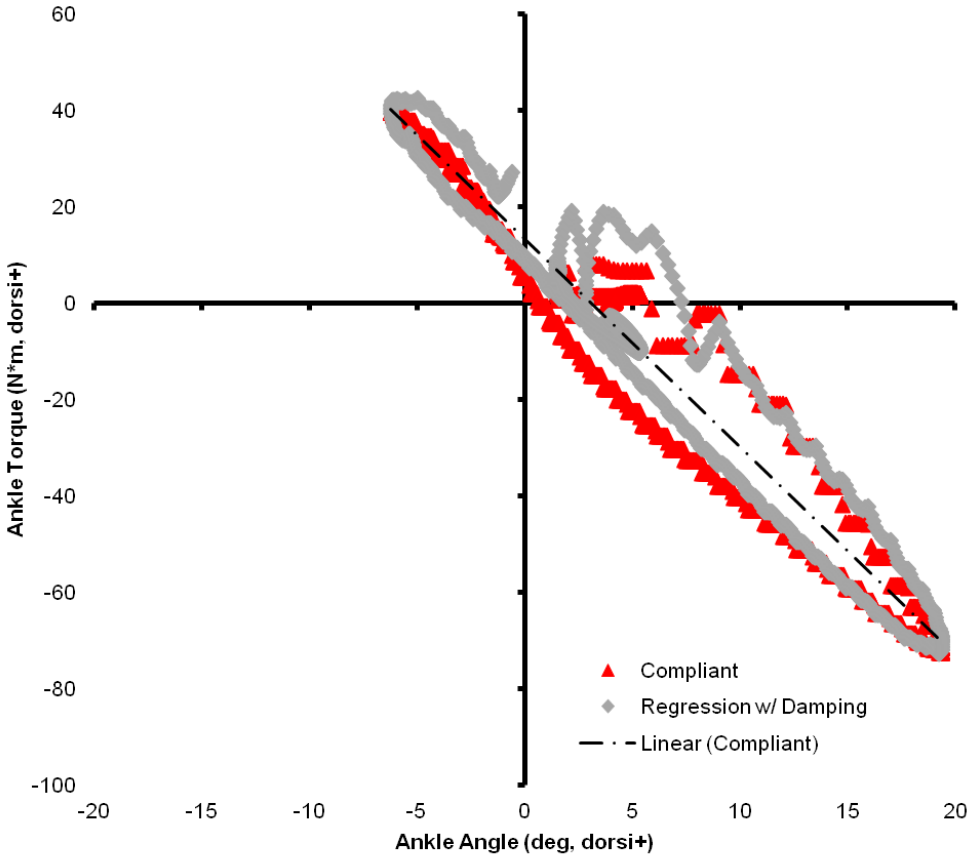

Figure A5: In order to estimate the damping of the three prosthetic feet, a linear regression equation was computed (Linear (Compliant)) to first predict the experimental residual leg ankle torque (Compliant) from the residual ankle angle. Next, this regression equation was modified to also include damping. The damping constant was multiplied by the ankle angular velocity such that the predicted regression model (Regression w/ Damping) took into account both ankle angle and velocity to predict the experimentally-measured ankle torque.

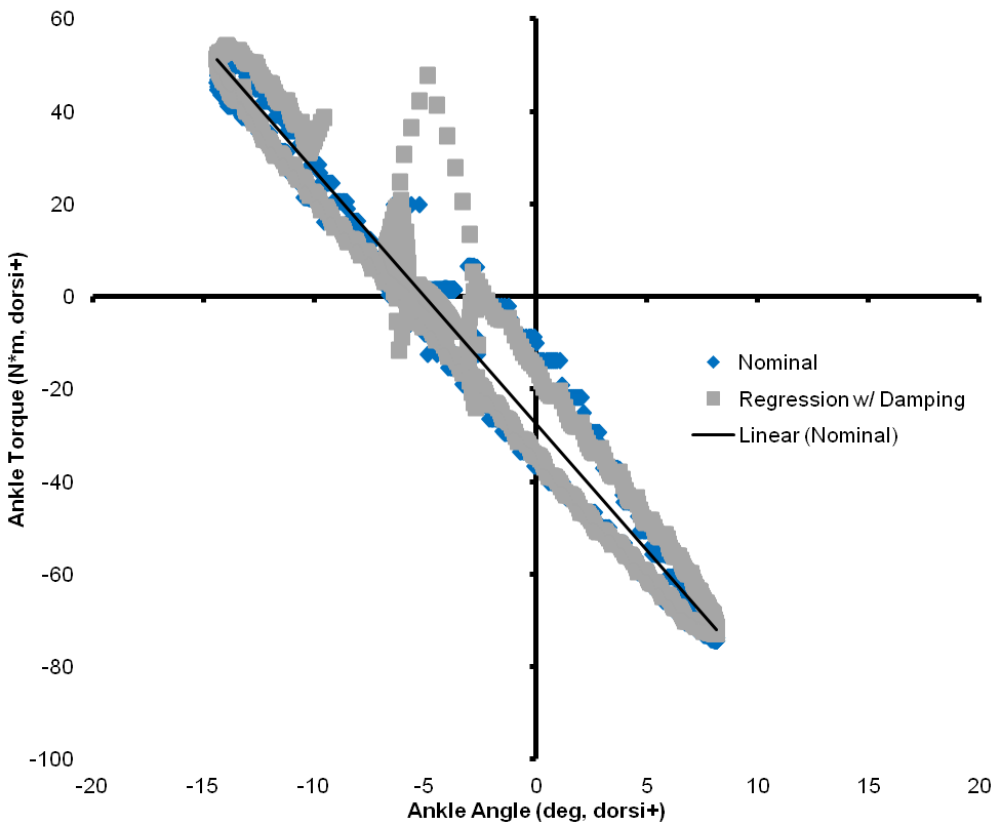

Figure A6: In order to estimate the damping of the three prosthetic feet, a linear regression equation was computed (Linear (Nominal)) to first predict the experimental residual leg ankle torque (Nominal) from the residual ankle angle. Next, this regression equation was modified to also include damping. The damping constant was multiplied by the ankle angular velocity such that the predicted regression model (Regression w/ Damping) took into account both ankle angle and velocity to predict the experimentally-measured ankle torque.

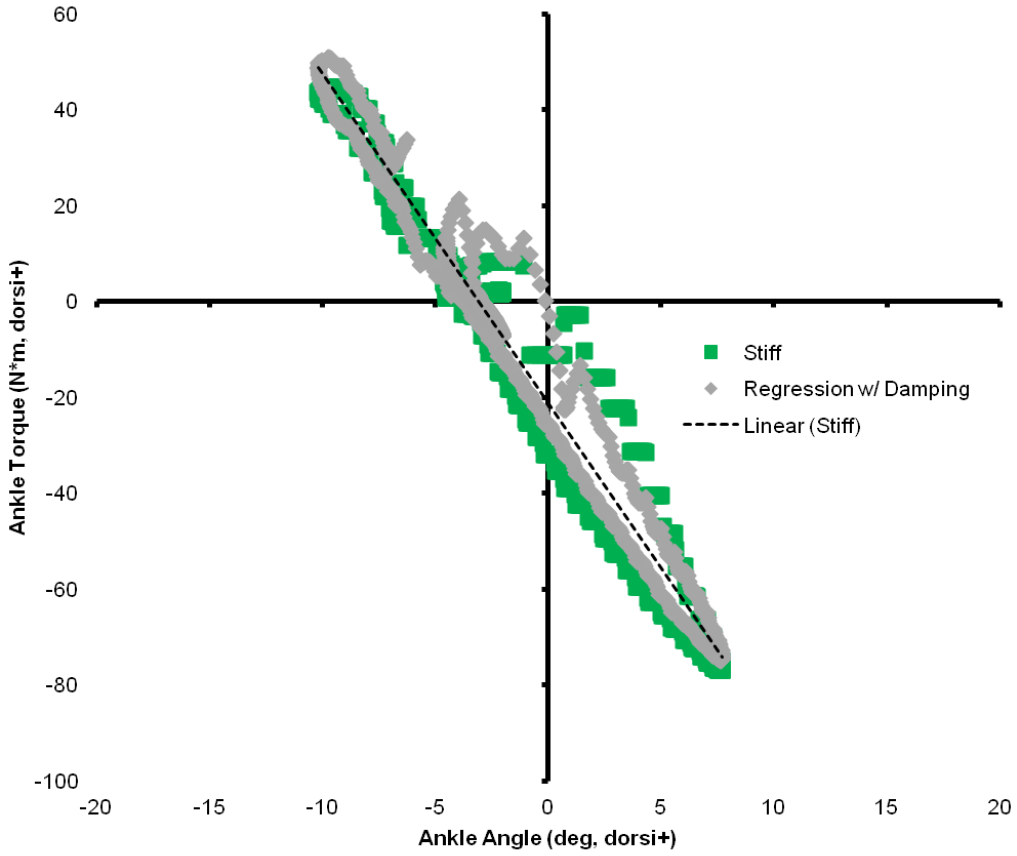

Figure A7: In order to estimate the damping of the three prosthetic feet, a linear regression equation was computed (Linear (Stiff)) to first predict the experimental residual leg ankle torque (Stiff) from the residual ankle angle. Next, this regression equation was modified to also include damping. The damping constant was multiplied by the ankle angular velocity such that the predicted regression model (Regression w/ Damping) took into account both ankle angle and velocity to predict the experimentally-measured ankle torque.

Appendix B: Additional Aim 3 Results

TRACKING COMPARISONS OF THE AMPUTEE WALKING SIMULATIONS

Below are comparisons of the three simulated motions with experimentally-collected data from the amputees walking using the nominal, compliant and stiff SLS ESAR feet (Figs. B1-B3).

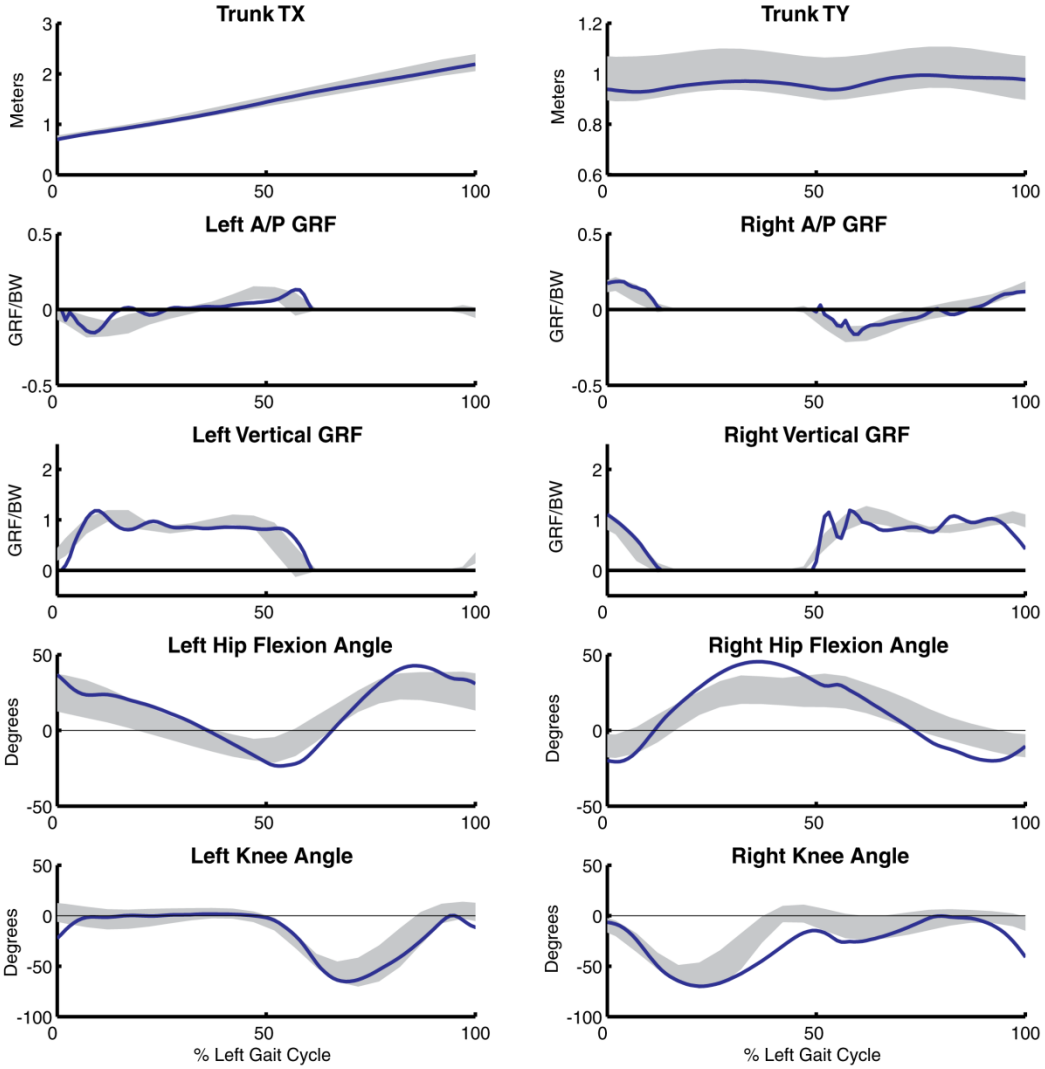

Figure B1: Representative simulation tracking comparison from the nominal amputee walking simulation. Simulated (blue) and experimental (gray, ± 2 SD) data are plotted.

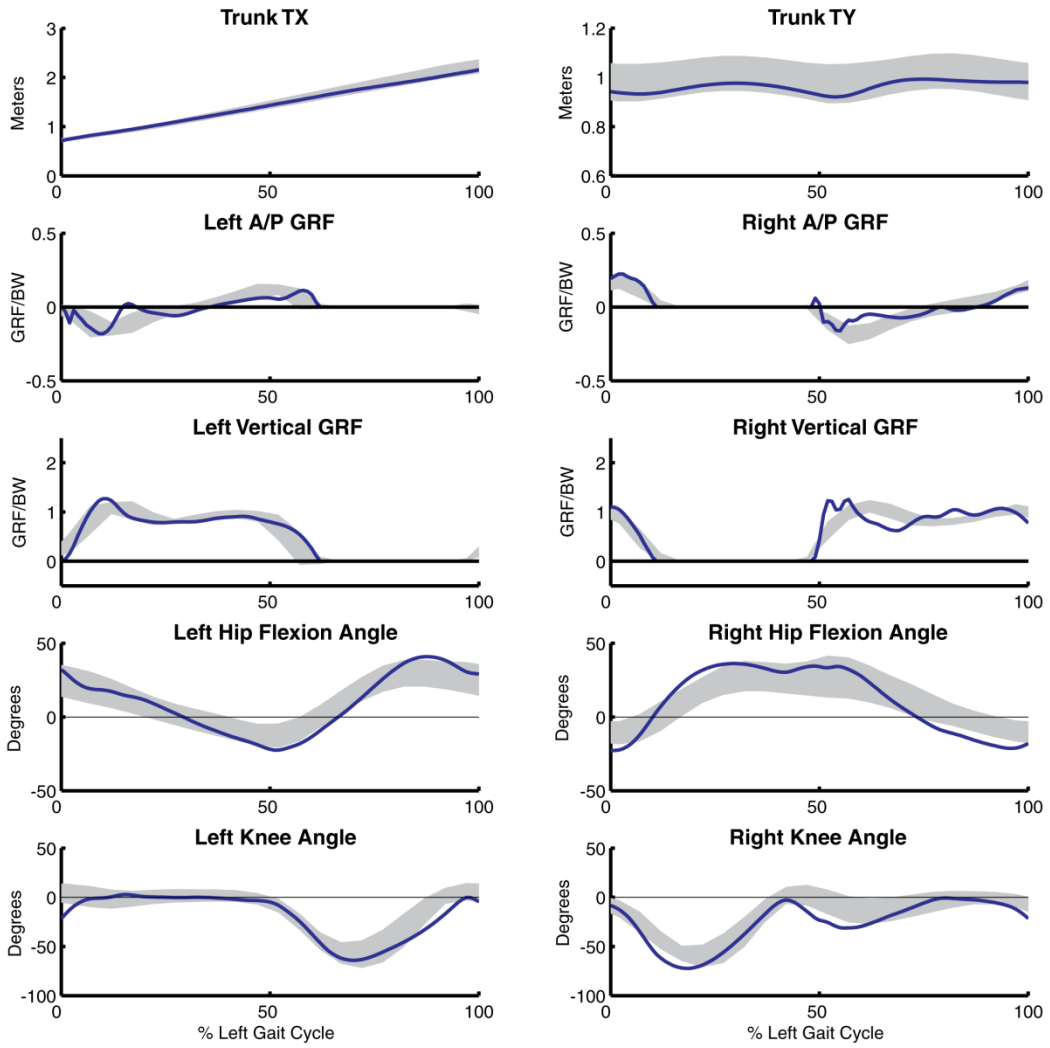

Figure B2: Representative simulation tracking comparison from the compliant amputee walking simulation. Simulated (blue) and experimental (gray, ± 2 SD) data are plotted.

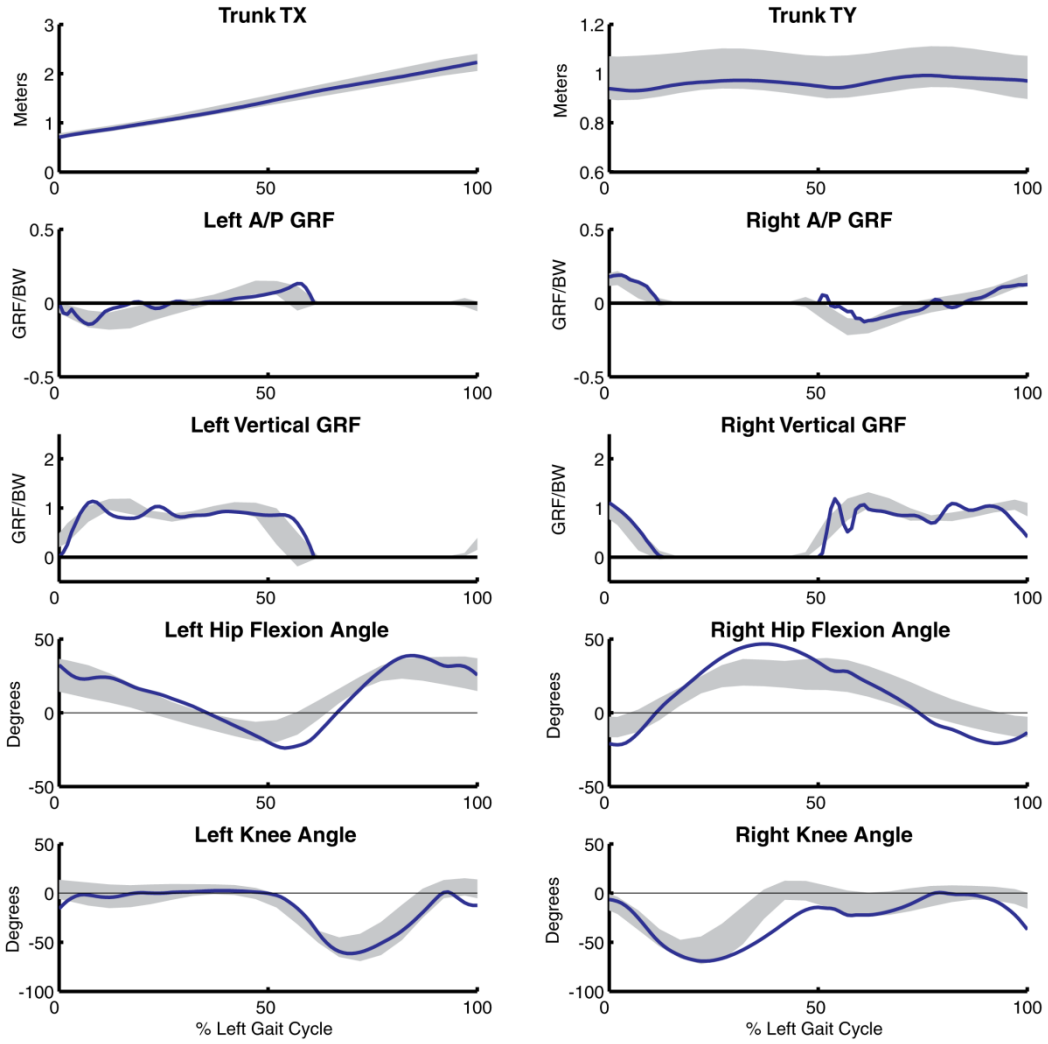

Figure B3: Representative simulation tracking comparison from the stiff amputee walking simulation. Simulated (blue) and experimental (gray, ± 2 SD) data are plotted.

PROSTHETIC FOOT DEFLECTIONS, TORQUES AND ENERGY STORAGE AND RETURN

Below are the individual prosthetic foot element deflections, torques and powers for each of the three simulations (Figs. B4-B6). As stiffness decreased (e.g., stiff simulation, Fig. B6, compared to the compliant simulation, Fig. B5), increased angular deflections were observed in the mid-foot (KR8-KR11) and ankle (KR1-KR7). Also as stiffness decreased, the plantarflexion moments produced by the keel elements in late stance and the dorsiflexion moments produced by the heel elements in early stance decreased. Lastly, as stiffness decreased, increased amounts of energy storage and return were observed in the mid-foot (KR8-KR11) such that energy storage and return throughout the keel was more uniform.

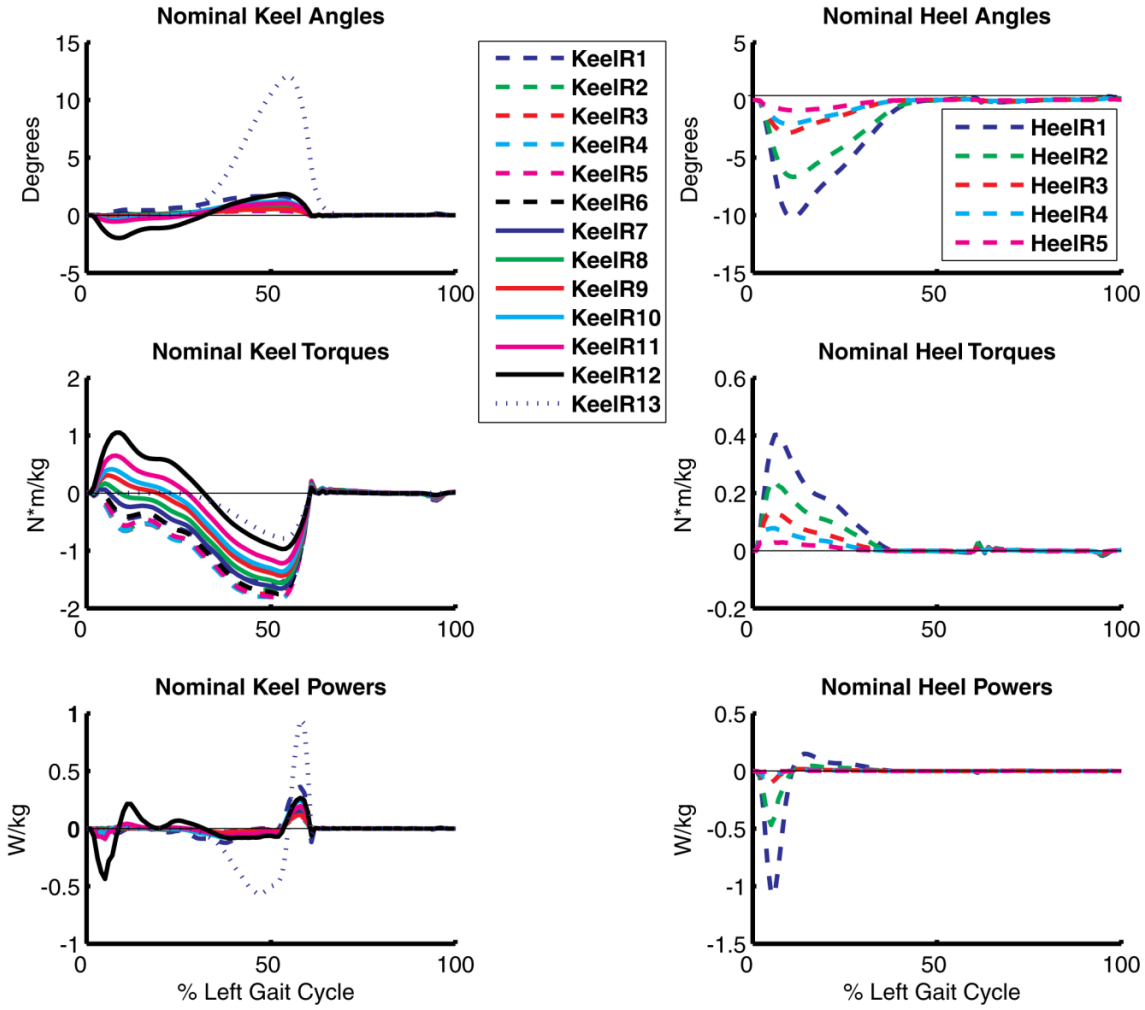

Figure B4: Keel (left column, KR1-KR13) and heel (right column, HR1-HR5) rotational element angular deflections (top row), torques (middle row) and powers (bottom row) in the nominal amputee walking simulation. Positive angular deflection and torque indicate dorsiflexion.

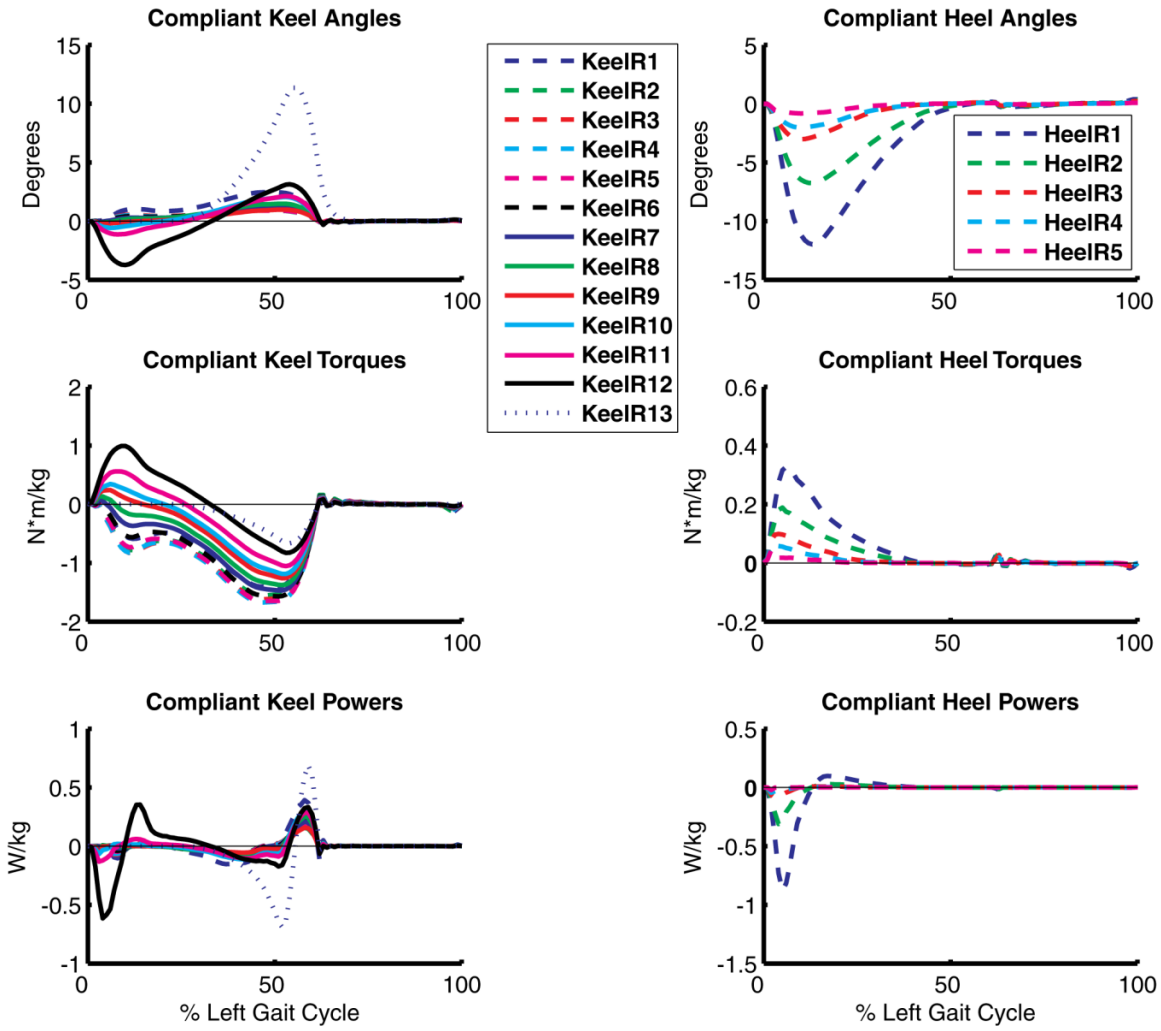

Figure B5: Keel (left column, KR1-KR13) and heel (right column, HR1-HR5) rotational element angular deflections (top row), torques (middle row) and powers (bottom row) in the compliant amputee walking simulation. Positive angular deflection and torque indicate dorsiflexion.

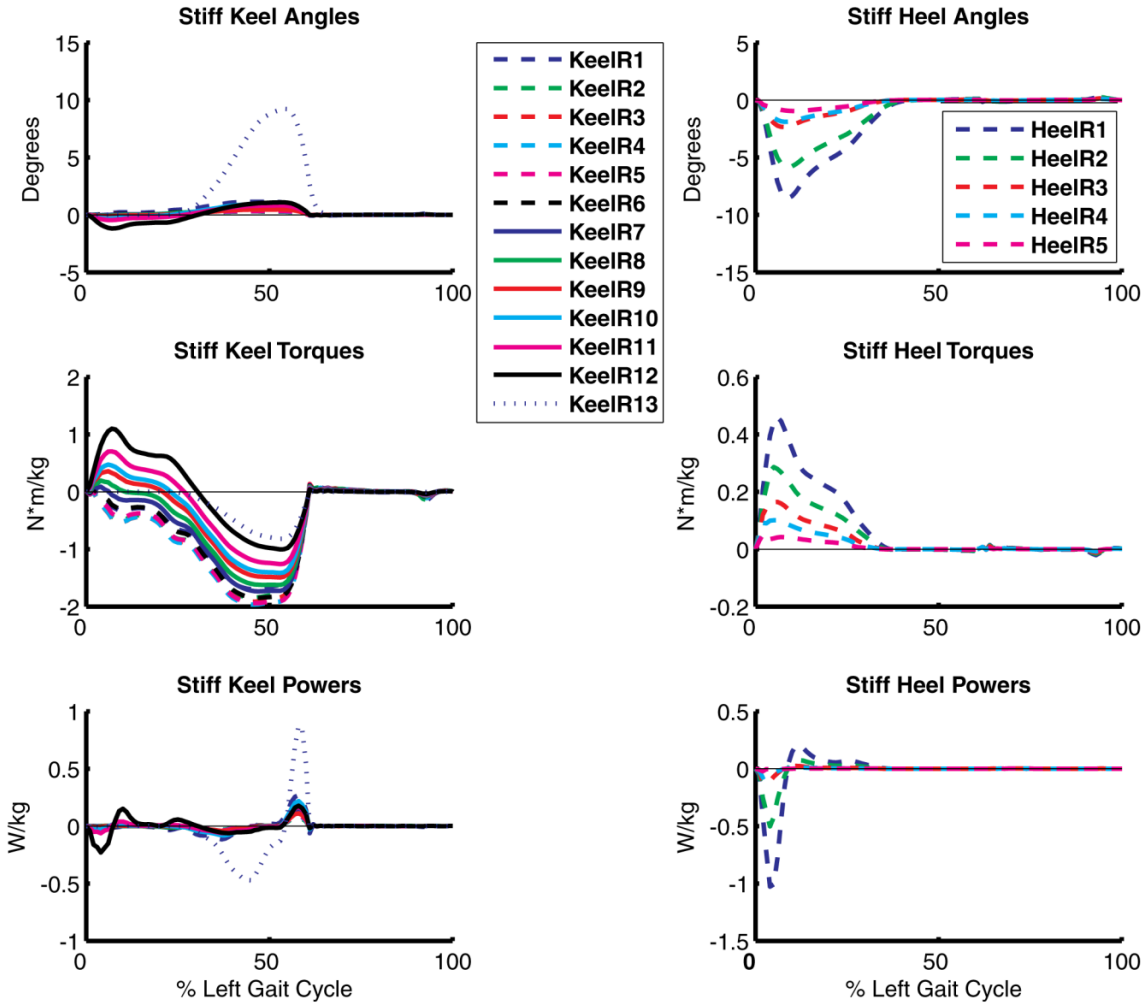

Figure B6: Keel (left column, KR1-KR13) and heel (right column, HR1-HR5) rotational element angular deflections (top row), torques (middle row) and powers (bottom row) in the stiff amputee walking simulation. Positive angular deflection and torque indicate dorsiflexion.

Appendix C: Additional Aim 4 Results

TRACKING COMPARISONS OF THE AMPUTEE WALKING SIMULATIONS

Below are comparisons of the simulated motions with the experimental tracking data for each of the three simulations (Figs. C1-C3).

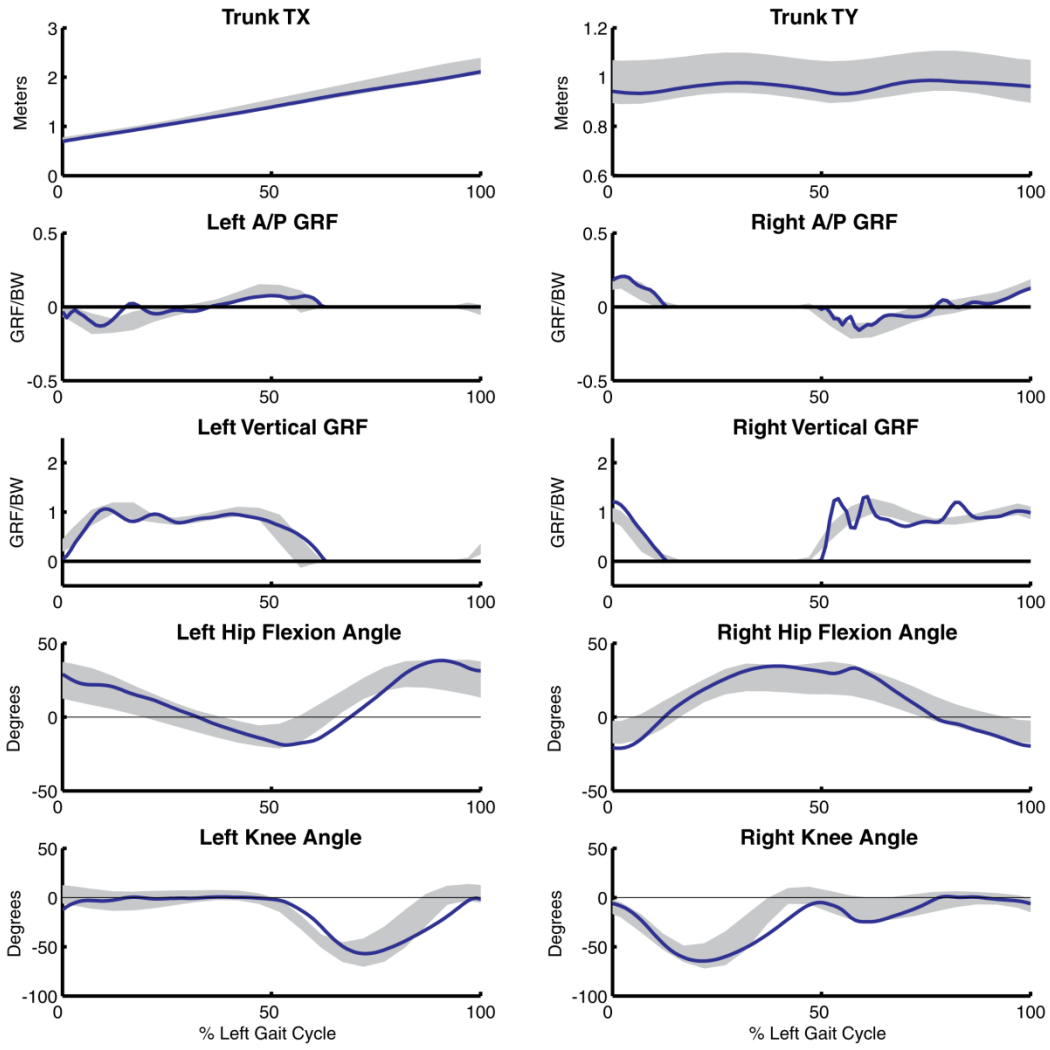

Figure C1: Representative simulation tracking comparison from the amputee walking simulation for minimizing metabolic cost. Simulated data (blue) are plotted with experimental tracking data of the amputees walking with the SLS ESAR foot (gray, ± 2 SD).

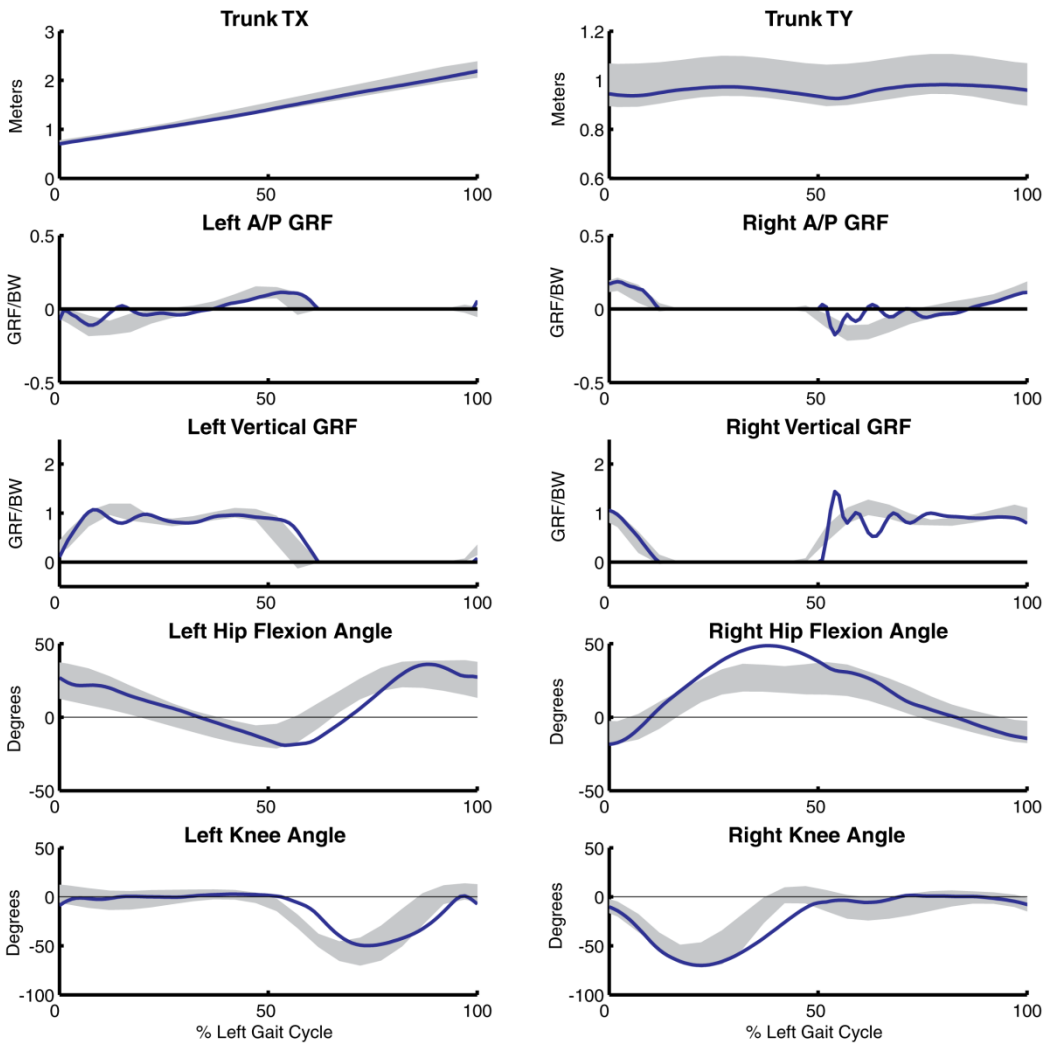

Figure C2: Representative simulation tracking comparison from the amputee walking simulation for minimizing both metabolic cost and intact knee contact force. Simulated data (blue) are plotted with experimental tracking data of the amputees walking with the SLS ESAR foot (gray, ± 2 SD).

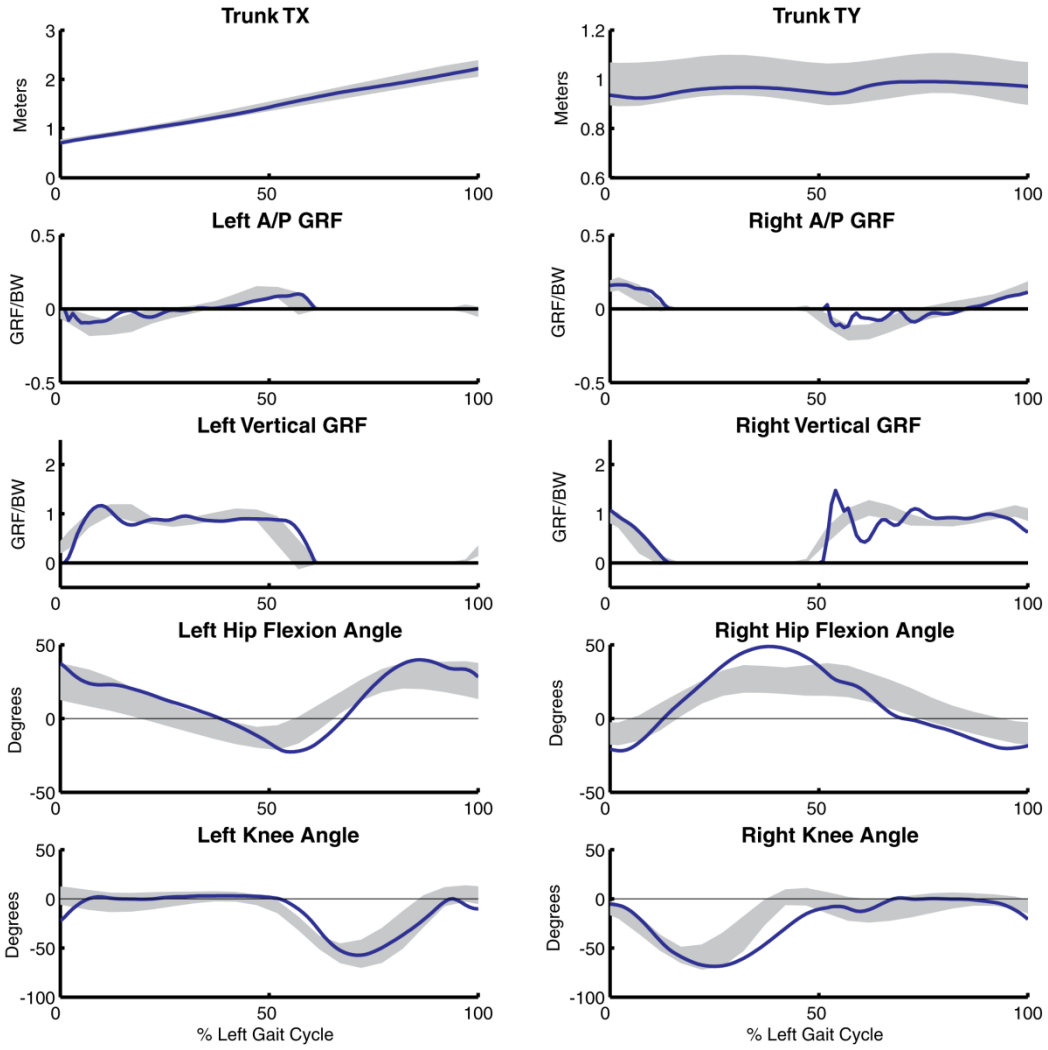

Figure C3: Representative simulation tracking comparison from the amputee walking simulation for minimizing intact knee contact force. Simulated data (blue) are plotted with experimental tracking data of the amputees walking with the SLS ESAR foot (gray, ± 2 SD).

PROSTHETIC FOOT DEFLECTIONS, TORQUES, AND ENERGY STORAGE AND RETURN

Below are the individual prosthetic element deflections, torques and powers for each of the three simulations (Figs. C4-C6). These profiles were similar across all simulations. However, due to the altered foot stiffness characteristics across simulations, differences in magnitude were observed.

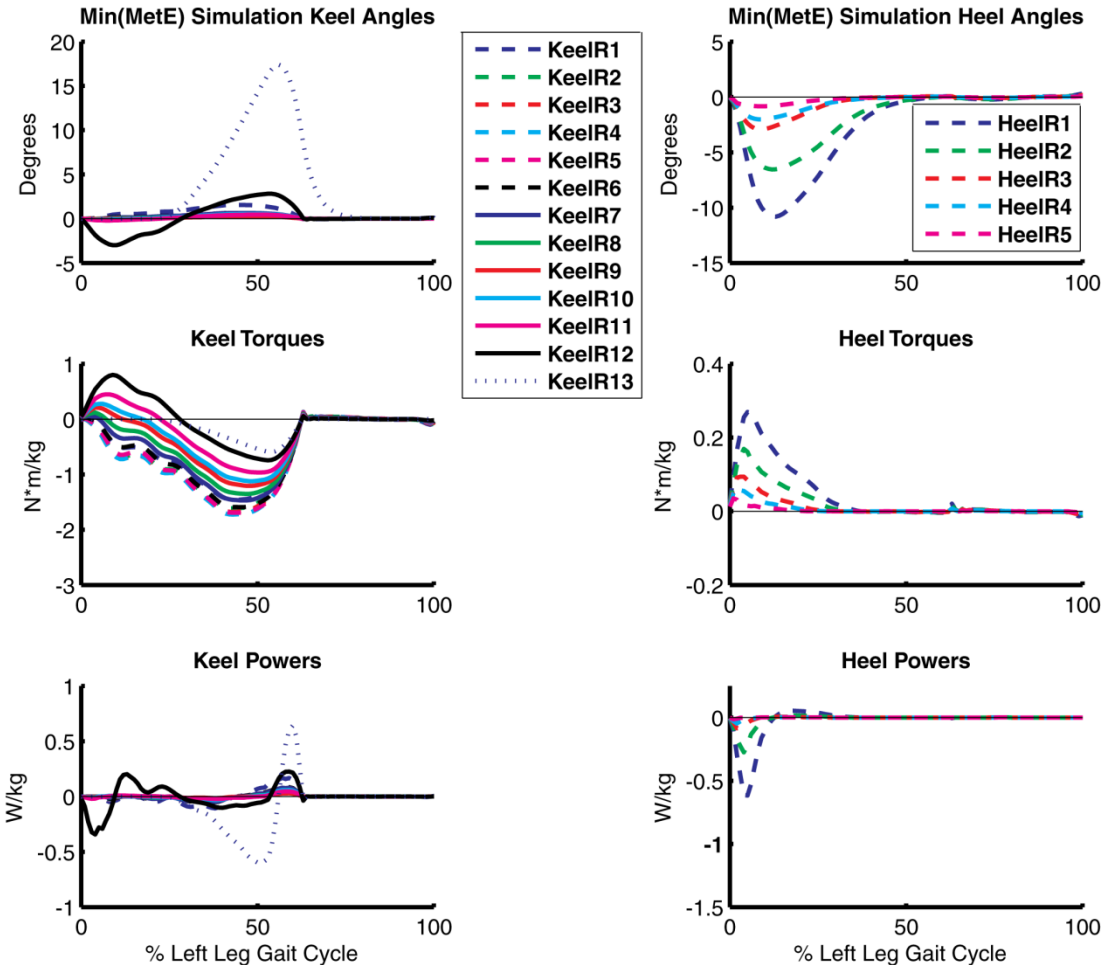

Figure C4: Keel (left column, KR1-KR13) and heel (right column, HR1-HR5) rotational element angular deflections (top row), torques (middle row) and powers (bottom row) in the amputee walking simulation for minimizing metabolic cost. Positive angular deflection and torque indicate dorsiflexion.

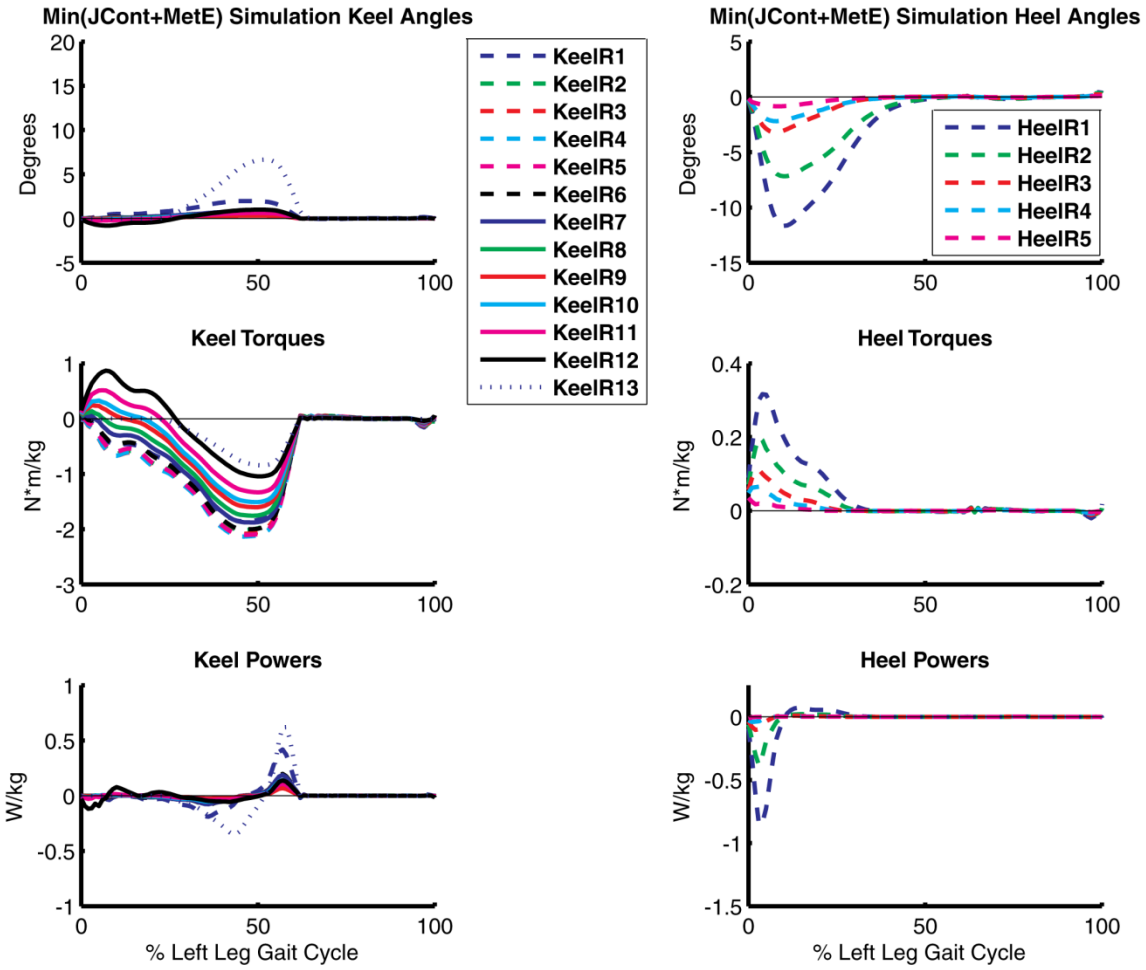

Figure C5: Keel (left column, KR1-KR13) and heel (right column, HR1-HR5) rotational element angular deflections (top row), torques (middle row) and powers (bottom row) in the amputee walking simulation for minimizing both metabolic cost and intact knee contact force. Positive angular deflection and torque indicate dorsiflexion.

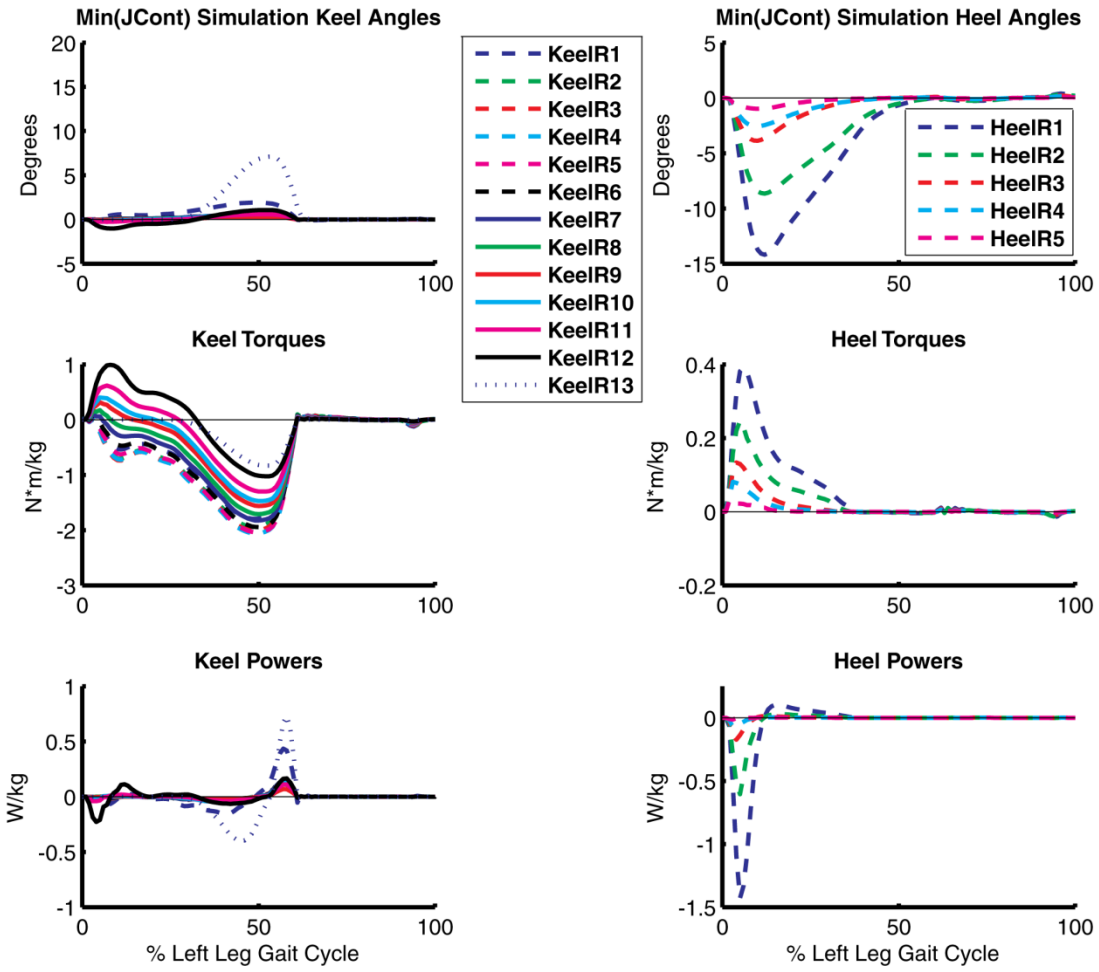

Figure C6: Keel (left column, KR1-KR13) and heel (right column, HR1-HR5) rotational element angular deflections (top row), torques (middle row) and powers (bottom row) in the amputee walking simulation for minimizing intact knee contact force. Positive angular deflection and torque indicate dorsiflexion.

TOTAL PROSTHETIC FOOT ENERGY STORAGE AND RETURN

Below are the profiles of total energy storage and return for each of the three simulations (Fig. C7). Minimizing only intact knee contact force resulted in increased early stance heel energy storage and late stance keel energy return. Minimizing only metabolic cost resulted in decreased early stance heel energy storage and late stance keel

energy return. Minimizing both objectives resulted in moderate early stance heel energy storage and increased late stance keel energy return.

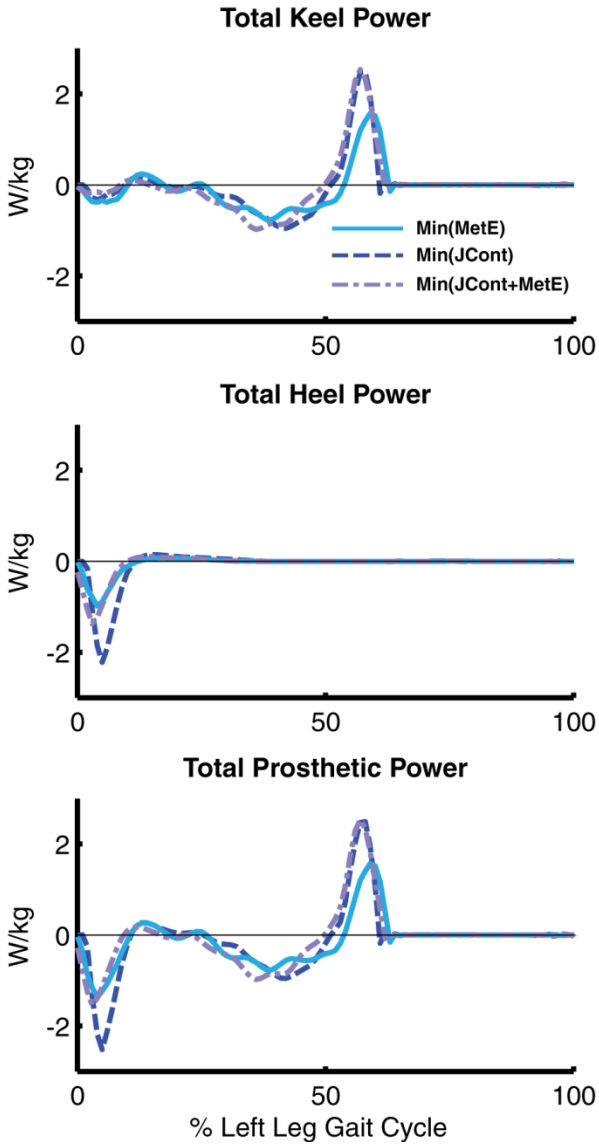

Figure C7: Keel, heel and total (keel + heel) power curves in the amputee walking simulations. Keel and heel powers were calculated by summing the powers across rotational elements within each region of the foot.

TOTAL METABOLIC POWER OF AMPUTEE WALKING

Below are the profiles of total metabolic cost for each of the three simulations (Fig. C8). Consistent with the metabolic cost profiles of the individual muscle groups (Fig. 4.10), there were differences in the total metabolic cost profiles of both the residual and intact legs during all regions of the gait cycle.

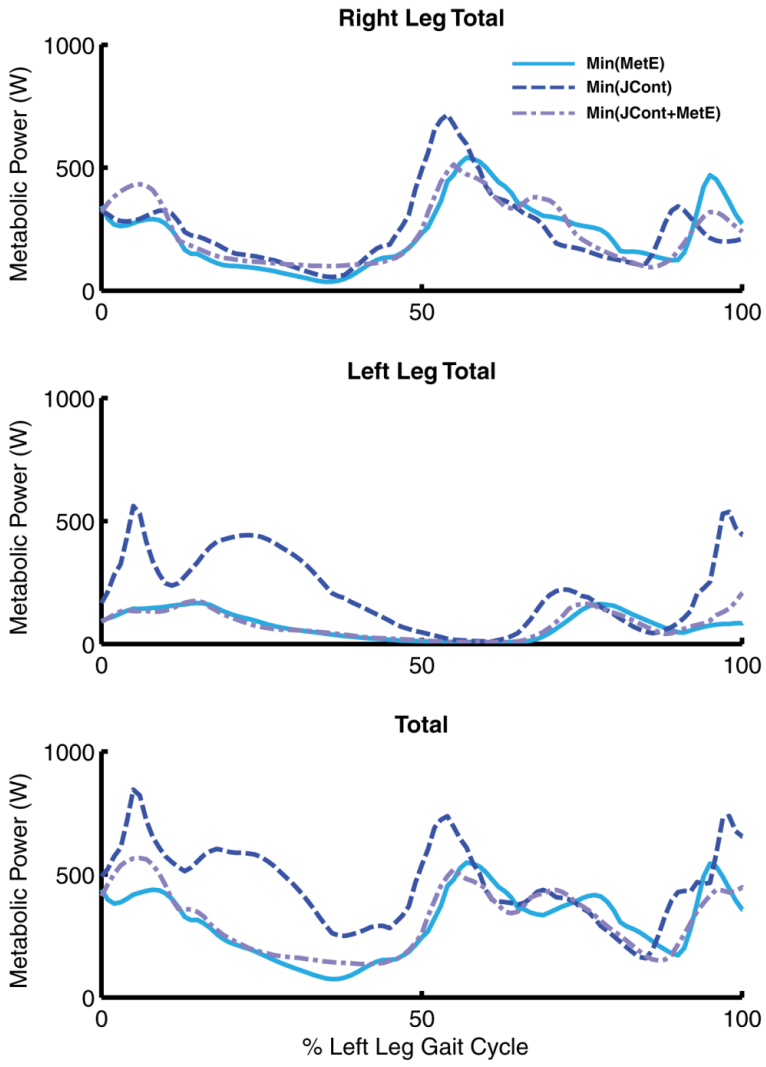

Figure C8: Metabolic cost profiles of the intact (right leg) and residual (left leg) legs as well as the total (right + left) metabolic cost profile for the three simulations.

References

Anderson, F.C. and Pandy, M.G., 1999. A dynamic optimization solution for vertical jumping in three dimensions. Comput Methods Biomech Biomed Engin 2 (3), 201-231.

Anderson, F.C. and Pandy, M.G., 2003. Individual muscle contributions to support in normal walking. Gait Posture 17 (2), 159-69.

Astephen, J.L., Deluzio, K.J., Caldwell, G.E., Dunbar, M.J. and Hubley-Kozey, C.L., 2008. Gait and neuromuscular pattern changes are associated with differences in knee osteoarthritis severity levels. J Biomech 41 (4), 868-76.

Barr, A.E., Siegel, K.L., Danoff, J.V., McGarvey, C.L., 3rd, Tomasko, A., Sable, I. and Stanhope, S.J., 1992. Biomechanical comparison of the energy-storing capabilities of sach and carbon copy ii prosthetic feet during the stance phase of gait in a person with below-knee amputation. Phys Ther 72 (5), 344-54.

Barrios, J.A., Crossley, K.M. and Davis, I.S., 2010. Gait retraining to reduce the knee adduction moment through real-time visual feedback of dynamic knee alignment. J Biomech 43 (11), 2208-13.

Bateni, H. and Olney, S.J., 2002. Kinematic and kinetic variations of below-knee amputee gait. J Prosthet Orthot 14 (1), 2-10.

Beaman, J.J., 1997. Solid freeform fabrication: A new direction in manufacturing: With research and applications in thermal laser processing.

Beyaert, C., Grumillier, C., Martinet, N., Paysant, J. and Andre, J.M., 2008. Compensatory mechanism involving the knee joint of the intact limb during gait in unilateral below-knee amputees. Gait Posture

Burke, M.J., Roman, V. and Wright, V., 1978. Bone and joint changes in lower limb amputees. Ann Rheum Dis 37 (3), 252-4.

Childs, J.D., Sparto, P.J., Fitzgerald, G.K., Bizzini, M. and Irrgang, J.J., 2004. Alterations in lower extremity movement and muscle activation patterns in individuals with knee osteoarthritis. Clin Biomech (Bristol, Avon) 19 (1), 44-9.

Culham, E.G., Peat, M. and Newell, E., 1986. Below-knee amputation: A comparison of the effect of the sach foot and single axis foot on electromyographic patterns during locomotion. Prosthet Orthot Int 10 (1), 15-22.

Czerniecki, J.M., Gitter, A. and Munro, C., 1991. Joint moment and muscle power output characteristics of below knee amputees during running: The influence of energy storing prosthetic feet. J Biomech 24 (1), 63-75.

Czerniecki, J.M., 1996. Rehabilitation in limb deficiency. 1. Gait and motion analysis. Arch Phys Med Rehabil 77 (3 Suppl), S3-8.

Davy, D.T. and Audu, M.L., 1987. A dynamic optimization technique for predicting muscle forces in the swing phase of gait. J Biomech 20 (2), 187-201.

Delp, S.L., Loan, J.P., Hoy, M.G., Zajac, F.E., Topp, E.L. and Rosen, J.M., 1990. An interactive graphics-based model of the lower extremity to study orthopaedic surgical procedures. IEEE Trans Biomed Eng 37 (8), 757-67.

Deluzio, K.J. and Astephen, J.L., 2007. Biomechanical features of gait waveform data associated with knee osteoarthritis: An application of principal component analysis. Gait Posture 25 (1), 86-93.
Dillingham, T.R., Pezzin, L.E. and MacKenzie, E.J., 2002. Limb amputation and limb deficiency: Epidemiology and recent trends in the united states. South Med J 95 (8), 875-83.
Ehara, Y., Beppu, M., Nomura, S., Kunimi, Y. and Takahashi, S., 1993. Energy storing property of so-called energy-storing prosthetic feet. Arch Phys Med Rehabil 74 (1), 68-72.
Engsberg, J.R., Lee, A.G., Patterson, J.L. and Harder, J.A., 1991. External loading comparisons between able-bodied and below-knee-amputee children during walking. Arch Phys Med Rehabil 72 (9), 657-61.
Ephraim, P.L., Wegener, S.T., MacKenzie, E.J., Dillingham, T.R. and Pezzin, L.E., 2005. Phantom pain, residual limb pain, and back pain in amputees: Results of a national survey. Arch Phys Med Rehabil 86 (10), 1910-9.
Eschenauer, H.A. and Olhoff, N., 2001. Topology optimization of continuum structures: A review. Applied Mechanics Reviews 54 (4), 331-389.
Faustini, M.C., Crawford, R.H., Neptune, R.R., Rogers, W.E. and Bosker, G., 2005. Design and analysis of orthogonally compliant features for local contact pressure relief in transtibial prostheses. J Biomech Eng 127 (6), 946-51.
Faustini, M.C., Neptune, R.R. and Crawford, R.H., 2006a. The quasi-static response of compliant prosthetic sockets for transtibial amputees using finite element methods. Med Eng Phys 28 (2), 114-21.
Faustini, M.C., Neptune, R.R., Crawford, R.H., Rogers, W.E. and Bosker, G., 2006b. An experimental and theoretical framework for manufacturing prosthetic sockets for transtibial amputees. IEEE Trans Neural Syst Rehabil Eng 14 (3), 304-10.
Faustini, M.C., Neptune, R.R., Crawford, R.H. and Stanhope, S.J., 2008. Manufacture of passive dynamic ankle-foot orthoses using selective laser sintering. IEEE Trans Biomed Eng 55 (2), 784-90.
Fey, N.P., Silverman, A.K. and Neptune, R.R., 2010. The influence of increasing steady-state walking speed on muscle activity in below-knee amputees. J Electromyogr Kinesiol 20 (1), 155-61.
Fey, N.P., Klute, G.K. and Neptune, R.R., 2011. The influence of energy storage and return foot stiffness on walking mechanics and muscle activity in below-knee amputees. Clin Biomech (Bristol, Avon)
Foroughi, N., Smith, R. and Vanwanseele, B., 2009. The association of external knee adduction moment with biomechanical variables in osteoarthritis: A systematic review. Knee 16 (5), 303-9.
Fregly, B.J. and Zajac, F.E., 1996. A state-space analysis of mechanical energy generation, absorption, and transfer during pedaling. J Biomech 29 (1), 81-90.
Fregly, B.J., D'Lima, D.D. and Colwell, C.W., Jr., 2009. Effective gait patterns for offloading the medial compartment of the knee. J Orthop Res 27 (8), 1016-21.

Gailey, R., Allen, K., Castles, J., Kucharik, J. and Roeder, M., 2008. Review of secondary physical conditions associated with lower-limb amputation and long-term prosthesis use. J Rehabil Res Dev 45 (1), 15-29.
Geil, M.D., 2001. Energy loss and stiffness properties of dynamic elastic response prosthetic feet. JPO: Journal of Prosthetics and Orthotics 13 (3), 70-73.
Genin, J.J., Bastien, G.J., Franck, B., Detrembleur, C. and Willems, P.A., 2008. Effect of speed on the energy cost of walking in unilateral traumatic lower limb amputees. Eur J Appl Physiol 103 (6), 655-63.
Gitter, A., Czerniecki, J.M. and DeGroot, D.M., 1991. Biomechanical analysis of the influence of prosthetic feet on below-knee amputee walking. Am J Phys Med Rehabil 70 (3), 142-8.
Goffe, W.L., Ferrier, G.D. and Rogers, J., 1994. Global optimization of statistical functions with simulated annealing. Journal of Econometrics 60 ((1-2)), 65-99.
Hafner, B.J., Sanders, J.E., Czerniecki, J. and Fergason, J., 2002a. Energy storage and return prostheses: Does patient perception correlate with biomechanical analysis? Clin Biomech (Bristol, Avon) 17 (5), 325-44.
Hafner, B.J., Sanders, J.E., Czerniecki, J.M. and Fergason, J., 2002b. Transtibial energy-storage-and-return prosthetic devices: A review of energy concepts and a proposed nomenclature. J Rehabil Res Dev 39 (1), 1-11.
Hall, A.L., Peterson, C.L., Kautz, S.A. and Neptune, R.R., 2011. Relationships between muscle contributions to walking subtasks and functional walking status in persons with post-stroke hemiparesis. Clin Biomech (Bristol, Avon) 26 (5), 509-15.
Halloran, J.P., Erdemir, A. and van den Bogert, A.J., 2009. Adaptive surrogate modeling for efficient coupling of musculoskeletal control and tissue deformation models. J Biomech Eng 131 (1), 011014.
Halloran, J.P., Ackermann, M., Erdemir, A. and van den Bogert, A.J., 2010. Concurrent musculoskeletal dynamics and finite element analysis predicts altered gait patterns to reduce foot tissue loading. J Biomech
Hansen, A.H., Meier, M.R., Sessoms, P.H. and Childress, D.S., 2006. The effects of prosthetic foot roll-over shape arc length on the gait of trans-tibial prosthesis users. Prosthet Orthot Int 30 (3), 286-99.
Hermodsson, Y., Ekdahl, C., Persson, B.M. and Roxendal, G., 1994. Gait in male trans-tibial amputees: A comparative study with healthy subjects in relation to walking speed. Prosthet Orthot Int 18 (2), 68-77.
Hurley, G.R., McKenney, R., Robinson, M., Zadravec, M. and Pierrynowski, M.R., 1990. The role of the contralateral limb in below-knee amputee gait. Prosthet Orthot Int 14 (1), 33-42.
Isakov, E., Keren, O. and Benjuya, N., 2000. Trans-tibial amputee gait: Time-distance parameters and emg activity. Prosthet Orthot Int 24 (3), 216-20.
Isakov, E., Burger, H., Krajnik, J., Gregoric, M. and Marincek, C., 2001. Knee muscle activity during ambulation of trans-tibial amputees. J Rehabil Med 33 (5), 196-9.

Johnson, V.J., Kondziela, S. and Gottschalk, F., 1995. Pre and post-amputation mobility of trans-tibial amputees: Correlation to medical problems, age and mortality. Prosthet Orthot Int 19 (3), 159-64.
Kepple, T.M., Siegel, K.L. and Stanhope, S.J., 1997. Relative contributions of the lower extremity joint moments to forward progression and support during gait. Gait Posture 6 (1), 1-8.
Kim, H.J., Fernandez, J.W., Akbarshahi, M., Walter, J.P., Fregly, B.J. and Pandy, M.G., 2009. Evaluation of predicted knee-joint muscle forces during gait using an instrumented knee implant. J Orthop Res 27 (10), 1326-31.
Klute, G.K., Kallfelz, C.F. and Czerniecki, J.M., 2001. Mechanical properties of prosthetic limbs: Adapting to the patient. J Rehabil Res Dev 38 (3), 299-307.
Koo, S. and Andriacchi, T.P., 2007. A comparison of the influence of global functional loads vs. Local contact anatomy on articular cartilage thickness at the knee. J Biomech 40 (13), 2961-6.
Kulkarni, J., Gaine, W.J., Buckley, J.G., Rankine, J.J. and Adams, J., 2005. Chronic low back pain in traumatic lower limb amputees. Clin Rehabil 19 (1), 81-6.
Lemaire, E.D. and Fisher, F.R., 1994. Osteoarthritis and elderly amputee gait. Arch Phys Med Rehabil 75 (10), 1094-9.
Lin, C.Y., Kikuchi, N. and Hollister, S.J., 2004. A novel method for biomaterial scaffold internal architecture design to match bone elastic properties with desired porosity. J Biomech 37 (5), 623-36.
Lin, Y.-C., Kim, H.J. and Pandy, M.G., 2011. A computationally efficient method for assessing muscle function during human locomotion. International Journal for Numerical Methods in Biomedical Engineering 27 (3), 436.
Lin, Y.C., Walter, J.P., Banks, S.A., Pandy, M.G. and Fregly, B.J., 2010. Simultaneous prediction of muscle and contact forces in the knee during gait. J Biomech 43 (5), 945-52.
Liu, M.Q., Anderson, F.C., Pandy, M.G. and Delp, S.L., 2006. Muscles that support the body also modulate forward progression during walking. J Biomech 39 (14), 2623-30.
Lloyd, C.H., Stanhope, S.J., Davis, I.S. and Royer, T.D., 2010. Strength asymmetry and osteoarthritis risk factors in unilateral trans-tibial, amputee gait. Gait Posture 32 (3), 296-300.
Mattes, S.J., Martin, P.E. and Royer, T.D., 2000. Walking symmetry and energy cost in persons with unilateral transtibial amputations: Matching prosthetic and intact limb inertial properties. Arch Phys Med Rehabil 81 (5), 561-8.
McGowan, C.P., Kram, R. and Neptune, R.R., 2009. Modulation of leg muscle function in response to altered demand for body support and forward propulsion during walking. J Biomech 42 (7), 850-6.
Miyazaki, T., Wada, M., Kawahara, H., Sato, M., Baba, H. and Shimada, S., 2002. Dynamic load at baseline can predict radiographic disease progression in medial compartment knee osteoarthritis. Ann Rheum Dis 61 (7), 617-22.

Mundermann, A., Dyrby, C.O., Hurwitz, D.E., Sharma, L. and Andriacchi, T.P., 2004. Potential strategies to reduce medial compartment loading in patients with knee osteoarthritis of varying severity: Reduced walking speed. Arthritis Rheum 50 (4), 1172-8.

Neptune, R.R., Wright, I.C. and Van Den Bogert, A.J., 2000. A method for numerical simulation of single limb ground contact events: Application to heel-toe running. Comput Methods Biomech Biomed Engin 3 (4), 321-334.

Neptune, R.R. and Kautz, S.A., 2000. Knee joint loading in forward versus backward pedaling: Implications for rehabilitation strategies. Clin Biomech (Bristol, Avon) 15 (7), 528-35.

Neptune, R.R., Kautz, S.A. and Zajac, F.E., 2001. Contributions of the individual ankle plantar flexors to support, forward progression and swing initiation during walking. J Biomech 34 (11), 1387-98.

Neptune, R.R., Zajac, F.E. and Kautz, S.A., 2004. Muscle force redistributes segmental power for body progression during walking. Gait Posture 19 (2), 194-205.

Neptune, R.R., Sasaki, K. and Kautz, S.A., 2008. The effect of walking speed on muscle function and mechanical energetics. Gait Posture 28 (1), 135-43.

Nolan, L. and Lees, A., 2000. The functional demands on the intact limb during walking for active trans-femoral and trans-tibial amputees. Prosthet Orthot Int 24 (2), 117-25.

Nolan, L., Wit, A., Dudzinski, K., Lees, A., Lake, M. and Wychowanski, M., 2003. Adjustments in gait symmetry with walking speed in trans-femoral and trans-tibial amputees. Gait Posture 17 (2), 142-51.

Ohsaki, M. and Swan, C.C. (2002). Topology and geometry optimization of trusses and frames. Recent advances in optimal structural design. S. A. Burns. Reston, VA, American Society of Civil Engineers.

Orendurff, M.S., Bernatz, G.C., Schoen, J.A. and Klute, G.K., 2008. Kinetic mechanisms to alter walking speed. Gait Posture 27 (4), 603-10.

Perotto, A. and Delagi, E.F. (1994). Anatomical guide for the electromyographer: The limbs and trunk. Springfield, Ill., USA, Charles C. Thomas.

Perry, J., 1992. Gait analysis: Normal and pathological function. Journal of Pediatric Orthopaedics

Perry, J. and Shanfield, S., 1993. Efficiency of dynamic elastic response prosthetic feet. J Rehabil Res Dev 30 (1), 137-43.

Perry, J., Boyd, L.A., Rao, S.S. and Mulroy, S.J., 1997. Prosthetic weight acceptance mechanics in transtibial amputees wearing the single axis, seattle lite, and flex foot. IEEE Trans Rehabil Eng 5 (4), 283-9.

Pinzur, M.S., Asselmeier, M. and Smith, D., 1991. Dynamic electromyography in active and limited walking below-knee amputees. Orthopedics 14 (5), 535-7; discussion 537-8.

Powers, C.M., Rao, S. and Perry, J., 1998. Knee kinetics in trans-tibial amputee gait. Gait Posture 8 (1), 1-7.

Raasch, C.C., Zajac, F.E., Ma, B. and Levine, W.S., 1997. Muscle coordination of maximum-speed pedaling. J Biomech 30 (6), 595-602.
Rankin, J.W. and Neptune, R.R., 2008. A theoretical analysis of an optimal chainring shape to maximize crank power during isokinetic pedaling. J Biomech 41 (7), 1494-502.
Rankin, J.W. and Neptune, R.R., 2010. The influence of seat configuration on maximal average crank power during pedaling: A simulation study. Journal of Applied Biomechanics
Rietman, J.S., Postema, K. and Geertzen, J.H., 2002. Gait analysis in prosthetics: Opinions, ideas and conclusions. Prosthet Orthot Int 26 (1), 50-7.
Robinson, J.L., Smidt, G.L. and Arora, J.S., 1977. Accelerographic, temporal, and distance gait factors in below-knee amputees. Phys Ther 57 (8), 898-904.
Rogers, B., Bosker, G.W., Crawford, R.H., Faustini, M.C., Neptune, R.R., Walden, G. and Gitter, A.J., 2007. Advanced trans-tibial socket fabrication using selective laser sintering. Prosthet Orthot Int 31 (1), 88-100.
Royer, T. and Koenig, M., 2005. Joint loading and bone mineral density in persons with unilateral, trans-tibial amputation. Clin Biomech (Bristol, Avon) 20 (10), 1119-25.
Royer, T.D. and Wasilewski, C.A., 2006. Hip and knee frontal plane moments in persons with unilateral, trans-tibial amputation. Gait Posture 23 (3), 303-6.
Sanderson, D.J. and Martin, P.E., 1997. Lower extremity kinematic and kinetic adaptations in unilateral below-knee amputees during walking. Gait Posture 6 126-136.
Sasaki, K., Neptune, R.R. and Kautz, S.A., 2009. The relationships between muscle, external, internal and joint mechanical work during normal walking. J Exp Biol 212 (Pt 5), 738-44.
Sasaki, K. and Neptune, R.R., 2010. Individual muscle contributions to the axial knee joint contact force during normal walking. J Biomech
Schmalz, T., Blumentritt, S. and Reimers, C.D., 2001. Selective thigh muscle atrophy in trans-tibial amputees: An ultrasonographic study. Arch Orthop Trauma Surg 121 (6), 307-12.
Sharma, L., Hurwitz, D.E., Thonar, E.J., Sum, J.A., Lenz, M.E., Dunlop, D.D., Schnitzer, T.J., Kirwan-Mellis, G. and Andriacchi, T.P., 1998. Knee adduction moment, serum hyaluronan level, and disease severity in medial tibiofemoral osteoarthritis. Arthritis Rheum 41 (7), 1233-40.
Shelburne, K.B., Torry, M.R. and Pandy, M.G., 2005. Muscle, ligament, and joint-contact forces at the knee during walking. Med Sci Sports Exerc 37 (11), 1948-56.
Silverman, A.K., Fey, N.P., Portillo, A., Walden, J.G., Bosker, G. and Neptune, R.R., 2008. Compensatory mechanisms in below-knee amputee gait in response to increasing steady-state walking speeds. Gait Posture 28 (4), 602-9.
Silverman, A.K. and Neptune, R.R., 2011. Differences in whole-body angular momentum between below-knee amputees and non-amputees across walking speeds. J Biomech 44 (3), 379-85.

Smith, D.G., Ehde, D.M., Legro, M.W., Reiber, G.E., del Aguila, M. and Boone, D.A., 1999. Phantom limb, residual limb, and back pain after lower extremity amputations. Clin Orthop Relat Res (361), 29-38.

Soto, C., 2001. Structural topology optimization: From minimizing compliance to maximizing energy absorption. International Journal of Vehicle Design 25 (1/2), 142-160.

South, B.J., Fey, N.P., Bosker, G. and Neptune, R.R., 2010. Manufacture of energy storage and return prosthetic feet using selective laser sintering. J Biomech Eng 132 (1), 015001.

Torburn, L., Perry, J., Ayyappa, E. and Shanfield, S.L., 1990. Below-knee amputee gait with dynamic elastic response prosthetic feet: A pilot study. J Rehabil Res Dev 27 (4), 369-84.

Umberger, B.R., Gerritsen, K.G. and Martin, P.E., 2003. A model of human muscle energy expenditure. Comput Methods Biomech Biomed Engin 6 (2), 99-111.

Umberger, B.R., 2010. Stance and swing phase costs in human walking. J R Soc Interface 7 (50), 1329-40.

Underwood, H.A., Tokuno, C.D. and Eng, J.J., 2004. A comparison of two prosthetic feet on the multi-joint and multi-plane kinetic gait compensations in individuals with a unilateral trans-tibial amputation. Clin Biomech (Bristol, Avon) 19 (6), 609-16.

Ventura, J.D., Klute, G.K. and Neptune, R.R., 2011. The effect of prosthetic ankle energy storage and return properties on muscle activity in below-knee amputee walking. Gait Posture 33 (2), 220-6.

Ventura, J.D., Klute, G.K. and Neptune, R.R., 2011. The effects of prosthetic ankle dorsiflexion and energy return on below-knee amputee leg loading. Clin Biomech (Bristol, Avon) 26 (3), 298-303.

Vrieling, A.H., van Keeken, H.G., Schoppen, T., Otten, E., Halbertsma, J.P., Hof, A.L. and Postema, K., 2008. Gait initiation in lower limb amputees. Gait Posture 27 (3), 423-30.

Waters, R.L., Perry, J., Antonelli, D. and Hislop, H., 1976. Energy cost of walking of amputees: The influence of level of amputation. J Bone Joint Surg Am 58 (1), 42-6.

Winby, C.R., Lloyd, D.G., Besier, T.F. and Kirk, T.B., 2009. Muscle and external load contribution to knee joint contact loads during normal gait. J Biomech 42 (14), 2294-300.

Winter, D.A. and Sienko, S.E., 1988. Biomechanics of below-knee amputee gait. J Biomech 21 (5), 361-7.

Winters, J.M. and Stark, L., 1988. Estimated mechanical properties of synergistic muscles involved in movements of a variety of human joints. J Biomech 21 (12), 1027-41.

Xinghua, Z., He, G. and Bingzhao, G., 2005. The application of topology optimization on the quantitative description of the external shape of bone structure. J Biomech 38 (8), 1612-20.

Zajac, F.E., 1989. Muscle and tendon: Properties, models, scaling, and application to biomechanics and motor control. Crit Rev Biomed Eng 17 (4), 359-411.
Zajac, F.E., Neptune, R.R. and Kautz, S.A., 2002. Biomechanics and muscle coordination of human walking. Part i: Introduction to concepts, power transfer, dynamics and simulations. Gait & Posture 16 (3), 215-32.
Zeni, J.A., Jr. and Higginson, J.S., 2009. Differences in gait parameters between healthy subjects and persons with moderate and severe knee osteoarthritis: A result of altered walking speed? Clin Biomech (Bristol, Avon) 24 (4), 372-8.
Ziegler-Graham, K., MacKenzie, E.J., Ephraim, P.L., Travison, T.G. and Brookmeyer, R., 2008. Estimating the prevalence of limb loss in the united states: 2005 to 2050. Arch Phys Med Rehabil 89 (3), 422-9.
Zmitrewicz, R.J., Neptune, R.R. and Sasaki, K., 2007. Mechanical energetic contributions from individual muscles and elastic prosthetic feet during symmetric unilateral transtibial amputee walking: A theoretical study. J Biomech 40 (8), 1824-31.

Vita

Nicholas Phillip Fey was born in San Antonio, Texas on March 25, 1984 to Timothy and Sharlene Fey. He attended elementary school at Our Lady of Perpetual Help Catholic School in Selma, TX and Comal Elementary in New Braunfels, TX. In 2002, he graduated *summa cum laude* from Canyon High School in New Braunfels, Texas. Next, he attended college at The University of Texas at Austin, where he graduated in May of 2006 with High Honors from the Cockrell School of Engineering with a Bachelor of Science degree in Mechanical Engineering. During the summer of 2005, Nicholas was a corporate intern for Caterpillar Inc. in Peoria, Illinois, where he worked in the Service Training Department of the Product Support Division. In July of 2006, he began graduate research at The University of Texas at Austin as a member of the Neuromuscular Biomechanics Laboratory. He subsequently enrolled in graduate school at The University of Texas at Austin in the fall of 2006. In May of 2008, Nicholas earned a Master of Science in Engineering degree. While in graduate school, Nicholas has also served as a research mentor to undergraduate mechanical engineering students and a teaching assistant in mechanical engineering courses. His graduate research has focused on the walking mechanics of lower-limb amputees and prosthetic foot design methods to improve amputee mobility.

Permanent email address: nicholas.fey@gmail.com

This dissertation was typed by the author.